BABEȘ-BOLYAI UNIVERSITY

Doctoral School of Engineering

DOCTORAL THESIS

Doctoral supervisors:

Professor Gilbert-Rainer GILLICH
Assoc.prof.habil István BIRÓ

Phd Student:

Tatian-Cristian MĂLIN

2021

BABEȘ-BOLYAI UNIVERSITY

Doctoral School of Engineering

DOCTORAL THESIS

Researches regarding the behaviour of structures isolated by friction pendulums

Cercetări privind comportamentul structurilor izolate cu pendule de frecare

Author: Eng. Tatian-Cristian MĂLIN

DOCTORAL COMMITTEE:

President:	Assoc.prof.habil. Zoltan Iosif KORKA	from Babeş-Bolyai University
Doctoral supervisors:	Prof. Gilbert-Rainer GILLICH	from Babeş-Bolyai University
	Assoc.prof.habil. István BIRÓ	from University of Szeged, Hungary
Official reviewers:	Prof. Dorian NEDELCU	from Babeş-Bolyai University
	Prof.habil. Mircea Cristian DUDESCU	from Technical University of Cluj-Napoca
	Prof. Elena MEREUȚĂ	from "Dunărea de Jos" University of Galați

REŞIŢA 2021

ACKNOWLEDGEMENTS

The elaboration of this doctoral thesis would have been impossible without the help, support, and guidance of special people who, through a high degree of professionalism and dedication, have contributed to my training as a researcher.

I would like to express my sincere gratitude to my esteemed scientific supervisors, Prof. Gilbert-Rainer Gillich and Assoc.prof.habil. István Biró, for their invaluable advice, noble guidance, continuous support, and patience during my PhD study.

I would also like to thank the guidance committee members, namely Prof. Dorian Nedelcu for his immense knowledge, plentiful experience and all the technical support provided on my study, Assoc.prof.habil. Zoltan Iosif Korka and Lecturer Vasile Iancu for their assistance at every stage of the research project.

My gratitude extends to the Faculty of Engineering for the funding opportunity to undertake my studies at the Department of the Doctoral School of Babeş-Bolyai University.

I would like to express my respect to Prof. Elena Mereuță from "Dunărea de Jos" University of Galați and to Prof.habil. Mircea Cristian Dudescu from Technical University of Cluj-Napoca which, as scientific reviewers, have contributed with competent suggestions and observations to the improvement of the current thesis.

My appreciation also goes out to my family and friends for their encouragement and support all through my studies.

Reşiţa, 25 November 2021 Author: Tatian-Cristian Mălin

TABLE OF CONTENTS

LIST OF TABLES

LIST OF FIGURES

LIST OF ABBREVIATIONS

A	Amplitude
a	Acceleration
D	Damping
Damp	Damping coefficient
d	Displacement
EDF	Electricite-de-France
FPS	Friction Pendulum System
FFT	Fast Fourier Transform
FR	Sampling frequency
f	Frequency
f_n	Natural frequency
g	Gravitational acceleration
HDRB	High-Damping Rubber Bearings
K	Lateral stiffness
k	Spring constant
LDRB	Low-Damping Rubber Bearings
LabVIEW	Laboratory Virtual Instrumentation Engineering Workbench
N	Number of samples
Ph	Phase
p(x)	Probability density for the Gaussian distribution
PySEMO	Python Seismic Motion
R	Radius
R_H	Semi-minor axis of the ellipse

R_V	Semi-major axis of the ellipse
R-FBI	Resilient-Friction Base Isolation
S	Signal
SFP	Simple friction pendulum
T	Natural period of vibration of a rigid structure
TMD	Tuned Mass Damper
t	Time
v	Velocity
W	Noise
w	Weight
x, *y*, *z*	Coordinates system
μ_S, μ_D	Static and dynamic friction coefficients
v_S, v_D	Static and dynamic velocity coefficients
φ_i	Initial phase

INTRODUCTION

Our society has been and still is affected by one of the deadliest and costly natural catastrophes that are earthquakes. High economic losses, thousands of casualties and even deaths are the consequences of earthquakes over time.

Earthquake is the definition for earth movements, consisting of vibrations produced in the internal areas of the Earth, propagated in the form of waves through the rocks.

The two main objectives of earthquake safety are life safety and collapse prevention, so the desire for high-performance buildings has increased.

The classic anti-seismic design of structures was based on the concept of increasing the rigidity of the structure against earthquakes by using retaining walls, braces, reinforcement shirts, etc. These traditional methods induce large vertical accelerations and horizontal displacements to the structures, therefore the structures can suffer major damages. Buildings that house high precision and fine machines, especially for strategic constructions and infrastructures like power plants (nuclear, hydro, and thermal), hospitals, schools, bridges, police and fire departments, communication centers, must remain operational after an earthquake.

Reducing the effects of earthquakes by reducing displacements and accelerations of the structures, imposed the concept of seismic isolation, by installing special devices between infrastructure (foundation) and superstructure (building). In this way it is ensured the isolation of the movement of the structure from that of the earth, practically decoupling them.

Regarding the development of innovative devices designed to reduce the effect of earthquakes on buildings, they are based on the following principles: use of inertia, dissipation of energy transmitted to the building, respectively by changing the oscillation period. The requirements for a high-performance seismic isolation device are the following: minimization of damage caused by earthquakes, maintenance in operation after the earthquake, low installation and operating costs, and autonomous operation, independent of energy sources.

Given the worldwide concern regarding the field of seismic isolation, there are currently numerous papers and studies on this subject. In this context, the results of the research regarding the behavior of structures isolated by friction pendulum systems had as essential objective to find out how the pendulum radii and friction coefficients, respectively the frequency of the excitation, influences the structural response. The idea is to design the mentioned devices based on the history of the place.

In these conditions, the specific objectives of the thesis can be summarized as follows:

- study of specialized literature and normative documents on the effects of earthquakes and methods to reduce their effects;
- elaboration of an algorithm regarding the digitization of earthquake signals stored as images;
- development of an algorithm to estimate the velocity and displacement of the earthquake signals with known acceleration;
- validation of the application designed to convert earthquake signals from acceleration in displacement and velocity for generated signals;
- determination of the effect of friction pendulum radius changes on the response of isolated structures by dynamic simulations;
- determination of the effect of the friction coefficient and the pendulum radius on the behavior of structures isolated with simple friction pendulums;
- design a friction pendulum system with variable radius and comparison of the performance with current friction pendulums (uniform radii);
- development of an isolation system with a plan sliding surface restrained by springs and with a counterweight on the top of the structure;
- validation the results obtained from dynamic simulations through experimental tests performed on a small-scale model;
- dissemination of the research results.

The proposed objectives led to the structure of the thesis in a number of six chapters, the content of which is presented below.

Chapter 1 *– ” Literature review”* presents the seismic activity from a global view and some basic earthquake principles: causes of earthquakes, fault types, seismic waves, and earthquake effects. Also, the earthquake magnitude and intensity scale are introduced. Further are presented the most devastating earthquakes recorded, their effects, and the new building design codes developed after each major event.

Chapter 2 *– ” Digital processing of earthquake signals”* presents some important web-based databases that can be used to re-analyze the past and present earthquakes. Further is presented a rapid and accurate method to extract the signals and the numerical values from an image with the help of the WebPlotDigitizer software. Also in this chapter is presented an application developed in the Python programming language that generates digital signals with known parameters (frequency, amplitude, phase, damping coefficient, existence of noise) and exemplify outcomes for different settings of the parameters. An algorithm was developed to

estimate the velocity and displacement of the earthquake signals with known acceleration. The algorithm, nominated as PySEMO, was implemented in the Python programming language and used to demonstrate the accuracy of the method. At the end of the Chapter, are presented some recommendations for the acquisition strategy to guarantee to find precise velocities and displacements.

Chapter 3 – *" Base isolation systems"* explain the concept of base isolation and present a short review of the history of base isolation. Further, the elastomeric (Low-Damping Rubber Bearings and High-Damping Rubber Bearings) and sliding based (Electricite-de-France System, Resilient-Friction Base Isolation System, Friction Pendulum System, and Tuned Mass Damper System) seismic isolation systems are briefly defined and described. Because friction pendulum systems with variable radii are little studied and used, it was a good opportunity to research the particularities of this system compared to those with spherical or cylindrical surfaces.

Chapter 4 – *" Dynamic simulations and behaviour of structures isolated by friction pendulum"* presents the results of simulations made on a rigid structure isolated with four simple friction pendulums. The structure was implemented in the Motion module of SolidWorks and the model was used to find out how the pendulum radii and friction coefficients, respectively the frequency of the excitation, influences the structural response.

Chapter 5 – *" Experimental research"* presents the experimental stand designed in the Laboratory for studying the seismic actions of the Babeş-Bolyai University and the virtual instrumentation. The software in which the data from accelerometers was processed and the input-output applications were developed is LabVIEW. Experimental tests performed on a small-scale model validated the results obtained by dynamic simulations.

Chapter 6 – *" Conclusions and further works"* presents the conclusions and the main personal contributions, theoretical and applied, included in the doctoral thesis, as well as the research directions that can be followed.

1. LITERATURE REVIEW

1.1. Seismic activity at a global view

94% of the Earth's surface is covered by seven major plaques with a thickness of up to 100 km. The seven major plaques (Figure 1.1) are in the order of magnitude: Pacific Plate, African Plate, Eurasian Plate, Australian Plate, North American Plate, Antarctic Plate, and South American Plate. The Pacific Plate is the only plate entirely made of oceanic crust, the other plaques containing both ocean bark and continental bark portions [1].

The dimensions of the tiles are permanently changed, and they can be expanded or shrunk. These processes take place at the edges of the plates and there is a deep balance between them. The boundaries of most of the plates are in the ocean, but some are marked by mountain chains, such as the Himalayan chain, which marks the limit between the Eurasian Plate and the Indian one.

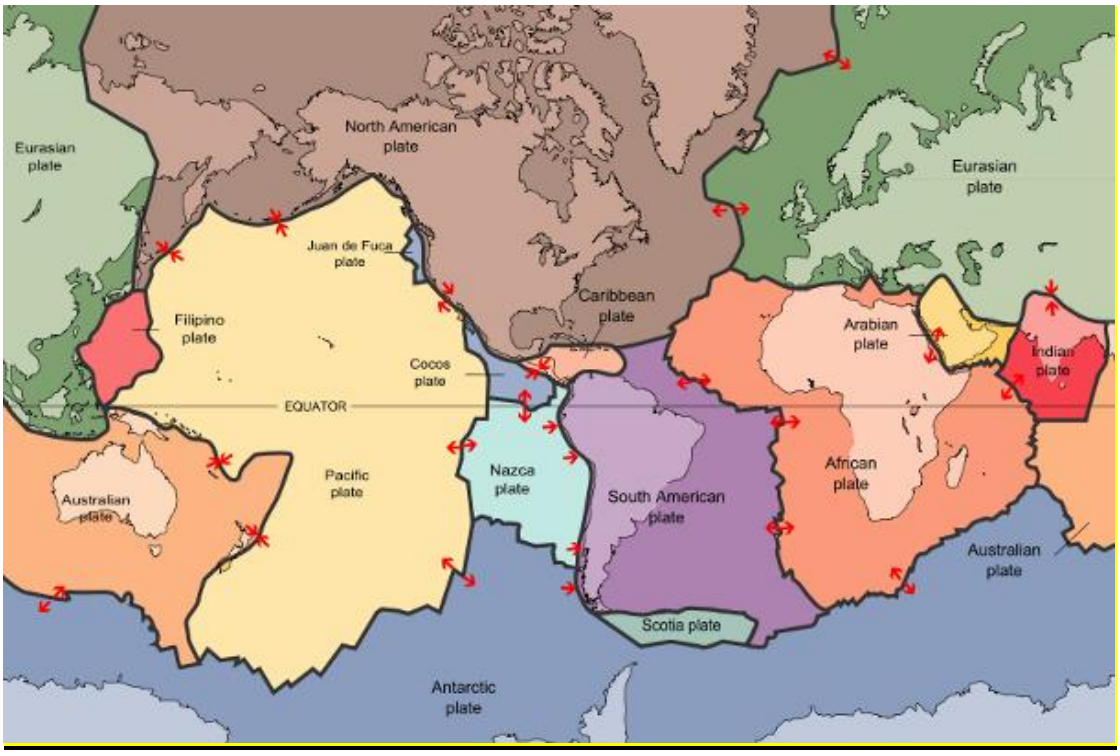

Figure 1.1 The main tectonic plates
https://en.wikipedia.org/wiki/List_of_tectonic_plates#/media/File:Plates_tect2_en.svg

Earthquakes are natural phenomena caused by the release of energy within the Earth following the fracture of the rocks subjected to the accumulated tensions.

Earthquake position has been analyzed in terms of seismic recordings from seismographic observatories. Areas with significant seismic activity (Figure 1.2) are concentrated along belts delimiting large continental and oceanic stretches:

- the Pacific Ring of Fire Belt with over 81% of the world's largest earthquakes, bordering the Pacific Ocean (from Chile to Alaska, Japan, the Philippines, and New Zealand);
- The Alpide belt with over 17% of the world's largest and most destructive earthquakes extends from Java to Sumatra through the Himalayas, the Mediterranean Sea to the Atlantic. The belt also includes the Vrancea seismic area of the Carpathian Mountains;
- Mid-Atlantic Ridge Belt in the middle of the Atlantic Ocean. In these areas, volcanic eruptions are frequent due to the presence of submarine mountain chains.

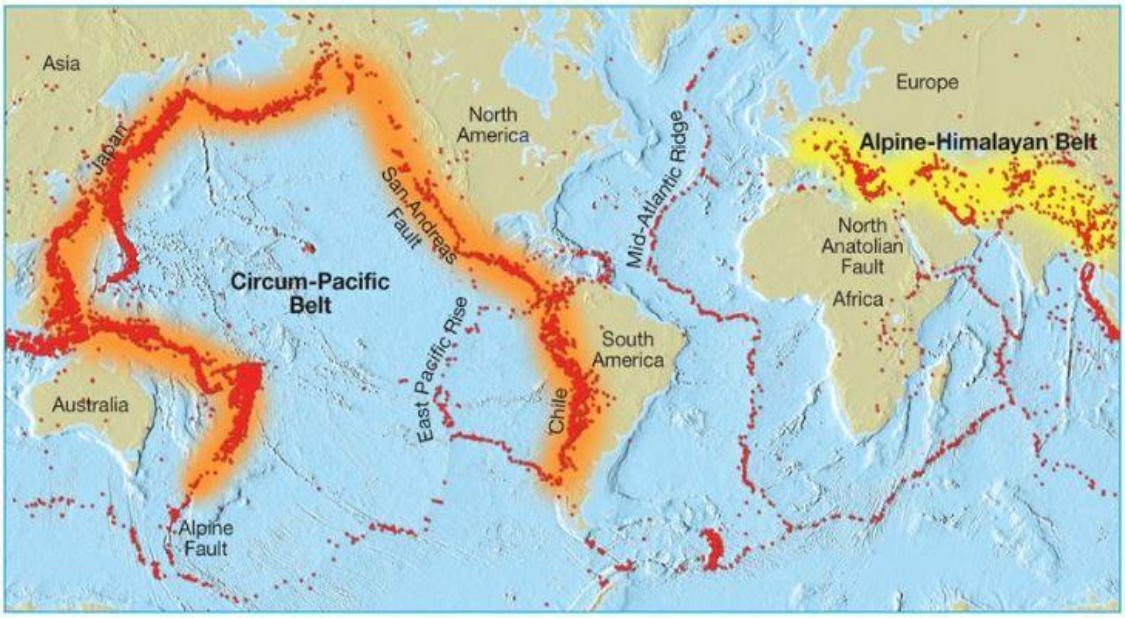

Figure 1.2 Areas with significant seismic activity
(http://belt.cchronicles.com/what-is-a-seismic-belt/)

The earthquake generates seismic waves that occur beneath the surface of the ground due to the sudden slippage of the edges of a fault. Seismic waves are responsible for producing destructive effects from the surface of the earth, causing the soil to move. The seismic source in which the seismic waves originate is called the focus or hypocenter.

The projection of the hypocenter on the surface of the terrain is called epicenter (Figure 1.3). The focuses are in many cases at low depths, but there are regions where they are located at hundreds of kilometers deep. Depending on the depth of the hypocenter, earthquakes can be classified as follows:

- Surface earthquakes with a hypocenter depth of less than 70 km
- Intermittent earthquakes, with a hypocenter depth between 70 and 300 km
- Deep earthquakes, with a hypocenter depth of more than 300 km

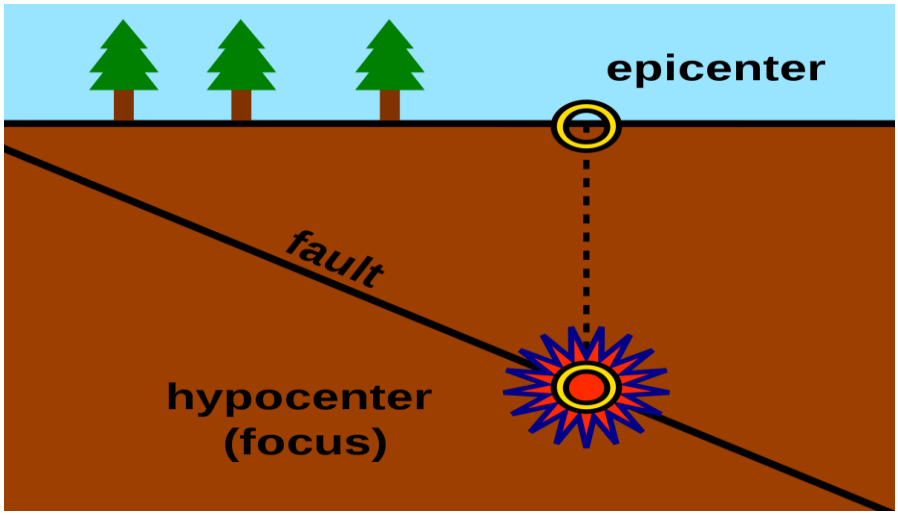

Figure 1.3. Hypocenter and epicenter of a ground earthquake
(https://en.wikipedia.org/wiki/Hypocenter)

With about 75% of the total seismic energy released by earthquakes worldwide, surface earthquakes have the most devastating consequences (located in California, Turkey, and Romania). Surface earthquakes are followed by post-shocks that may occur in a short period of time, like a few hours or a few months after the main shock. Post-shocks may be strong enough to cause significant damage. Earthquakes with intermediate focuses have a moderate duration, longer predominant periods, and a much larger area of manifestation. These earthquakes are quite low in number, being present in Afghanistan, Colombia, Mexico, and Romania.

Earthquakes with deep focuses are lesser in number, with longer duration and longer predominant periods. The most severe earthquake in the seismic record was the magnitude 8.3 Okhotsk Sea earthquake which occurred at a depth of 609 km in 2013 [2]. The deepest earthquake ever recorded was a small 4.2 earthquake in Vanuatu at a depth of 735.8 km in 2004 [3]. Deep earthquakes, up to 680 km, are concentrated in the islands' chains of the Pacific Ocean and the Eastern Caribbean.

1.2. Causes of earthquakes

The causes of producing earthquakes can be divided into natural and artificial:

Natural:

- tectonic: due to the tensions inside the Earth (90% of Earth's earthquakes);
- volcanic activity (7% of Earth's earthquakes);
- impact of meteorites;
- collapse of underground caverns.

Artificial:

- explosions;
- mining operations (such as mine collapses, excavation);
- filling of storage lakes.

Tectonic plates are huge masses of relatively stable rock that form the outer mantle of the Earth. The average thickness of the main tectonic plates is about 80 km. The heat generated in the core creates the convection movement in the mantle, which in turn causes the tectonic plates to move. The relative movement of the tectonic plates is responsible for an important part of the world's seismic activity. The collision between the lithospheric plates, the destruction of the tectonic plate edges in the converging zones, or the expansion in the divergent areas are mechanisms that can produce stresses and fractures in the earth's crust.

The inter-plate earthquakes are generated at the active edges of the tectonic plates. The most powerful inter-plate earthquakes are in Chile, Peru, Central America, Southern Mexico, California, Taiwan, South Alaska, Philippines, Japan, Indonesia, and New Zealand. Intra-plate earthquakes are devastating earthquakes that occur within the tectonic plates. Such earthquakes indicate that the lithospheric plates are not undeformable and that fractures can occur within them. The most representative intra-plate earthquakes are those in northeast Iran, Charleston (USA), New Madrid (USA), and northern China.

Volcanic earthquakes are relatively rare and of low intensity, and may be caused by volcanic explosions, magma motion, or the collapse of the solidified magma from the volcano basket on its hearth. Most volcanoes are located on the active edges of the tectonic plates, but there are also intra-plate volcanoes, such as the volcanoes of the Hawaii Islands.

Local earthquakes can be generated by *larger meteorites* that, due to their size, do not disintegrate into the atmosphere, reaching the terrestrial surface.

Earthquakes resulting from the crash of the ceiling of some *mines and caverns* have low intensities. Another means of producing these earthquakes is the *explosive* decomposition of large volumes of rock from mine walls due to accumulated stresses. Massive landslides can also cause minor earthquakes. Earthquakes can be produced by *underground detonations of chemical or nuclear devices*. Underground nuclear explosions that occurred in the past have generated earthquakes of magnitude up to six.

Increases in seismic activity were observed in areas where large water dams were built. The most plausible explanation is that the rock in the vicinity of the water dams is already in a state of tension. Filling the tank with water either increases the stress state and generates slippage, or crack water pressure reduces the strength of the fault, or both phenomena occur.

1.3. Fault types

Faults represent sudden changes in the structure of rocks that occur at the contact between two different tectonic blocks. They may have different lengths from a few meters to hundreds of kilometers.The slope of a fault is the angle that the surface of the fault creates with the horizontal plane and the direction of a fault is the direction of the projection of the fault on the land surface towards the North.

The relative displacements of the geological structures along the faults can be either slow slopes that do not produce seismic movements or sudden breaks that produce earthquakes. In most cases, the slides along the faults are not visible, not reaching to the surface of the terrain, but there are cases when the faults extend to the surface of the ground (Figure 1.4)

Figure 1.4 The effect of a transcurrent fault on the surface of the ground (https://www.sciencedirect.com/topics/earth-and-planetary-sciences/fault-displacement)

Depending on their geometry and the direction of relative sliding, the faults are classified (Figure 1.5) as follows:

- reverse faults - the sliding occurs in a vertical plane (parallel to the slope), the upper plate of the inclined fault moving upward from the lower plate;

- normal faults - the sliding occurs in a vertical plane (parallel to the slope), the upper plate of the inclined fault moving downwards from the lower plate;

- transcurrent faults - movement of rock blocks parallel to the fault;

- oblique faults - a combination of slopes in horizontally and vertically plane, being the most common in nature.

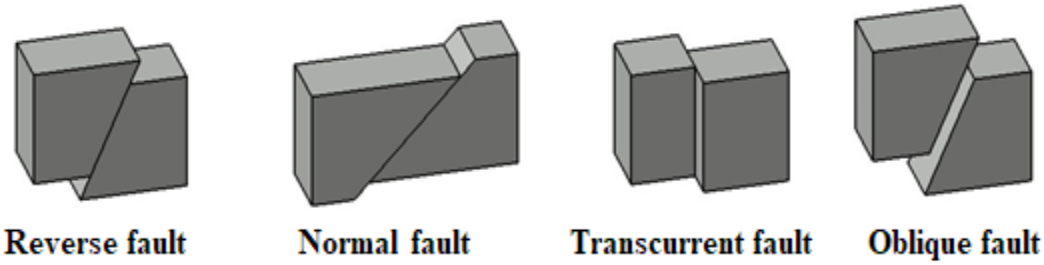

Figure 1.5 Fault types

1.4. Seismic waves

The seismic movement is due to the various types of waves generated by the sudden sliding of the tectonic plates along a fault.

There are known two major types of seismic waves:

- volume waves - propagate through the interior of the earth:
  - P-waves (also called primary, compression or longitudinal waves) generate a series of compressions and expansions of the material (liquid or solid) through which they propagate, have the highest speed, are the first to reach a given location, and the impact of the waves on seismic motion in a location is the smallest;

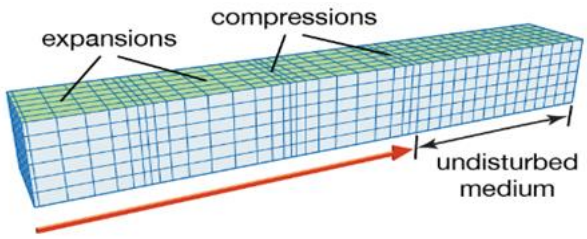

Figure 1.6 P-waves
(https://www.britannica.com/science/earthquake-geology)

- S-waves (also known as secondary, shear, or transverse) generate shear deformations in the propagating material (solid only), the propagation velocity is less than the P-waves, but the wave effect on the seismic motion in a location is the largest;

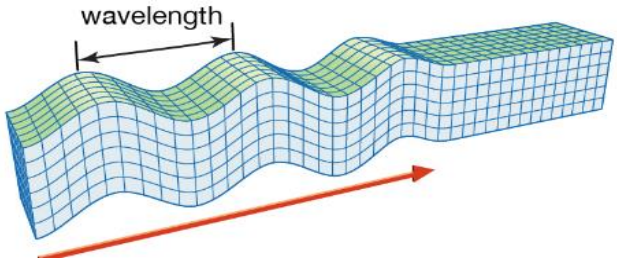

Figure 1.7 S-waves

(https://www.britannica.com/science/earthquake-geology)

- surface waves - propagate only near the surface of the land:
  - Rayleigh's waves are like waves created by a stone thrown into a pot of water. The movement of the particles takes place in a vertical plane;

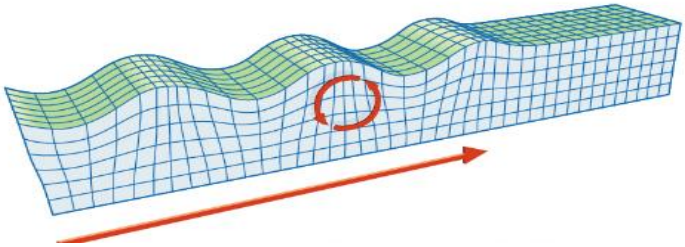

Figure 1.8 Rayleigh waves

(https://www.britannica.com/science/earthquake-geology)

- Love waves are similar to S-waves, being transversal waves propagating to the surface of the field, the movement of the ground particles taking place horizontally. Surface waves result from the interaction of volume waves with the surface of the ground.

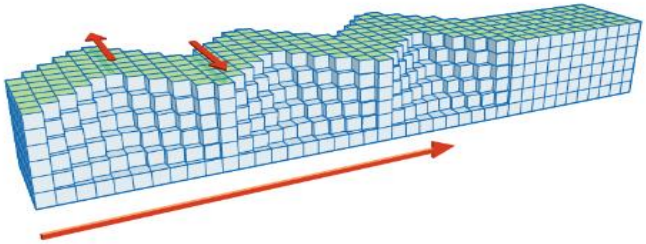

Figure 1.9 Love waves

(https://www.britannica.com/science/earthquake-geology)

1.5. Earthquake effects

The damage and destruction that may be caused by earthquakes is due to several earthquake effects, among which:

- inertial forces induced in the structure due to seismic motion
- fires caused by earthquakes
- modification of the physical properties of the foundation ground (consolidation, composting, liquefaction)
- the direct movement of the fault at the level of the land
- landslides
- changing the topography of the land
- earthquake-induced waves such as tsunami

The most significant and most common destruction of earthquakes is due to the vibrations induced in construction by seismic motion (Figure 1.10).

Another major danger resulting from an earthquake is fire. Thus, during the 1906 earthquake in San Francisco, only 20% of the total loss was due to direct destruction caused by seismic movements, the remaining 80% being caused by the fires that devastated the city for three days and which consumed an area of 12 km^2 and 521 blocks from downtown.

Figure 1.10 Partial collapse of a structure in Bucharest, Vrancea earthquake of March 4, 1977 (https://www.igsu.ro/)

Destruction due to base ground behavior has created major problems during the earthquakes in the past, for example the 1967 Niigata earthquake (Figure 1.11(a)). The development of the city has forced the use of poor land from the former Shinano River bed. As a result of the seismic movement, many buildings have leaned or overturned as a result of the

liquefaction of the foundation ground. A total of 3018 buildings have been destroyed and 9750 have suffered average to severe degradation, mostly due to uneven deposits and cracks in the ground.

The direct shifts of ground fault (Figure 1.11(b)), are probably the most shattering at the social level. This phenomenon is encountered relatively rarely, and the damage and the affected area are minor compared to those caused by the vibrations induced in constructions by the seismic movement.

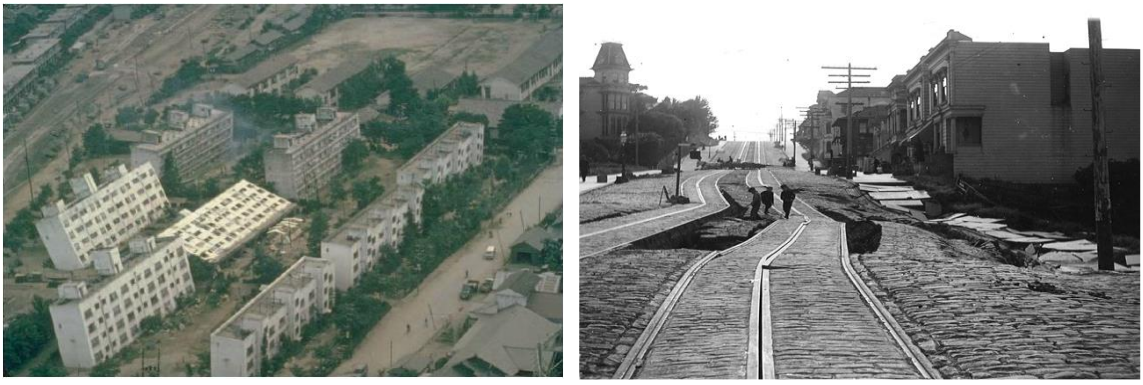

(a) (b)

(http://nisee.berkeley.edu/) (http://www.eas.slu.edu/)

Figure 1.11 Liquefaction at buildings foundation, Niigata earthquake, 1964 (a); tram tracks bent as result of the earthquakes produced during the 1906 San Francisco earthquake (b).

Landslides caused by earthquakes (Figure 1.12), although they represent a major hazard, do not occur very frequently.

Figure 1.12 A landslide triggered by the Kumamoto earthquake, Japan 2016
(https://blogs.agu.org/landslideblog/2016/04/18/kumamoto-earthquake-1/)

Topographic changes due to earthquakes do not directly lead to loss of life. The most important consequence of such changes is the destruction that structures such as bridges and dams can suffer.

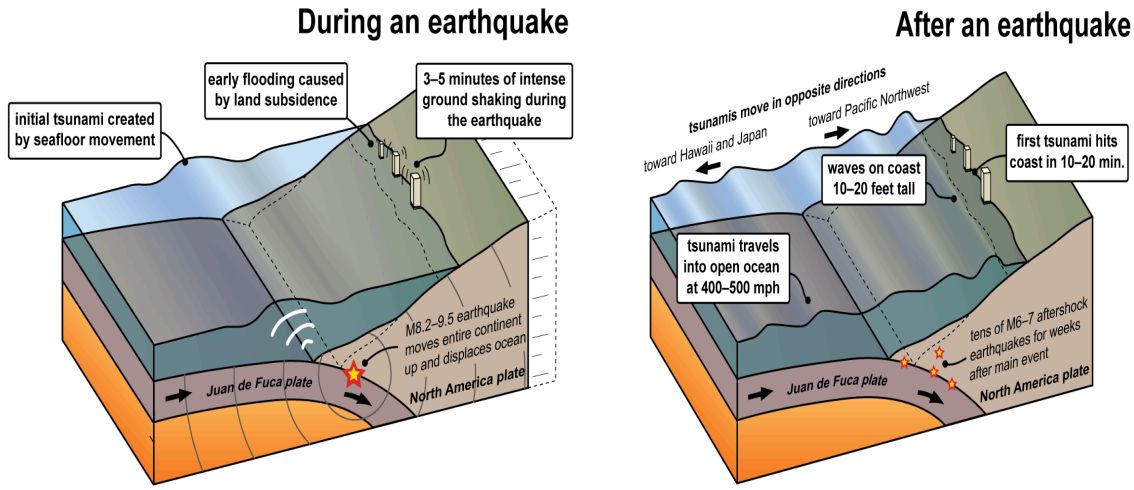

Figure 1.13 Tsunami generated by underwater earthquakes (https://www.dnr.wa.gov/)

Tsunami are ocean waves generated by underwater earthquakes and can cause significant damage to coastal localities (Figure 1.13). The Pacific Ocean is often the place for such events. For an earthquake to generate a tsunami, it must be associated with an inverse or normal fault.

Preventing human losses in the Pacific due to the tsunami is achieved through a monitoring and alert system composed of several dozen stations located in the Pacific Ocean. In addition to this system, the risk of huge waves can be reduced by specific coastal construction and avoiding the location of construction in low coastal areas.

1.6. Measuring earthquakes

The effects of the earthquake on the environment in the earthquake area are described using Richter and Mercalli (Table 1.1) seismic intensity scales [4],[5]. The Richter scale was built by Charles Richter and Beno Gutenberg (1935) for a measure of earthquake power [6]. It is a logarithmic scale because the magnitude corresponds to the logarithm of measuring the amplitude of the volume waves (type P and S) at 100 km from the epicenter and is graded from 1 to 9. Usually, the intensity of earthquakes is not expressed in whole numbers, but in fractional

numbers [7]. Because the Richter scale is logarithmic, a change of one degree on the Richter scale is correlated with a 10 times change in the amplitude of the seismic waves and about 30 times the energy released by the earthquake [8].

Table 1.1 Mercalli and Richter scales

Mercalli Scale	Category	Effects	Richter Scale
I.	Instrumental	Not felt.	1 - 2
II.	Weak	Felt by only a few people, especially on upper floors of tall buildings.	2 - 3
III.	Slight	Felt by some people inside the buildings in the upper stories of tall buildings.	3 - 4
IV.	Moderate	Felt by several people inside the buildings and few outside.	4
V.	Rather strong	Felt by everyone; sleeping people may be awakened.	4 - 5
VI.	Strong	Trees sway, chandeliers swing, some damage from falling objects.	5 - 6
VII.	Very strong	General alarm; walls and plaster crack.	6
VIII.	Destructive	Poorly constructed buildings seriously damaged; felt in moving vehicles.	6 - 7
IX.	Ruinous	Considerable damage; some houses collapse.	7
X.	Disastrous	Ground cracks; railroad tracks bent; some landslides.	7 - 8
XI.	Very disastrous	Few buildings survive; bridges damaged or destroyed; all services interrupted.	8
XII.	Extreme	Total destruction.	> 8

The Mercalli scale, invented by the Italian seismologist Giuseppe Mercalli, is a scale that determines the intensity of an earthquake based on personal, subjective observations, during the earthquake [9].

The intensity of the earthquakes is assessed by the severity of the destruction of buildings, by the type and magnitude of the deformations of the earth's surface and by the reactions of the population to the seismic shock. The effects of the shock diminish proportionally with the increase of the distance to the epicenter [10].

1.7. The biggest earthquakes recorded

1.7.1. The San Francisco Earthquake, 1906

One of the largest earthquakes of all time is the California earthquake from 18 April 1906. At around 5 a.m. was the first strong shock that was felt in the entire bay of San Francisco. The earthquake occurred 25 seconds later, with the epicenter near San Francisco. The powerful earthquake shocks lasted about 60 seconds and were felt in Oregon, Los Angeles, and Nevada [11].

The earthquake surprised geologists with its considerable rupture length and large horizontal displacements, 477 kilometers of the San Andreas fault.

This earthquake is remembered in the public's mind for the fire occurred in San Francisco, causing severe damage and a lot of deaths. Initially, there were an estimated 700 deaths, but it is now believed that there were 3 or 4 times more victims than the initial estimate.

Figure 1.14 San Francisco Earthquake, Sacramento Street
(https://earthquake.usgs.gov/earthquakes/events/1906calif/18april/)

1.7.2. El Centro Earthquake, 1940

Another important earthquake was the El Centro earthquake also known as the 1940 Imperial Valley earthquake. Originated from the San Andreas fault line, the earthquake occurred in Southern California (in the Imperial Valley) on 18 May at around 9 pm and had a maximum intensity of X (on the Mercalli intensity scale).The epicenter of the earthquake was detected 8.0 km north of Calexico (California) [12]. An hour after the mainshock, a magnitude 5.5 secondary quake happened near Brawley, causing physical damage to the town's residential and business area [13].

The El Centro earthquake caused extensive and widespread damage, directly caused the deaths of nine people and, indirectly, seven others.

Significant damage to irrigation systems were caused by the earthquake, leaving the Imperial Irrigation District with compromised canals in multiple locations resulting in water rationing during the following days. In Mexico, a 427 m wooden canal was completely destroyed, as well as water storage tanks at Holtville and Imperial [14],[15].

Close to the border, a surface rupture of approximately 60 km appeared during the earthquake, recording a displacement of 4.5 m and having a sense of movement nearly pure strike-slip, without any vertical displacement [12].

The same section of the fault was broken on the United States territory during the 1979 Imperial Valley earthquake having a similar displacement pattern as the rupture of the 1940 earthquake. The Mexican side was not affected by the 1979 earthquake, suggesting that the Imperial Fault slides in discrete patches, two of them rupturing in 1940, and only one of them in 1979 [16].

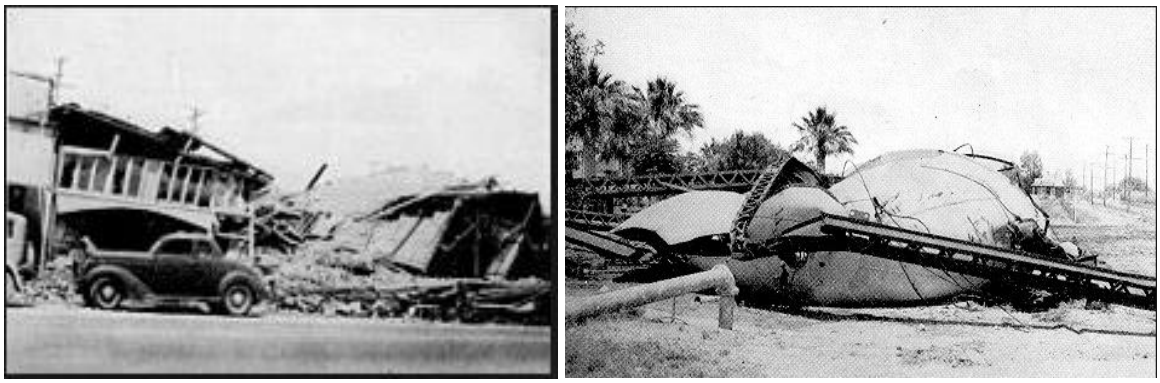

Figure 1.15 El Centro Earthquake
(https://en.wikipedia.org/wiki/1940_El_Centro_earthquake)

1.7.3. San Fernando Earthquake, 1971

On 9 February 1971, in southern California, at the base of San Gabriel Mountains a 6.5 magnitude and a maximum Mercalli intensity XI, San Fernando earthquake occurred at 6 am, with a 12 seconds duration.

The unanticipated earthquake produced severe damage in the northern San Fernando Valley and caused extensive surface faulting along city streets, affecting thousands of homes and businesses. Gas lines exploded, power lines fell, windows shattered, and telephone service cut. In Sylmar, the newly opened six-story tall psychiatric ward at the Olive View Community

Hospital collapsed, killing three people, but the most impacted was the San Fernando Veterans Administration Hospital with 44 dead [17].

At least a dozen bridges fell onto freeway lanes, and the transportation surrounding Los Angeles suffered roadway collapse, one of the most important being the partial crash of some major highway interchange nodes [18].

The Lower Van Norman Dam was so severely affected by the earthquake and threatened to burst, that 80.000 downstream residents had to be evacuated for three days so that the water level of the dam could be lowered as a precaution to prevent a possible collapse.

With 64 people dead, 2500 injured, and prejudice of more than 550 million US dollars, the San Fernando earthquake was at that time the 3rd worst earthquake regarding lost lives, and the 2nd in terms of property damage.

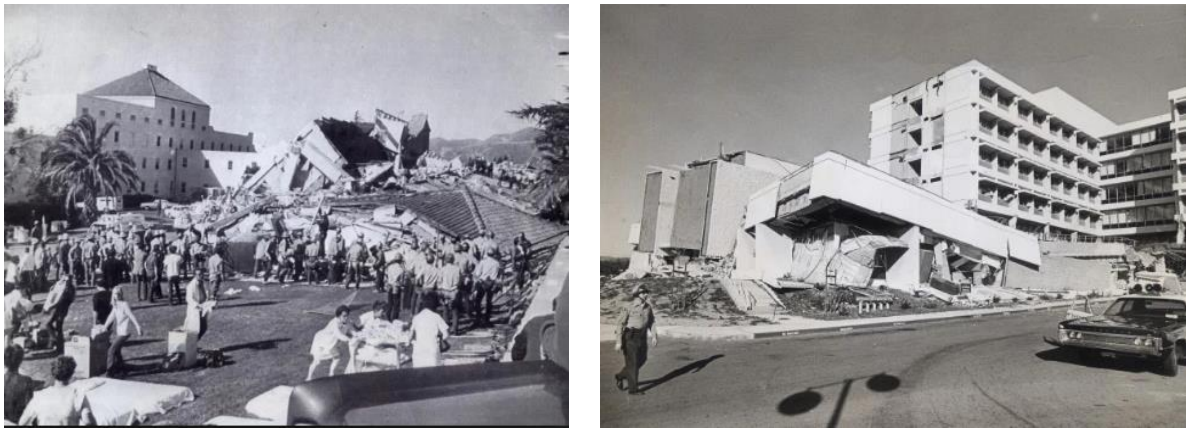

Figure 1.16 San Fernando Earthquake
(https://en.wikipedia.org/wiki/1971_San_Fernando_earthquake)

1.7.4. Vrancea Earthquake, 1977

On 4 March 1977 occurred the Vrancea earthquake, the second most powerful earthquake registered in Romania, with a magnitude of 7.2. The epicenter was localized at a depth of 94 km in the Vrancea Mountains, making the earthquake felt in the Balkans area [19].

The earthquake was so powerful that the communist dictator Nicolae Ceaușescu declared a state of urgency, due to a large number of victims, around 13.000 people and about 1.578 people were killed [20]. Even though the authorities at that time never confirmed it and a detailed damage report was never published, the economic losses were believed to be huge, around two billion US dollars [19].

Because most of the country's buildings were constructed before WW II and were not consolidated, the earthquake left about 32.900 buildings damaged or even destroyed and 35.000 families homeless, Bucharest was the most affected city with around 33 buildings collapsed.

The earthquake caused damage in Bulgaria also, deteriorating many buildings, including the Church of the Holy Trinity and the collapse of three blocks in Svishtov, taking the lives of more than 100 people.

Figure 1.17 Vrancea Earthquake
(https://en.wikipedia.org/wiki/1977_Vrancea_earthquake)

1.7.5. Northridge, 1994 and Kobe,1995 Earthquakes

With a magnitude of 6.7, the Northridge earthquake (17 January 1994) caused 44 billion US dollars material damage, considered to be the biggest damage in history [21]. The earthquake showed the weakness of the buildings constructed until then. The number of victims resulted was quite small, 57, even though the event occurred in a very populated area.

With a similar magnitude, 6.9, the Kobe earthquake occurred one year after the Northridge earthquake, but the number of victims was considerably higher killing 6.427 people. The seismic movement determined the land rupture 20 km southwest of Kobe city, the intense acceleration of the land causing the collapse of more than 100.000 buildings and damaging another 80.000 structures severely. Most of the damaged buildings were traditional Japanese, having wooden design and heavy roof, not efficient for earthquake action because they were missing the elements that ease catching horizontal dynamic demands of the earthquake [22].

The Kobe earthquake had a long pulse with a period of approximate 0.8-1.2 seconds, causing the collapse of many buildings with metal structures and the breakdown of Hanshin highway piles and reinforced concrete pillars due to shear force (Figure 1.18).

The liquefaction of the land was another cause that resulted in the partial or total collapse of some structures and the destruction of the Kobe port.

Figure 1.18 Collapse of the Hanshin Motorway, Kobe, Japan (https://www.researchgate.net/figure/Flexural-failure-at-the-base-of-bridge-pier-during-1995-kobe-earthquake-Hanshin_fig2_273573779)

1.8. Conclusions

The field of seismic engineering went through a process of continuous development, and after each major event, new building design codes were developed. Currently, they help construct buildings, making them much safer and reducing human and material losses.

The first important step in the seismic design of buildings was taken in 1914 when the lateral force method was included in a design code (UBC 1927).

The importance of the foundation ground on the design forces was known from the beginning, as well as the positive influence of the appropriate structural detailing. A more dynamic approach to seismic engineering was brought by the first recording of an earthquake, El Centro 1940, being recognized the influence of the rigidity of the building on the shear force base. In the 1950s, the main objective was to set resistance standards for design to ensure the safety of human life. After the massive earthquake of 1977, Romania developed the P100 design code, a document where the local design prescriptions were aligned to international standards. A better knowledge of the specific of Vrancea earthquakes was determined by the records of earthquakes from 1977, 1986 and 1990.

The ATC-3.06 report in the US and the P100-78 norm in Romania have set down the foundations for today's construction codes. The lateral force method and linear spectral analysis are still used today to design structures.

The destruction caused by the Northridge and Kobe earthquakes has highlighted the vulnerability of design codes and design in the elastic field. With the spreading of personal computers, structural analysis in the inelastic field has become widely available.

2. DIGITAL PROCESSING OF EARTHQUAKE SIGNALS

The historical view related to earthquakes is an important concern for seismic risk evaluation, especially for strategic constructions and infrastructures like nuclear power plants, hospitals, schools, bridges, etc. The knowledge about the evolution of earthquakes over long time ranges is imperative.

Due to the availability of historical instrumental data, so important from the scientific point of view, the earthquake instrumental catalogs were developed over 100 years. The original recordings, like printed bulletins and analog seismograms, are kept still in most observatories around the world. To keep the unique seismological heritage, new digital archiving techniques have been created. The digital format and the modern techniques allowed the re-analysis of past earthquakes and the re-evaluation of seismic hazards [26],[27].

2.1. Earthquake registrations database

2.1.1 PEER Ground Motion Database

The web-based PEER Ground Motion Database (Pacific Earthquake Engineering Research Center) contains many archives of seismograms and tools that allow the user to search, select and download ground motion data from historical earthquakes [23]. The web-based database is accessible on the website: https://ngawest2.berkeley.edu.

The PEER database provides two types of search: event or station characteristics and parameters for the response spectra. In Figure 2.1 are provided the results of the search for the 1995 Kobe earthquake.

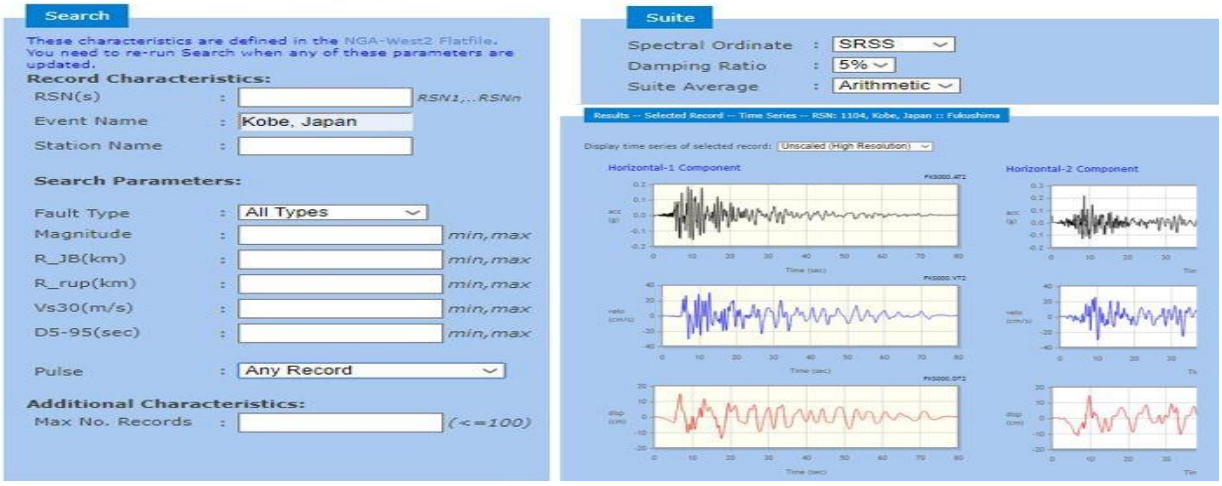

Figure 2.1 Search options from PEER database

2.1.2 Center for Engineering Strong-Motion Data (CESMD)

The USGS (U.S. Geological Survey) and CGS (California Geological Survey) have developed the CESMD (Center for Engineering Strong Motion Data) as a unified database to provide earthquake strong-motion data for engineering applications [24]. The CESMD database is accessible on the website: https://www.strongmotioncenter.org.

In the CSMD database, the earthquake records are searchable in many ways, depending on the user's interests. The search parameters can be a combination of earthquakes name, station, and record parameters.

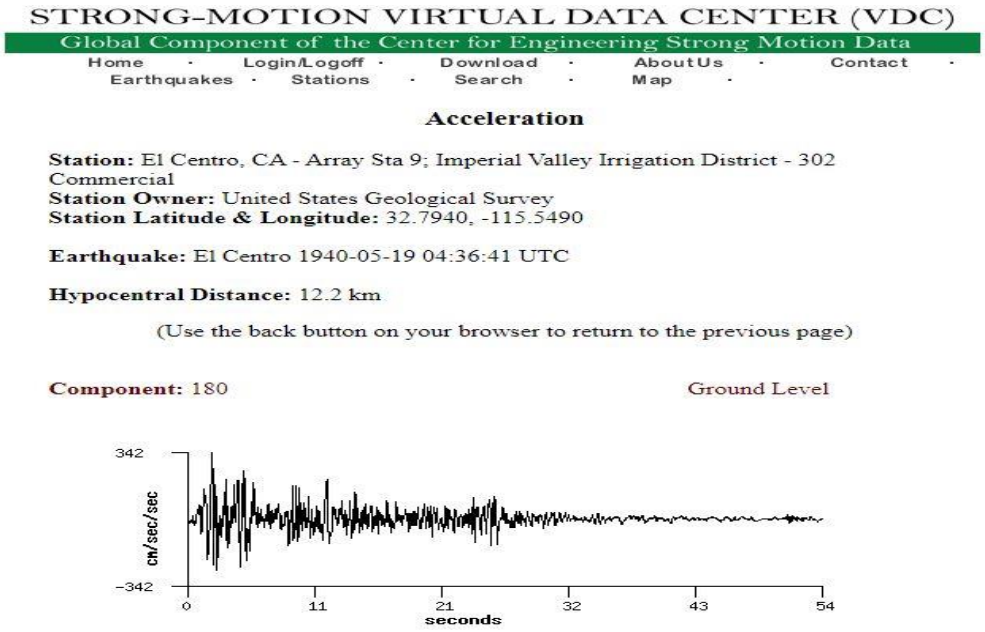

Figure 2.2 Search results from CESMD database

2.1.3 Strong-Motion Seismograph Networks K-NET and KiK-net

K-NET (Kyoshin network) and KiK-net (Kiban Kyoshin network) are two Japanese strong-motion seismograph databases, consisting of more than 1700 observation stations that uniformly cover the entire country. K-NET and KiK-net are operated by the NIED (National Research Institute for Earth Science and Disaster Resilience).

The strong-motion data recorded by both networks are immediately transmitted to the NIED and the data is widely available to the public through the internet from this website: http://www.kyoshin.bosai.go.jp [25].

In the K-NET and KiK-net database, the earthquake records are searchable based on several parameters (Figure 2.3).

Figure 2.3 Search options from K-NET and KiK-net database

There are many other web-based earthquake databases, but the above provides a reasonable representation of the data freely available for download.

If the earthquake records are presented in their raw format, then are required baseline correction and filtering.

2.2. Digitization of earthquake signals stored as images

The retrieval of information from historical analogical records is essential for the study of the seismic activity and of the seismic danger in the vulnerable areas during the earthquake. This is possible due to modern techniques and methods of processing and converting analog data into digital data.

Below is presented a method of the digitization of earthquake signals stored as images. For this method, the software WebPlotDigitizer has been used to extract the signals and the numerical values from an image.

WebPlotDigitizer is an open source software and can be used directly from the website https://automeris.io/WebPlotDigitizer/. The software WebPlotDigitizer runs within most popular web browsers and does not require to be installed by the user [28].

WebPlotDigitizer is a semi-automated tool that makes easy and accurate data extraction:

- works with many types of charts (XY, bar, polar, maps, etc.);
- makes easier to extract many data points with automatic extraction algorithms;

- useful for measuring distances and angles between diverse features;
- permits manual adjusting and other intervention of the user;
- open source software and free to use.

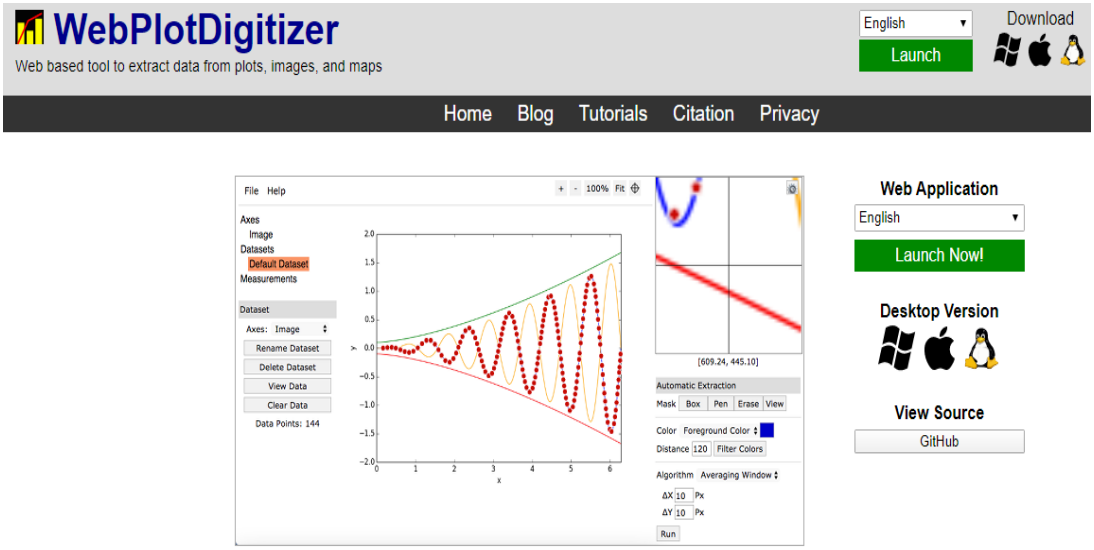

Figure 2.4 WebPlotDigitizer software interface

Depending on the browser used, the image format supported is JPEG, PNG, GIF, and BMP, but not PDF files.

After the application is launched, the image file can be uploaded into the software like this: File Menu → Load Image, Drag & Drop Operation and Copy-Paste from Clipboard (Figure 2.5).

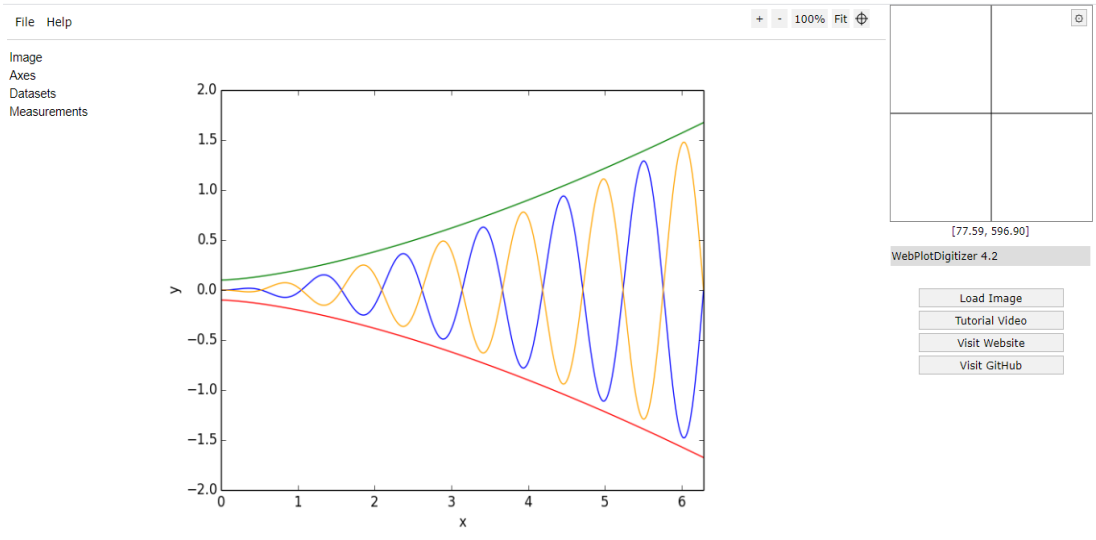

Figure 2.5 Loading images

In the flowchart displayed in Figure 2.6 is explained the procedure followed to extract the signals from an image.

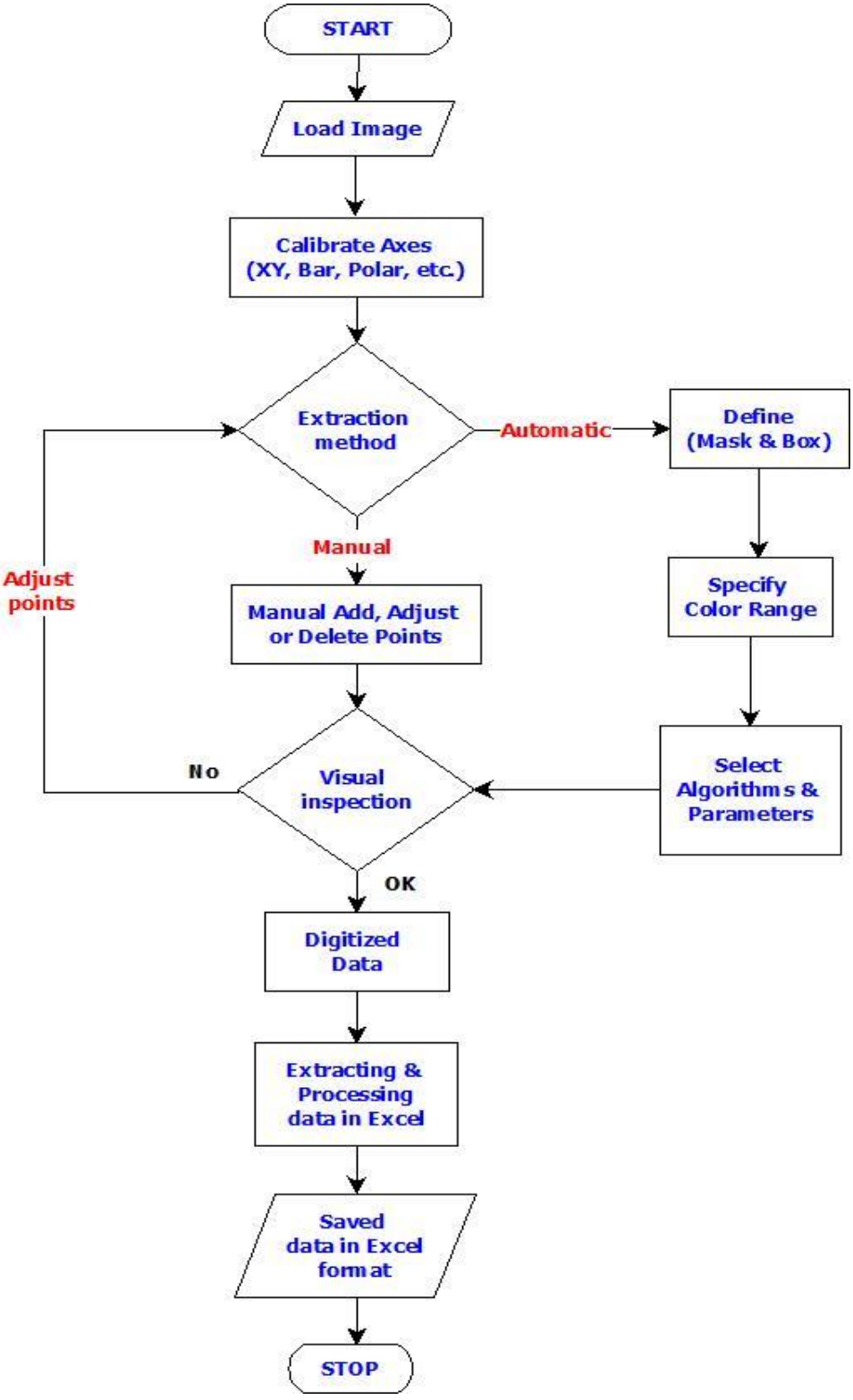

Figure 2.6 Flowchart for the extraction of the signals with WebPlotDigitizer

To exemplify the process of digitization, a registration in form of .jpg image taken from PEER Ground Motion Database [23] is used. The .jpg file is saved on the computer and uploaded in the WebPlotDigitizer software.

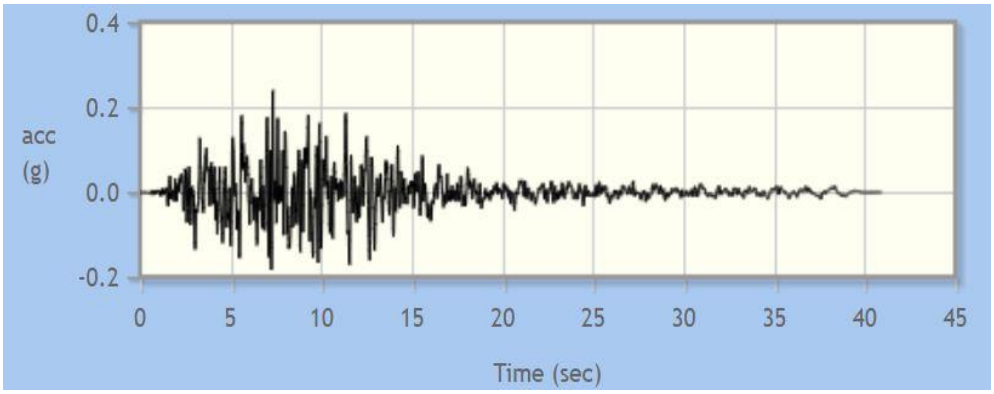

Figure 2.7 Kobe Earthquake, 1995, Japan (https://ngawest2.berkeley.edu)

After loading the image as shown in Figure 2.7, it must be specified the type of axis; for this analysis has been used 2D X-Y Plot presented in the Figure 2.8. The software required this to map the image pixels.

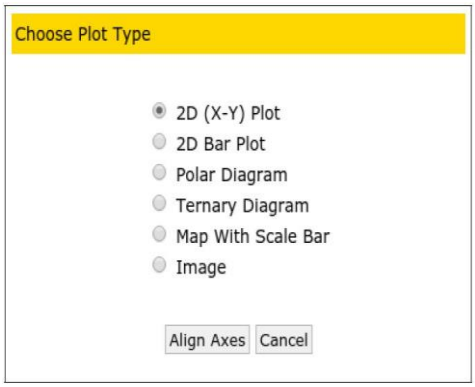

Figure 2.8 Type of axis

Figure 2.9 Data acquisition controls

Once the axis XY of the signal has been calibrated, the automatic extraction method was chosen and was set up the controls for data acquisition as shown in Figure 2.9. Automatic data extraction is based on separating the color of the data points or curves from the background in the image. The controls from the Mask tab are used to mark the region for the extraction algorithms, from this tab, has been used the Box tool to mark the searching region like it is presented in the Figure 2.10.

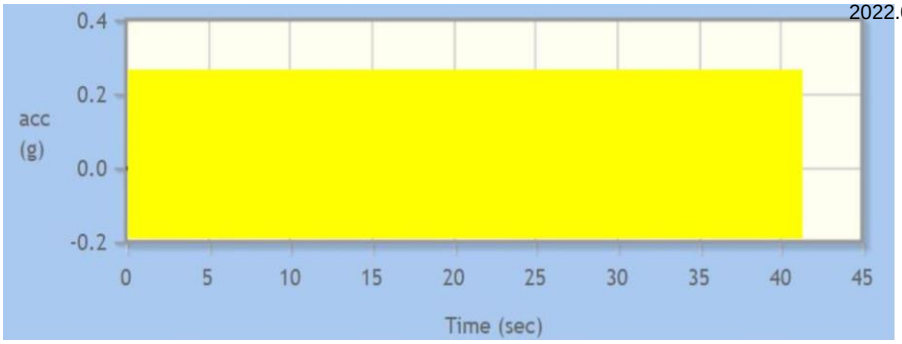

Figure 2.10 Rectangular region used for the extraction data points

After the region was marked for the extraction data points, the color controls was used to specify the color of the data points. From the drop-down menu of the Color tab the Background Color was chosen white, the color selection was made and the specified distance value from the Filter Colors tab was extracted as shown in Figure 2.11.

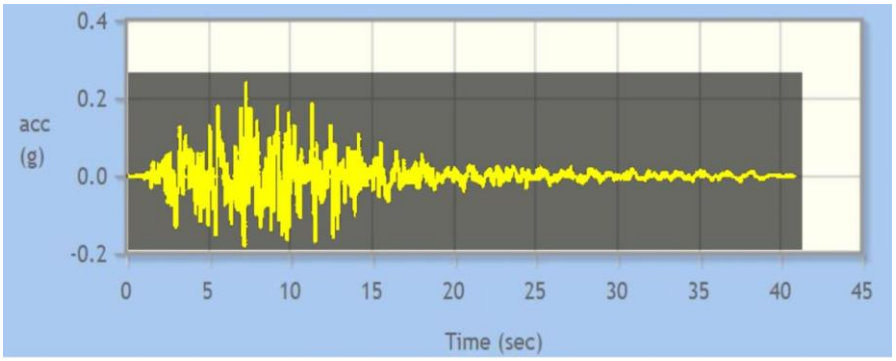

Figure 2.11 The region used by the automatic extraction algorithms

Once all the settings were done, the auto-detection algorithm was started from the Run button. Figure 2.12 presents the points extracted in WebPlotDigitizer software after the auto-detection is completed.

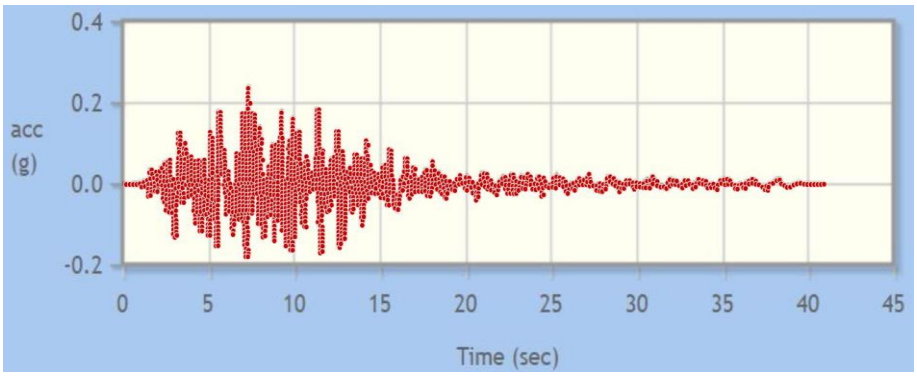

Figure 2.12 Points extracted in WebPlotDigitizer

In the Figure 2.13 is presented the acquired data and can be viewed from the View Data tab and exported to a .CSV file. After the data has been obtained, the numerical values were downloaded as .CSV file and were processed in an Excel file.

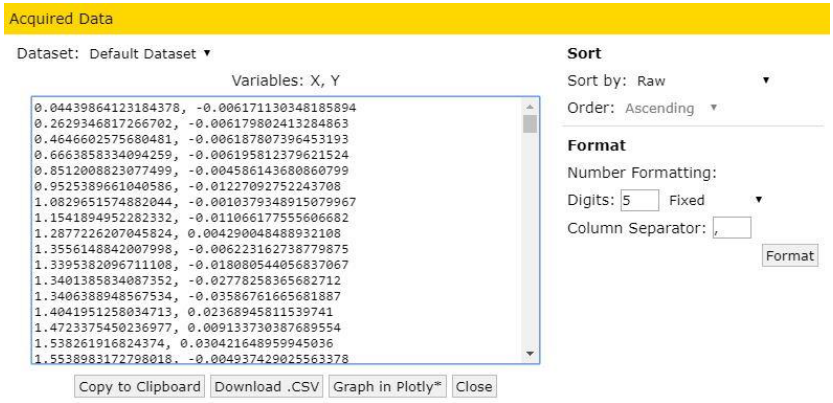

Figure 2.13 Acquired data

1648 points from the signal processing were obtained from the initial picture and were used to digitize the signal in Excel as shown in Figure 2.14.

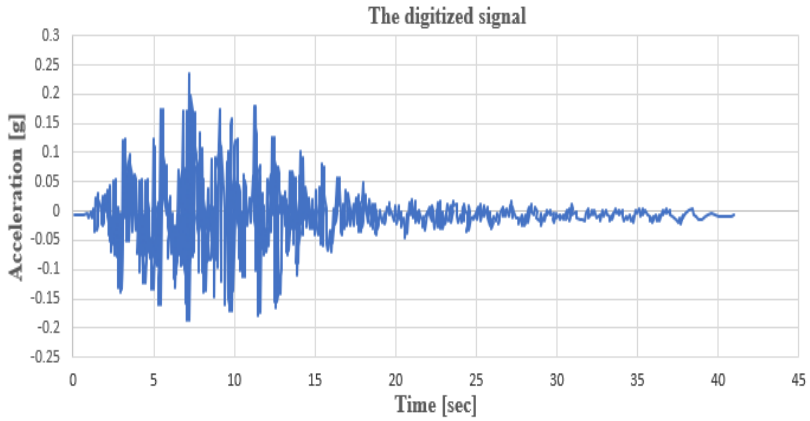

Figure 2.14 The digitized signal in Excel

Above it was presented a rapid and accurate method to extract the signals and the numerical values from an image with the help of the WebPlotDigitizer software. Once the digital signal is aquired, the Fast Fourier Transform (FFT) can be applied to convert the signal from the time domain to the frequency domain. The FFT can be used to simply characterize the magnitude and phase of a signal and the main advantage of this type of analysis is that little information is lost from the signal during the transformation. In Figure 2.15 is presented the digitized signal converted from time domain to frequency domain with FFT.

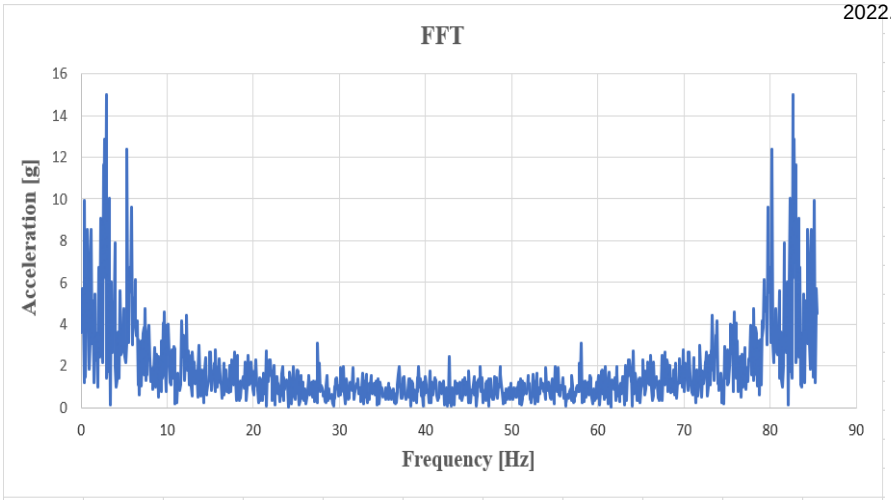

Figure 2.15 FFT of the digitized signal

A sample of digital signal (t=5s) was analyzed like is shown in Figure 2.16, and the FFT was applied to this sample of signal (Figure 2.17).

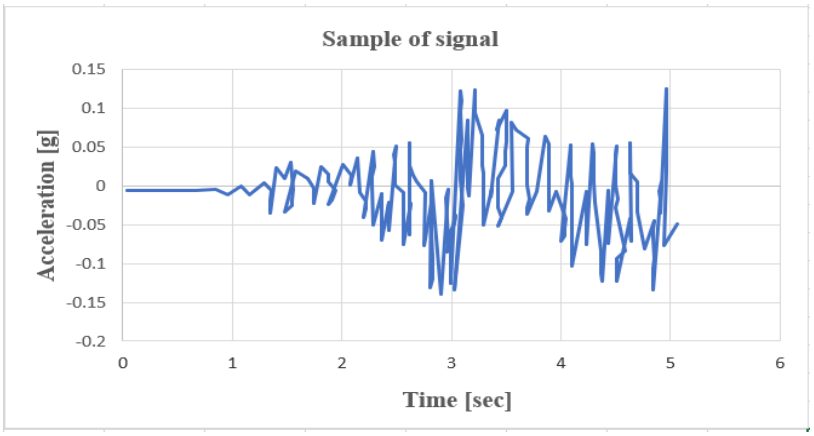

Figure 2.16 Sample of signal (*t*=5s)

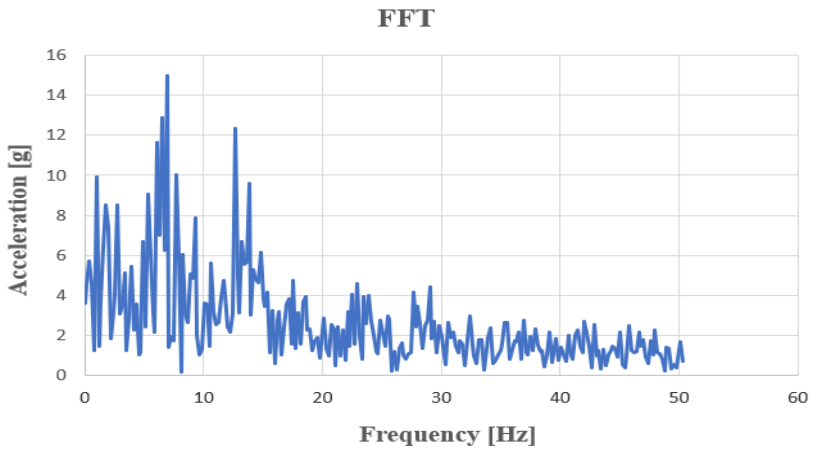

Figure 2.17 FFT of the signal sample

The frequency-domain representation of a signal allows the observation of some characteristics of the signal, for example, the cyclic behavior of a signal which would otherwise be difficult to observe in the time domain.

2.3. Development of a Python application to generate digital signals

The typical sensor for measuring the dynamic response of structures is the accelerometer. It generates a digital signal that is represented by a sequence of discrete values [29]-[31]. When interpreting earthquake response signals measured with accelerometers, estimation of velocities and displacements is often required [32].

To study the behavior of structures during earthquakes, digital signals are needed to present different earthquake movements. A list of databases that can be accessed on the Web that contain earthquake accelerograms in digital form are detailed in [33]. Due to modern techniques and methods of processing and converting analog data into digital data, the original recordings from bulletins and seismograms can be digitized and re-analyzed [34].

2.3.1 Application description

For our research, digital signals were needed with known parameters, to calculate the velocity and displacement from accelerograms and to use them as input for dynamic simulations, made for base-isolated structures.

Hence, an application developed in the Python programming language was created for generating digital signals with known parameters (frequency, amplitude, phase, damping coefficient, existence of noise) and exemplifying outcomes for different settings of the parameters.

In the proposed application the signals were generated with up to three harmonic components S_i (i=1…3), which have the amplitudes a, b and c, the frequencies f_i and the phase Ph_i. Thus, the harmonic components of the signal can be written as follows:

- the first sinusoidal component is:

$$S_1 = a \cdot sin(2 \cdot \pi \cdot f_1 \cdot t + \pi \cdot Ph_1) \quad (2.1)$$

- the second sinusoidal component is:

$$S_2 = b \cdot sin(2 \cdot \pi \cdot f_2 \cdot t + \pi \cdot Ph_2) \quad (2.2)$$

- the third sinusoidal component is:

$$S_3 = c \cdot sin(2 \cdot \pi \cdot f_3 \cdot t + \pi \cdot Ph_3) \quad (2.3)$$

Both noise *W* and damping *D* can be added also to the signal. The damping is generated by involving the term:

$$D = e^{Damp \cdot t} \tag{2.4}$$

where *Damp* is the damping coefficient. Note that, the damping coefficient can get associated positive values in the case of increasing the amplitude of the signal, or negative values in the case the intend is to decrease the amplitudes.

In relations (2.1) to (2.4), *t* represents the time, i.e., the length of the signal.

The effect of noise can be expressed as:

$$W = p(x) \cdot Noise/max[\mathrm{p(x)}] \tag{2.5}$$

where *p(x)* is the probability density for the Gaussian distribution and *Noise* is a randomly generated value for each discrete time moment.

Finally, the most complex form of the signal is:

$$S = D \cdot (S_1 + S_2 + S_3 + W) \tag{2.6}$$

The signal is used to test application that derivate or integrate signals, for which the signal parameters should be known.

The *SignalGeneration* application was developed based on the Python programming language and is defined by four classes: "SignalGeneration", "Table_Grid", "Plot" and "Plot-Notebook" and four public functions: "ExtragTextMemory", "ExtragImageMemory", "IsNu-meric" and "Put_Clipboard". The main window represents a notebook control, which manage one chart window with the named tab: "Signal Generated". The "Plot" and "PlotNotebook" classes create the main window where the notebook with the chart windows will be created.

The public function "ExtragTextMemory" extract the Excel template from database to be saved as Excel file into "RESULTS" folder created by application. The template contains chart that will be updated at the end of the transfer. The public function "ExtragImageMemory", extracts the icons from database to memory to be used as icons when creating the toolbar.

The public function "Put_Clipboard" copies a string into Windows Clipboard and is called by "OnExcel" function from "SignalGeneration" class. When the results are exported to Excel file, these are memorized in strings copied to Windows Clipboard and pasted into Excel. The reason of this operation is a significative short time required for transfer comparing with export values cell by cell. The "Table_Grid" show the numerical results on screen into a grid control.

The application uses a SQLite database to memorize the toolbar icons as image format and the "Excel template.xls" file, where the numerical and charts results will be exported. These files were loaded as Binaly Large Objects (BLOB) in "Config.db" application's file. Features of the toolbar are shown in Figures 2.18 and 2.19.

Figure 2.18 The toolbar of the *SignalGeneration* application – input data

Figure 2.19 The toolbar of the *SignalGeneration* application – processing buttons

The *SignalGeneration* application use the dependencies presented in Table 2.1.

Table 2.1 Dependencies used by the *SignalGeneration* program

Python(x, y)	A free scientific and engineering development software for numerical computations, data analysis and data visualization based on Python programming language.	https://python-xy.github.io/
Matplotlib	A Python 2D plotting library which produces publication quality charts.	https://matplotlib.org/
wxPython	The cross-platform Graphical User Interface toolkit for the Python language.	https://wxpython.org/
SQLite	A C-language library that implements a small, fast, self-contained, high-reliability, full-featured, SQL database engine.	https://www.sqlite.org/index.html
numpy	The fundamental package for scientific computing with Python.	https://numpy.org/

The application's toolbar is located at the top-left of the main window and includes text and button controls marked, with the functions described in Table 2.2.

Table 2.2 Functions of the *SignalGeneration* toolbar

	**Open** – Load signal form CSV saved previous file.
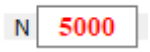	Text control to input ‘Number of samples’ **N** variable.
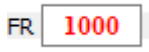	Text control to input ‘Sampling frequency’ **FR** variable.
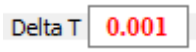	Text control to show ‘Time interval’ **Delta T** variable (Read Only – computed by application).
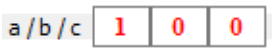	Text controls to input ‘First/Second/ Third Amplitude’ values of the **A1/ A2/A3** variables.
	Text controls to input ‘First/Second/Third Target Frequency’ values of the **f1/f2/f3** variables.
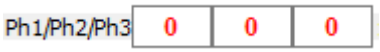	Text controls to input ‘First/Second/ Third Phase’ coefficients of the **Ph1/ Ph2/Ph3** variables.
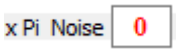	Text control to input ‘White Noise’ **Noise** variable.
	Text control to input ‘Damping coefficient’ **Damp** variable.
	**Generate** – Calculate the signal based on equation (2.6) and create the chart of the signal.
	**Data table** – Shows the table of the signal values, calling "Table_Grid " class.
	**Word** – Save application’s graphical results to Word file.
	**Excel** – Save application’s results (graphical and numerical) to Excel file.
	**Fit Chart** – Returns to initial view in the chart windows.
	**Zoom** - Enlarges selected area in chart windows.
	**Pan** - zoom in/out with the right mouse button pressed.
	**Exit** – Quit the application, calling "OnClose" function from "SignalGeneration" class.

2.3.2 Exemples of signals generated with the application

The signals, which represent measured accelerations in *mm/s*^{2} are generated with a number of samples *N*=6000 by a sampling frequency *FR*=1000 Hz.

In Table 2.3 are presented different settings of the parameters used to generate signals with the *SignalGeneration* application.

Table 2.3 Parameter settings for the generated signals

Curve	a	b	c	f_1	f_2	f_3	Ph_1	Ph_2	Ph_3	Damp	Noise	Figure
1	1	0	0	1	0	0	0	0	0	0	0	2.20
2	1	0	0	1	0	0	1	0	0	0	0.5	2.21
3	1	0	0	1	0	0	1	0	0	0.5	0	2.22
4	1	1	0	1	15	0	0	0	0	-0.5	0.5	2.23
5	1	1	1	1	5	10	0	0	0	0	0	2.24
6	1	1	1	1	5	10	0	0	0	-0.5	0	2.25
7	1	1	1	1	5	10	1	1	1	-0.5	0.5	2.26

In Figures 2.20 to 2.26, the generated signals with the parameter settings from Table 2.3 are shown. The different signals are represented in these figures with different colors (*green* – damping, *gray* – noise, *cyan* – signal with one to three components in the absence of damping and noise) and with *red* is represented the resulted signal. These digital signals, since have known parameters, can be used to create benchmarks for test and numerical simulation.

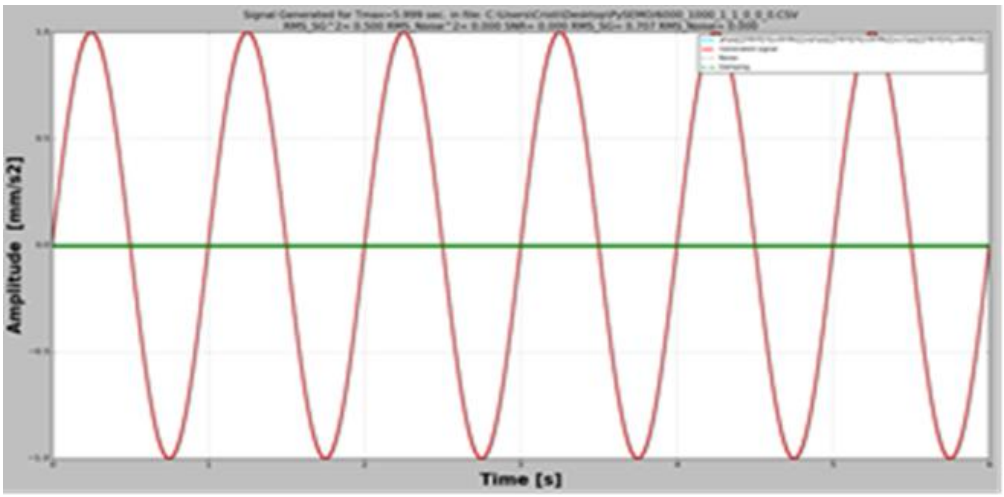

Figure 2.20 Generated Curve 1 - the signal with one harmonic component

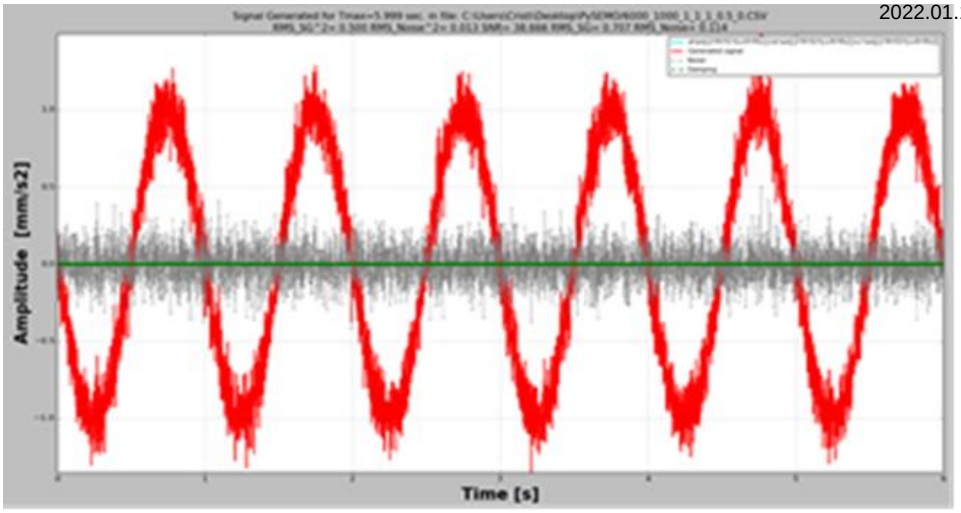

Figure 2.21 Generated Curve 2 - the signal with one harmonic component polluted with noise

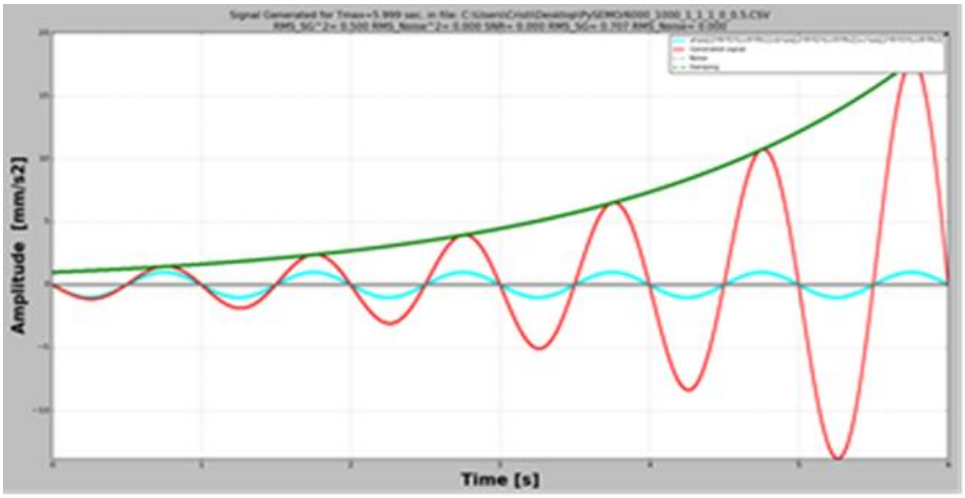

Figure 2.22 Generated Curve 3 - the signal with progressively increasing amplitude

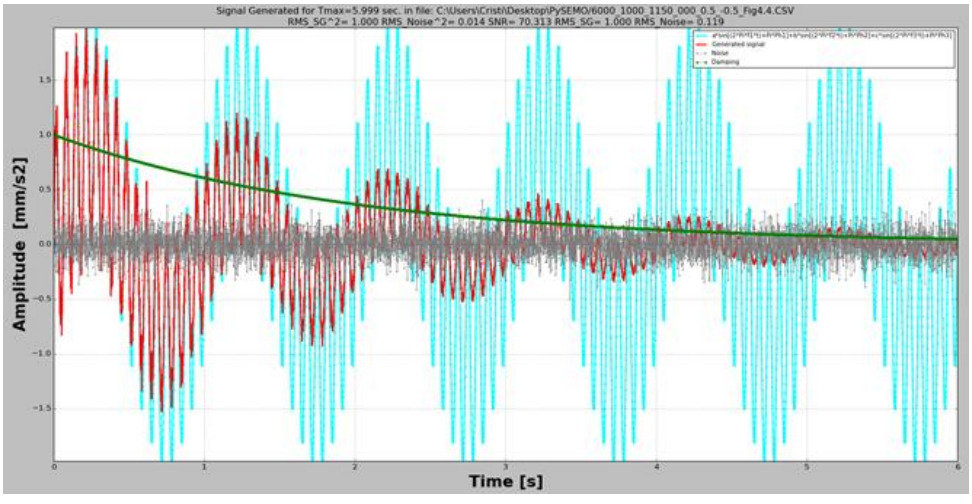

Figure 2.23 Generated Curve 4 - damped signal with two components

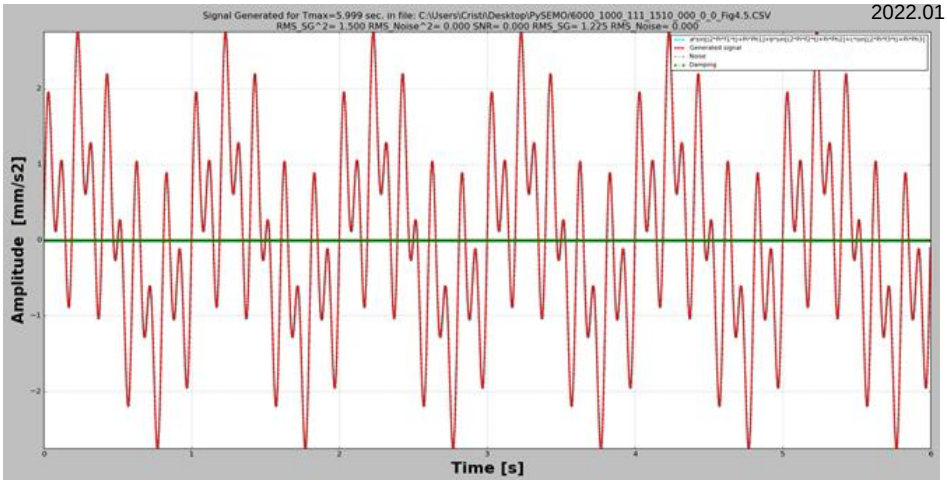

Figure 2.24 Generated Curve 5 - signal with three components

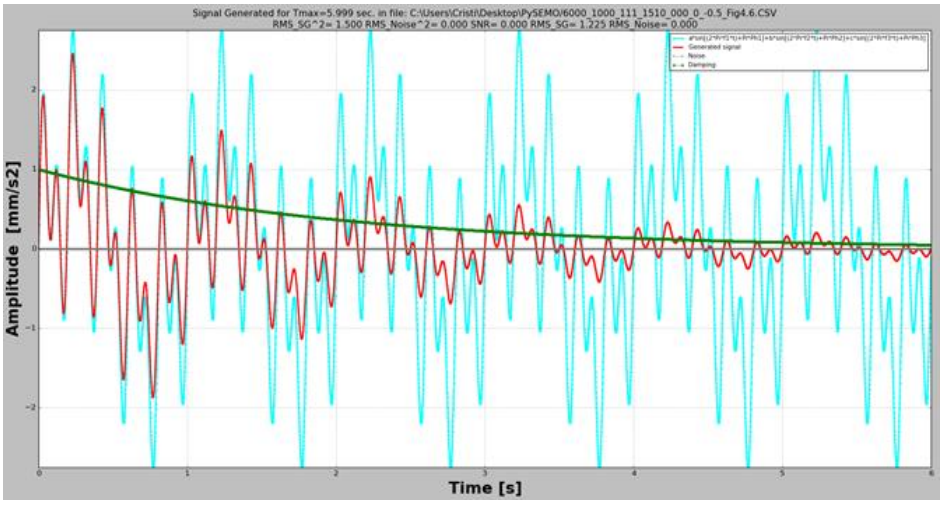

Figure 2.25 Generated Curve 6 - damped signal with three components

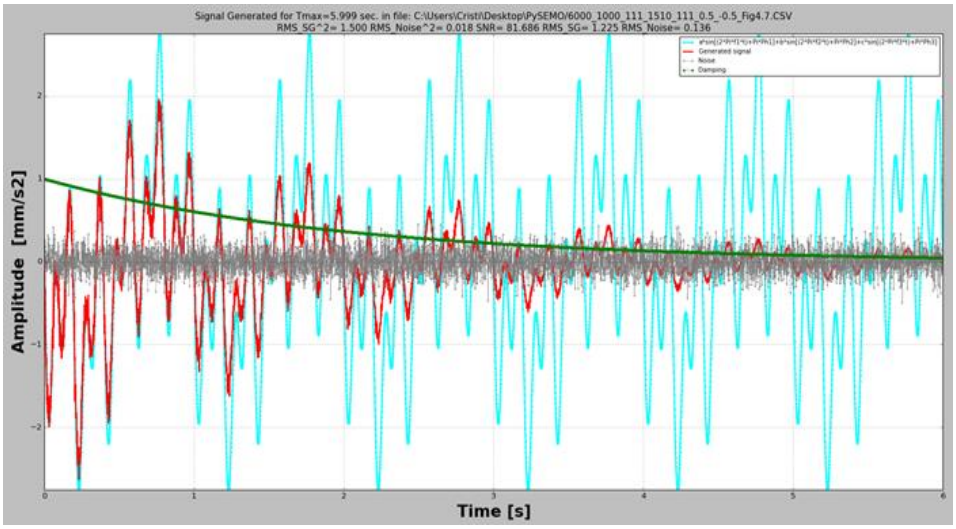

Figure 2.26 Generated Curve 7 - damped signal with three components polluted with noise

2.4. Algorithm development to estimate the velocity and displacement of the earthquake signals with known acceleration

When interpreting technical standards and norms, estimation of velocities and displacements is often required [35]. The velocity is the antiderivative of the acceleration, while the displacement is the antiderivative of the velocity [36]. Numerical methods allow finding the antiderivative (or primitive integral) as a discrete function by integration. This implies calculating integrals for the original function for all intervals limited by two consecutive samples.

The most difficult problem in calculating the antiderivative is finding the initial value, which implies finding the integration constant [37]. As far as is known, there is no method to calculate the antiderivative as a discrete function from an original discrete function. Herein is presented a numerical method to calculate the antiderivative of alternating signals which integral has an insignificant value. The vibration of rotating machinery [38-40] and the response of structures to impulsive excitation [41] are indicated as examples.

An algorithm to find the velocity and afterwards the displacement was developed by repetitively calculating the antiderivative of accelerograms. Two aspects are of importance in this calculus: finding the initial value and extraction of the zero-frequency component from the first antiderivative (i.e. the velocity).

The exemplification of how the development of the algorithm to repetitively calculate antiderivatives for a digital signal is made for a sinusoid. Afterward, the algorithm works for signals with more harmonic components as well.

It was considered the *i*-th harmonic component a^i of an acceleration signal a, expressed as:

$$a^i = \bar{a}^i \, sin\left(2\pi f^i t + \varphi^i\right) \tag{2.7}$$

where: $\bar{a}_i$ is the amplitude; f_i is the frequency, t is the time and φ_i is the initial phase. For the digital signal, the *k*-th sample is displayed at time:

$$t_k = (k-1)\Delta t \tag{2.8}$$

Hence, the signal with more components can be expressed:

$$a = a^1 + \ldots + a^i + \ldots \tag{2.9}$$

For the acceleration represented as a simple harmonic signal (for simplicity the index i was not used here), the velocity is:

$$v_{q+1} = v_q + \frac{a_k + a_{k+1}}{2} \Delta t \tag{2.10}$$

where

$$t_q = t_k + \frac{\Delta t}{2} \tag{2.11}$$

The problem is finding the initial value of the velocity v_0, in fact the constant of integration. It was achieved by calculating the average of the velocity signal that starts from the origin, i.e. the initial value equals zero. Or, in other words, it was subtracted the zero-frequency component from the signal resulted by integration involving Eq. (2.10) for the case $v_0 = 0$. The process is illustrated in Figure 2.27, which shows the velocity signal obtained for the initial condition $v_0 = 0$ and after subtracting the average.

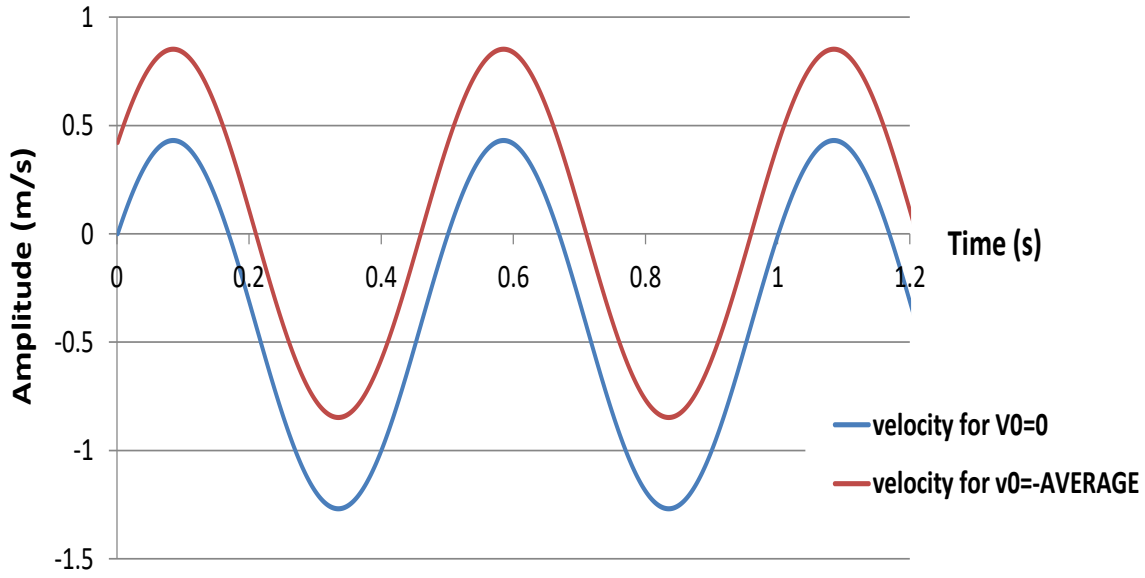

Figure 2.27 The velocity for the initial condition set to zero and after subtracting the average

In a similar way, by performing again the calculus of the antiderivative, the displacement was calculated with the mathematical relation:

$$d_{m+1} = d_m + \frac{v_q + a_{q+1}}{2} \Delta t \tag{2.12}$$

where

$$t_m = t_q + \frac{\Delta t}{2} \tag{2.13}$$

Because the velocity curve does usually not contain an integer number of cycles, the average can differ smoothly from the real zero-frequency component, thus slight increase or decrease of the next antiderivative is expected.

To find the real displacement, the trendline of the displacement curve was extracted. This has as result the subtraction of the average along with the rotation to get the curve to ensure it a horizontal axis. Observe that the trendline for the displacement calculated for $d_0 = 0$, which has the equation indicated in the Figure 2.28, is not perfectly parallel with the abscissa and is translated in the positive direction of the ordinate.

Dissimilar, the trendline after correction (subtraction of the previously calculated trendline) fit the abscissa, which means the displacement is now correctly calculated and displayed.

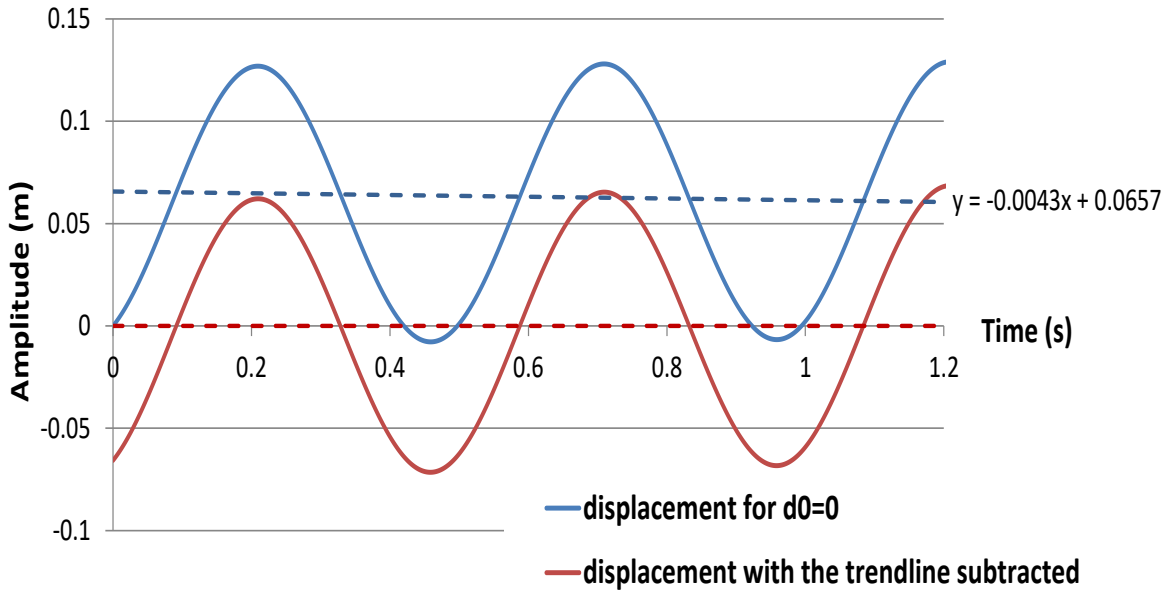

Figure 2.28 The displacement for the initial condition set to zero and after subtracting the trendline

The algorithm on which the application is based is comprehensively described in Figure 2.29.

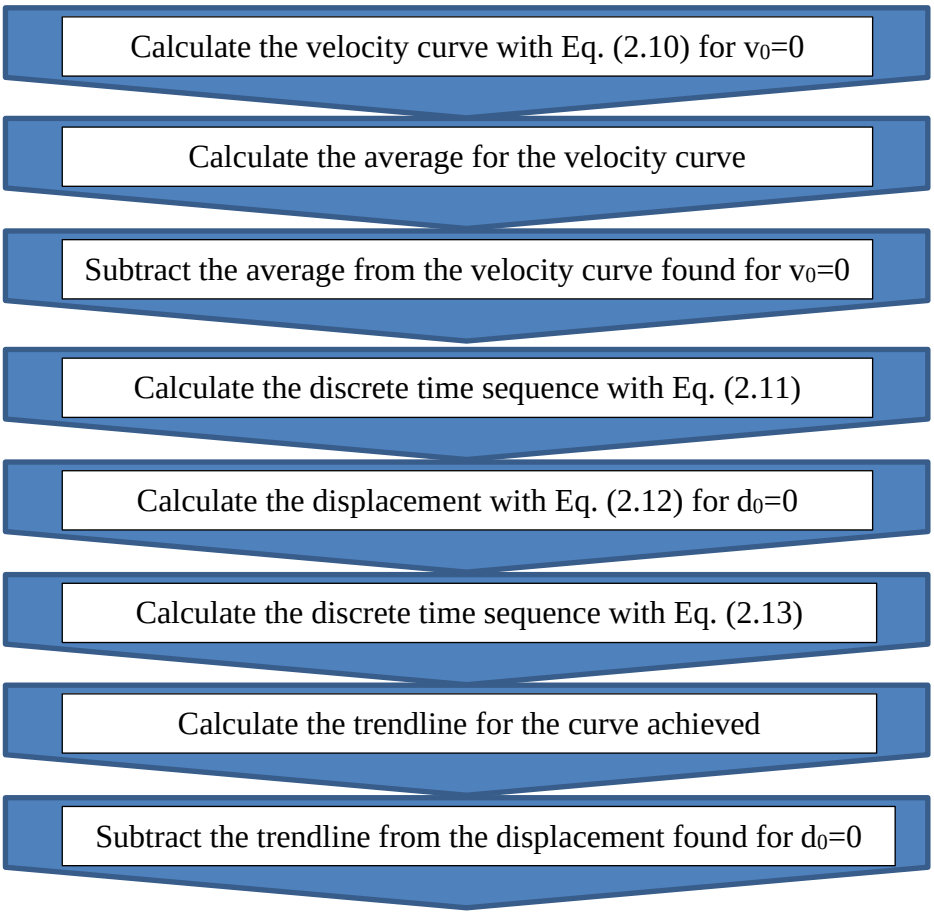

Figure 2.29 The algorithm to find the velocity and displacement curves from the accelerograms

2.5. Python Seismic Motion (PySEMO) application

2.5.1 Implementation of the algorithm in a Python application

The algorithm presented in Chapter 2.4 was implemented in a Python application named PySEMO (Python Seismic Motion), in order to perform fast simulation and prove it works well for signals with one or more components and in the absence or presence of damping. The interface of PySEMO application is presented in Figure 2.30.

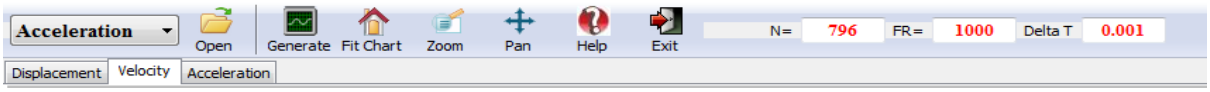

Figure 2.30 The interface of the PySEMO application to control the input data

It permits importing a digital real-world signal acquired with an acquisition system or generating one (especially for demonstration or didactic reasons). It is possible to mention the type of the signal, acceleration, velocity or displacement as shown in Figure 2.31, and the application generate the other two signals by calculating the antiderivative based on the proposed algorithm. It is possible to display any signal and to save these as images or export the results as Excel files.

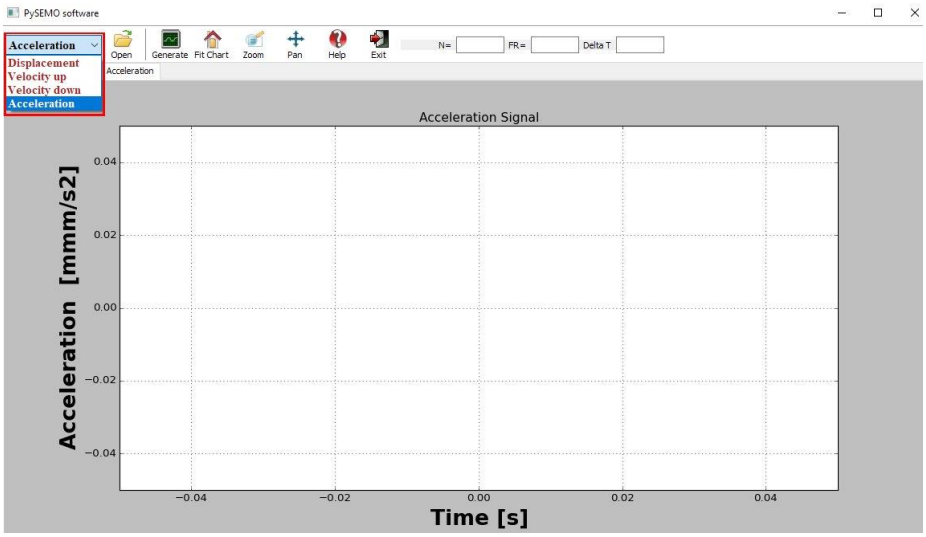

Figure 2.31 Calculation options

With *Open*  button it is possible to import a signal (acceleration, velocity or displacement) from an Excel file, like it is presented in Figure 2.32.

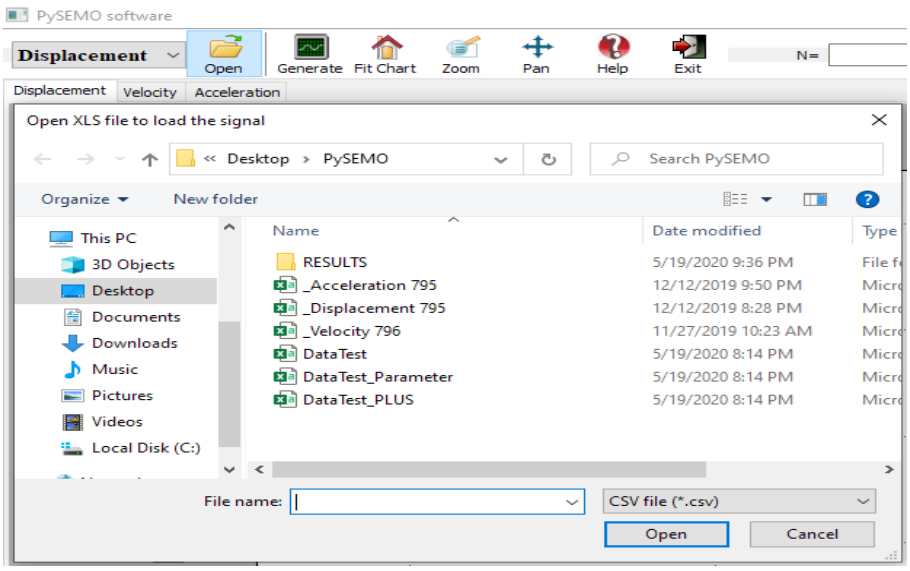

Figure 2.32 Import a signal from an Excel file

From *Generate*  button the application generate a signal; once the signal generation command has been launched, a new window opens like it is presented in Figure 2.33.

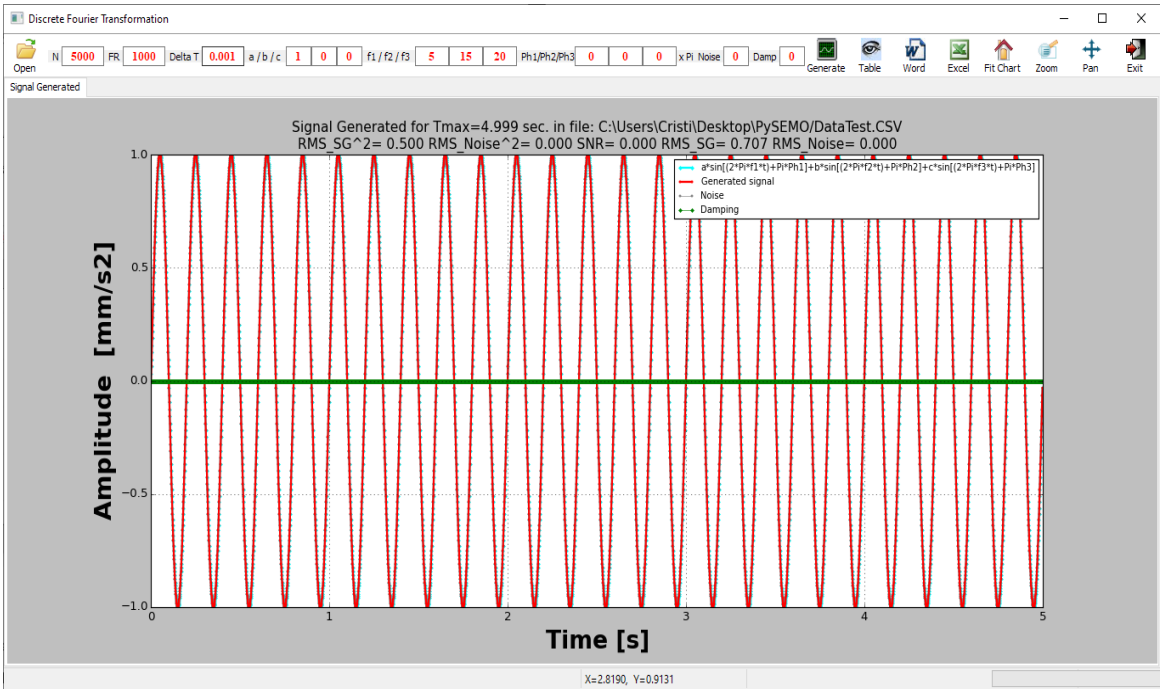

Figure 2.33 Signal generation window

After all the parameters required for signal generation are set, like presented in Chapter 2.3, it is necessary to push the *Generate* button in order to generate the signal. Figure 2.34 wait to input the name of the Excel file where the signal will be saved.

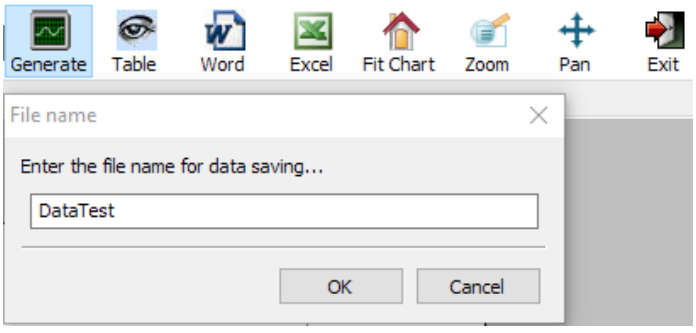

Figure 2.34 File name for signal generated

Help button  of PySEMO application shows the algorithm behind the application with all the steps followed for the calculation steps of the signal.

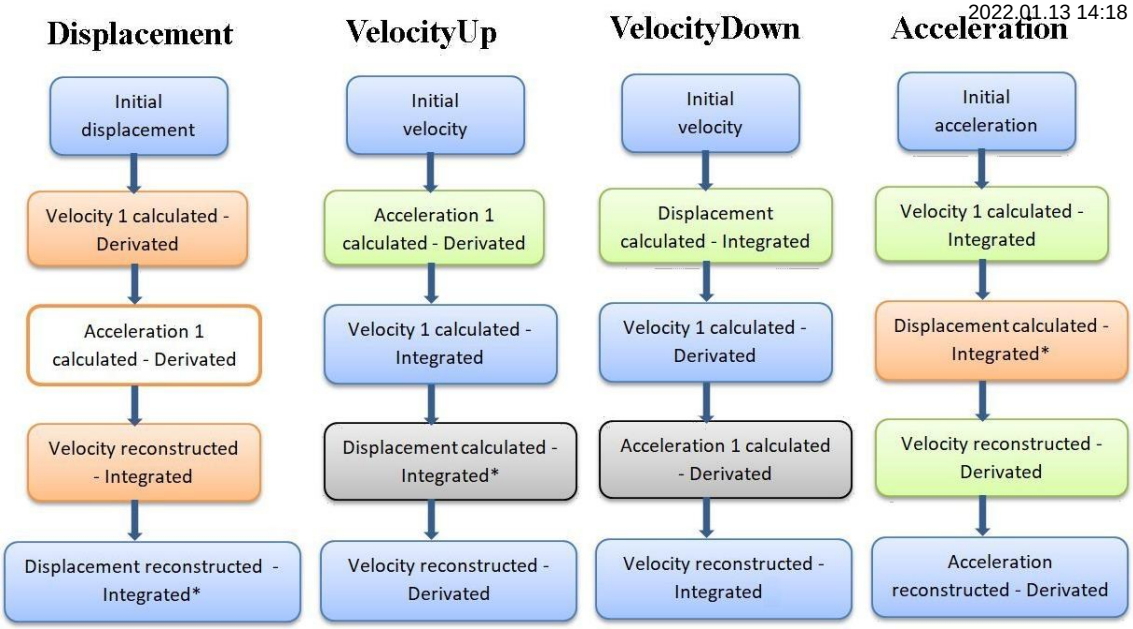

Figure 2.35 Help menu of PySEMO application

To demostrate the accuracy of the proposed method an aplication was developed to calculate the velocities and displacements from accelerograms. However, the application can be used for any signal alternating around zero, for instance those measured on rotating machines. In addition to performing two integrations, PySEMO is able to calculate the derivatives. Thus, the velocities and displacements can be introduced to calculate the other two curves. After calculating the velocity and the displacement the acceleration was reconstruct and compared with the original signal.

2.5.2 Examples processed in PySEMO application

For comparison and understanding the necessary conditions for an accurate calculus, simulations with the PySEMO application were made for 3 sets of signals. The signals, which represent measured accelerations, are generated with a sampling **frequency FR=1000 Hz** and all signals or components have the **amplitude a=1**.

The first set consists in a **short signal** (**t=1.5 s**) and a **long signal** (**t=5.5 s**), both having the **frequency f=1 Hz**. It was desired to find out how the signal length affects the accuracy of the calculated curves.

From the accelerations, velocities and displacement represented in the Figure 2.36 can be deduced that the achieved results are accurate for the long signal, while for the short signal the velocities (calculated as an antiderivative and reconstructed) are not perfectly overlapped.

The reason is that the displacement curve, even after rotation, has not the trendline aligned with the abscissa. Note that the short signal has an initial phase and the method still works.

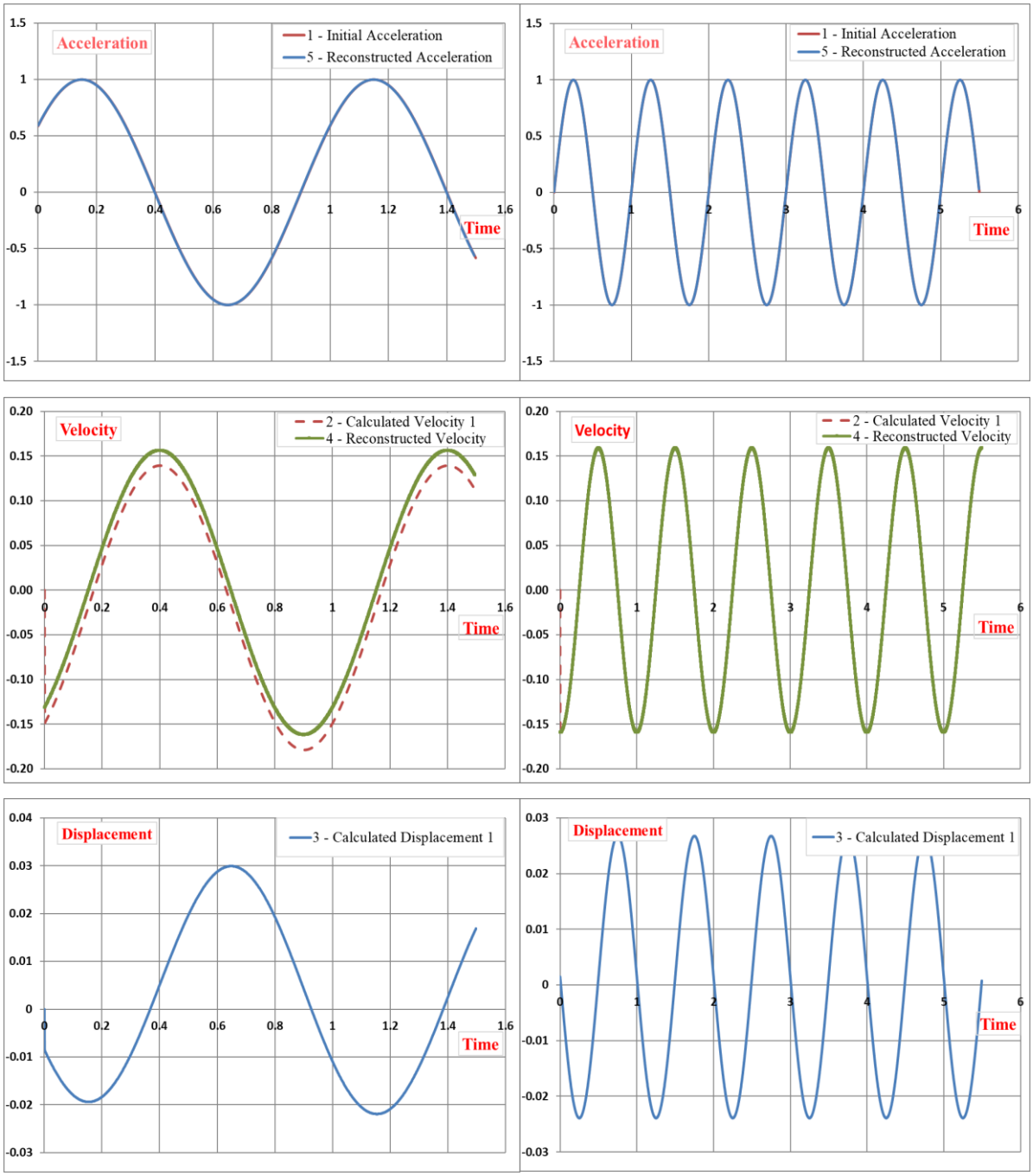

a. b.

Figure 2.36 Diagrams for the generated acceleration having the frequency f=1 Hz and the calculated velocities and displacement (a) short signal with t=1.5 s;
(b) long signal with t=5.5 s.

The second set of signals consist in a short signal with the frequency **f=5 Hz**, **undamped** and **damped** with the **damping ratio 0.5** respectively. Figure 2.37 represents the acceleration signal and its antiderivatives; in addition, the reconstructed velocities and accelerations are represented for a comparison.

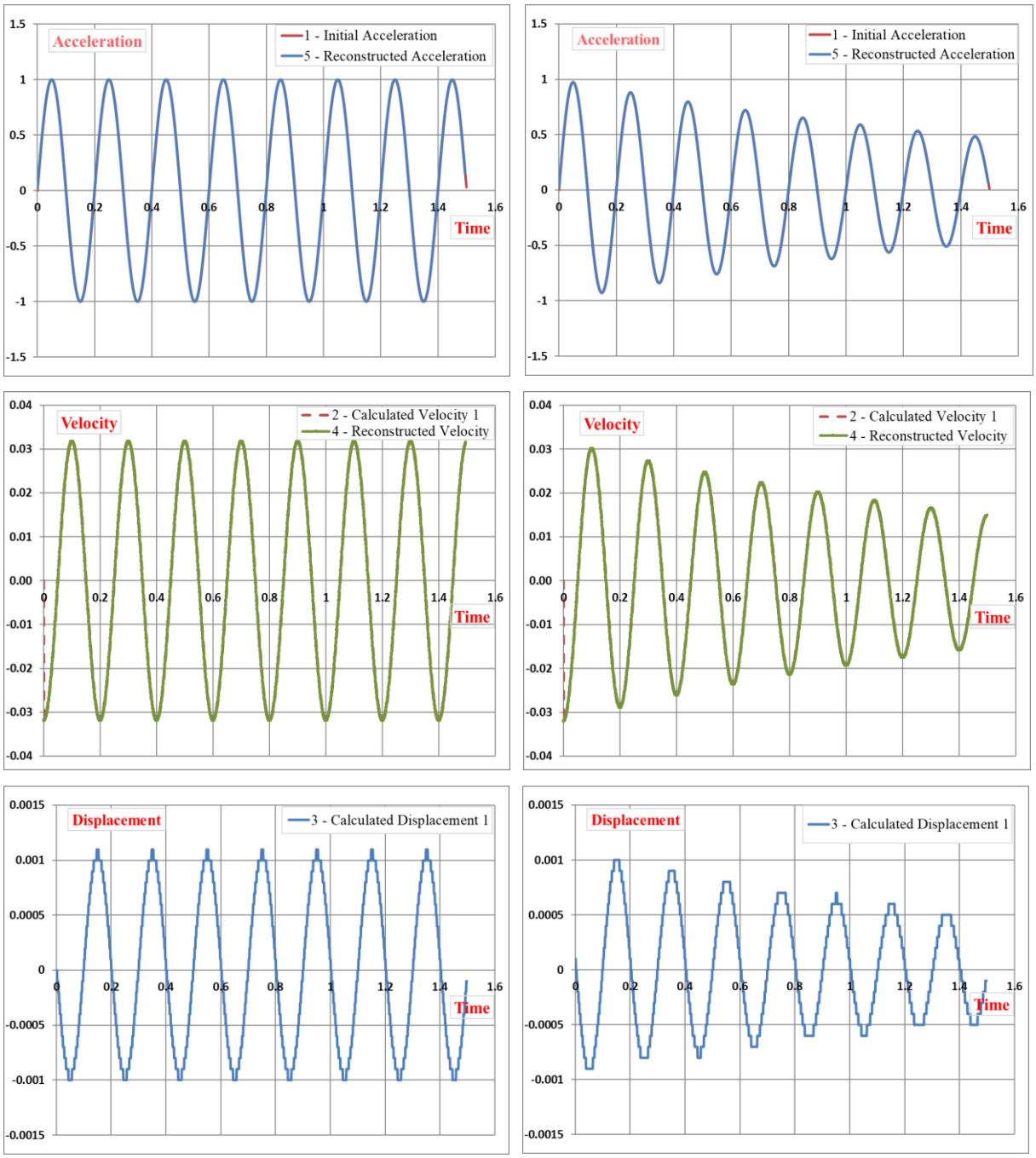

a. b.

Figure 2.37 Diagrams for the generated accelerations and calculated velocities and displacements(a) undamped signal; (b) damped signal.

One can observe the quality of the calculated velocities both for the undamped as well as for the damped signal. The curves representing the displacements are not smooth, so it was concluded that the sampling rate should be increased to achieve better results. Next approach is to demonstrate the algorithm works for a signal with more harmonic components.

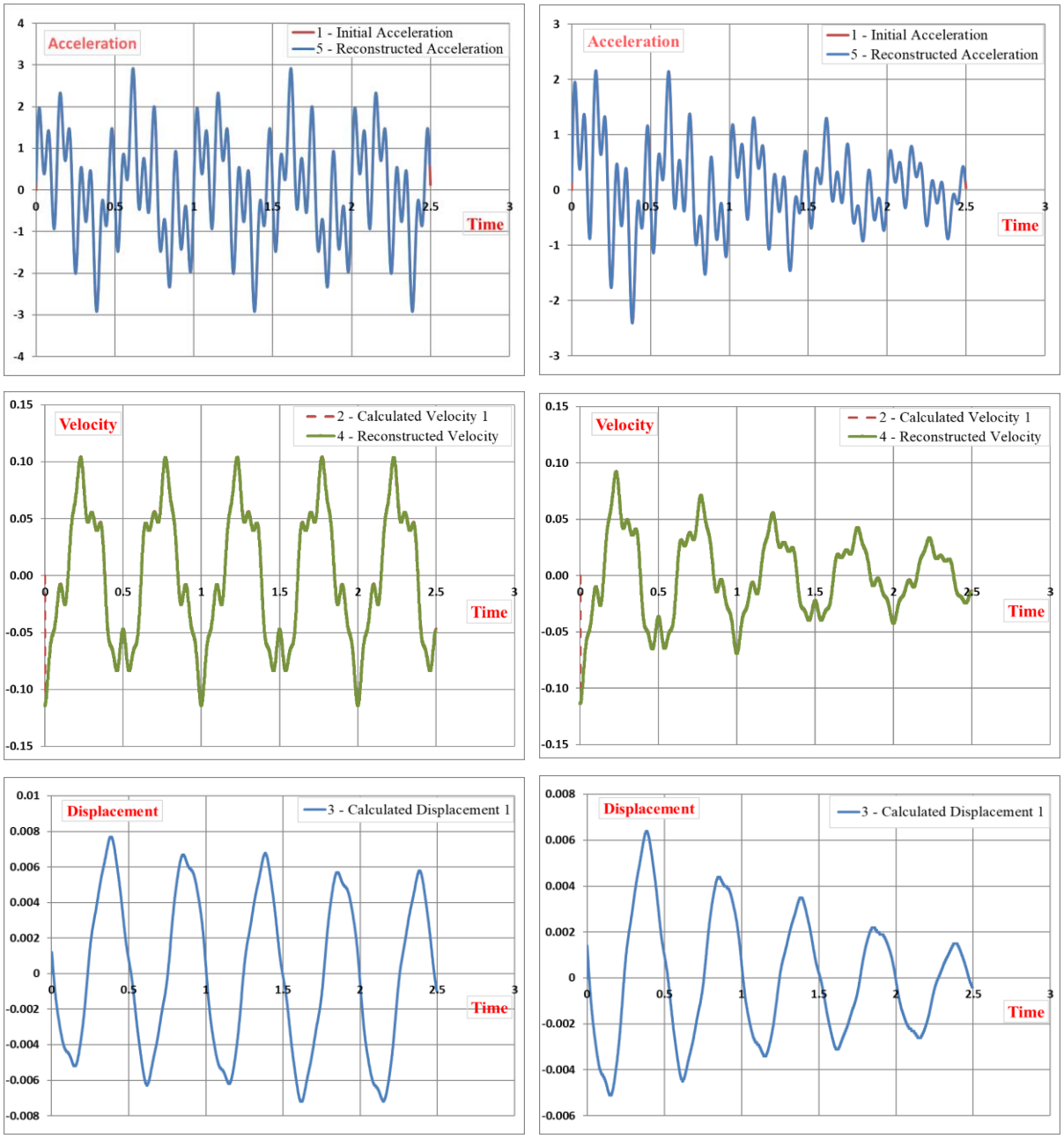

a. b.

Figure 2.38 Diagrams for the acceleration signal generated with three harmonic components and the calculated velocities and displacements
(a) undamped signal; (b) damped signal.

First, an undamped signal with the time length t=2.5 s that has three harmonic components with the frequencies: f1=2 Hz, f2=5 Hz and f3=12 Hz was tested. Secondly, the same signal, but with the damping ratio 0.5 was considered, and the signals were represented in Figure 2.38.

From Figure 2.38.b the conclusion is that the damping does not affect the method's accuracy, both the reconstructed velocity and acceleration fit the original one. Comparing the undamped and damped signals in Figures 2.37 and 2.38, it can be observed that the same sampling strategy lead to similar precision in calculating the antiderivatives.

Analysing the Figures 2.36 to 2.38 it is visible that the algorithm implemented in the PySEMO application is precise and can be used for calculating antiderivatives without knowing the initial conditions of the analysed system if some conditions are fulfilled.

First, the ratio between the frequencies of the signal components and the time length should be as big as possible, in order to ensure a sufficient big number of cycles in the signal. From experience, the signal must contain at least five cycles of the fundamental frequency.

A second condition concerns the time resolution, which depends on the sampling frequency. Here, it was discovered that each cycle of the highest frequency in the acceleration signal must include 200 samples to ensure a smooth displacement curve. Regarding the initial phase and the damping ratio, it was established that these do not affect the accuracy of the results obtained with the PySEMO application.

2.6. Conclusions and contributions

The old earthquake recordings are very important from the scientific point of view. Therefore, some important web-based database were presented to provide tools for searching, selecting, and downloading ground motion data. The earthquake databases shown can be used to re-analyze the past and present earthquakes. For this research, digital signals were needed to describe various earthquake movements.

In this chapter, an algorithm was developed to extract the signals and the numerical values from an image with the help of the WebPlotDigitizer software. The digital format allowed the re-analyzation of the past earthquakes and the usage of digital data as input for dynamic simulation made for base-isolated structures.

An application developed in the Python programming language was created to generate digital signals with known parameters (frequency, amplitude, phase, damping coefficient, existence of noise) and exemplify outcomes for different settings of the parameters. These digital

signals, since have known parameters, can be used to create benchmarks for test and numerical simulation.

In this Chapter also, an algorithm was designed to calculate the antiderivative of signals that have the integral close to null, as the signals measured on structures during earthquakes are. The method implies performing a series of numerical integration considering the initial value being zero. Afterward, the average value for the primitive function is calculated and considered as initial value: this solves the initial value problem with acceptable precision. Because of the minor errors, the second antiderivative that is the displacement in our case will gain a continuously slight increase. This problem was overcomed by finding the trendline and extracting it from the signal representing the second antiderivative. In this way, accurate instantaneous values for the displacement were obtained as well.

The algorithm, nominated as PySEMO, is implemented in the Python programming language and can be used to find the velocity and the displacement evolution for earthquake signals acquired with accelerometers. The algorithm can be used for other signals alternating around zero, e.g. those measured on rotating machines, as well.

The accuracy of the method of the signal processing was demonstrated involving a large variety of generated signals with known parameters.

3. BASE ISOLATION SYSTEMS

Protecting buildings from the devastating effects of earthquakes remains one of the oldest challenges for structural engineers.The behaviour of structures during earthquakes is a particular case that is actually the focus of this work. To avoid harmful effects, the structures are isolated by inserting between the ground and the superstructure devices that diminish the effect of inertial forces.

Two main types of devices are used: that based on dissipation of energy by friction [42-44] and that based on elastic supports which change the period of the system [45-47]. The latter are manufactured from various materials and can achieve different configurations [48]. The idea is to design the mentioned devices based on the history of the place, therefore the information stored in earthquake registrations is essential. Repositories containing earthquake accelerograms in digital form exist [23], [49], [50].

3.1. The concept of base isolation

The concept of base isolation systems is to interpose structural elements with low horizontal stiffness between the structure and the foundation in order to decouple the structure from the horizontal ground motion. Thus the seismic isolation system changes the fundamental period of the structure from a high value to a small one or dissipates the energy by damping, thus limiting the force that is transmitted to the structure which decreases drastically by reducing the acceleration (Figure 3.1).

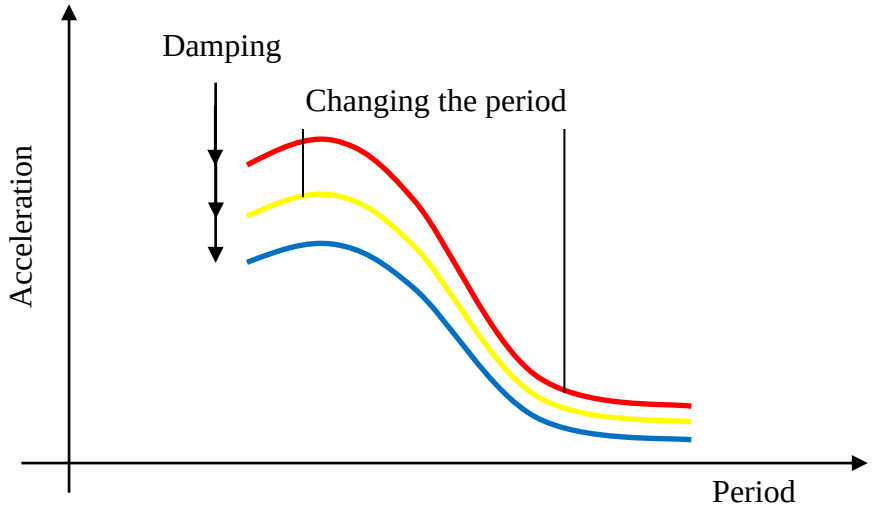

Figure 3.1 Response acceleration spectrum

Earthquake accelerations have a dominant period between 0.1 ÷ 1.0 s with a high danger of destruction in the interval of 0.1 ÷ 0.6 s. The structures that have a natural period of vibration between 0.1 ÷ 1.0 s. are vulnerable during earthquakes because they can resonate. The most important feature of seismic isolation systems is the increase of the natural period of the structure, higher than 1.5 s. Because the period increases beyond that of the earthquake, resonance is avoided and the seismic acceleration response is reduced [51].

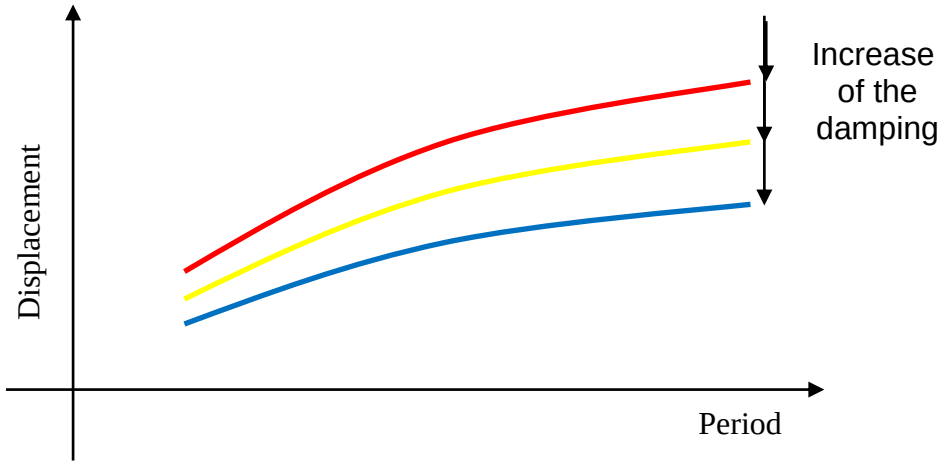

Figure 3.2 Displacement of the response spectrum

Dampers are important to suppress resonance at the isolation frequency. Figure 3.2 shows the effect of damping on the controlled displacement where it is observed that, with the increase of the damping, both the displacement and the acceleration of the structure are reduced [52].

3.2. History of base isolation

The idea of avoiding disastrous damages of earthquakes through insertion between the ground and the protected structure of devices that reduce the effect of ground movement on structures has a long history.

Jules Touaillon of San Francisco was among the first to obtain a patent on an earthquake-resistant ball system in February 1870 (Figure 3.3). To isolate the structures, he suggested using ball bearings between the base and the foundation of the structure [53].

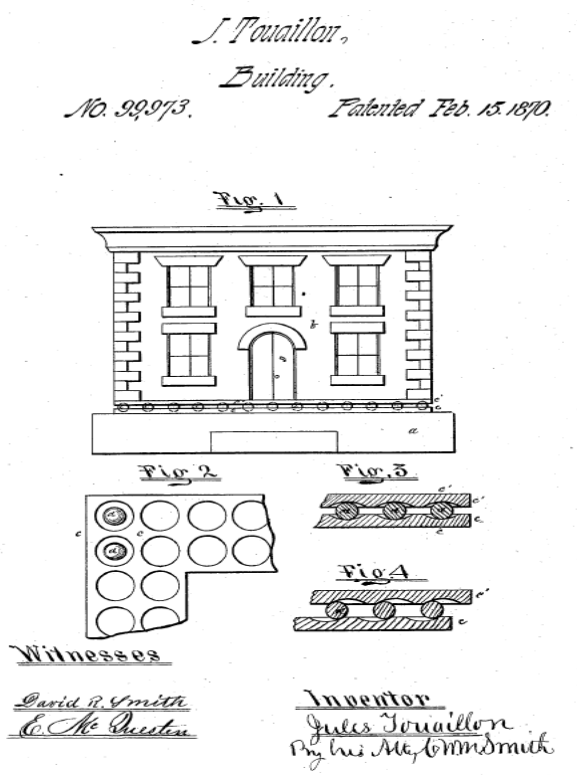

Figure 3.3 Jules Touaillon - earthquake-proof building [US Patent No. 99,973, 1870]

In 1891, Kozo Kawai published a method for seismic isolation in the Journal of the Architectural Institute of Japan [54]. In the paper "Structures free from the maximum vibrations during earthquake", he proposed a base-isolated structure with the foundation of the structure consisting of a concrete platform placed on several layers of timber logs assembled in a criss-scross pattern. The structure had a triangular shape to increase the stiffness and the design included a deep trench all around the building to cut off the surface waves (Figure 3.4).

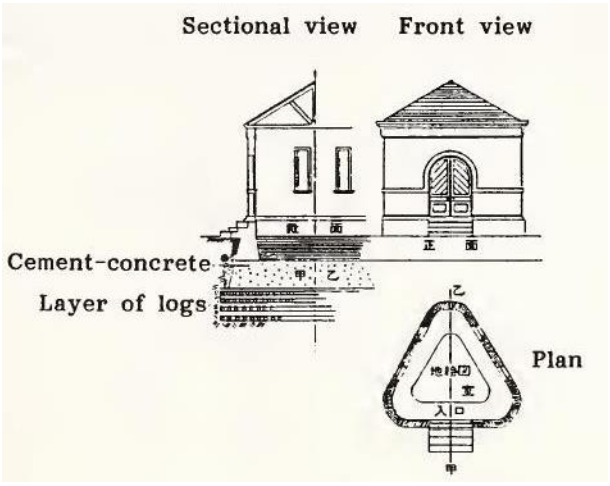

Figure 3.4 Kozo Kawai anti-seismic building [54]

Some years later in 1907, Jacob Bechtold obtained a patent in which he presented a structure on a rigid plate which supported on spherical mechanisms of hard material as an isolation layer [55].

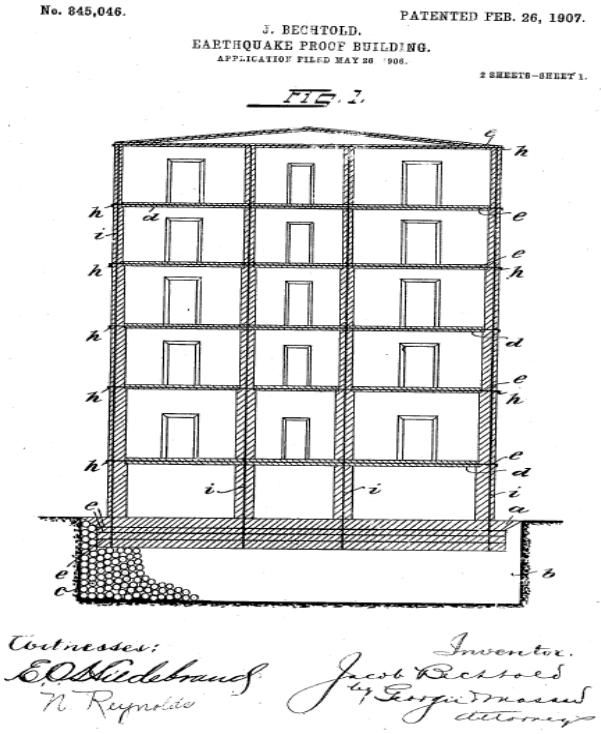

Figure 3.5 Jakob Bechtold - earthquake-proof building [US Patent No. 845,046, 1907]

In 1909 J. A. Calantarients proposed the construction of buildings on sliding foundations. His construction method was to build the superstructure on a layer of fine sand, talc, and mica to create a lubricated surface that allows the building to slide during earthquake motion [56].

The first natural rubber isolation system was used in 1969 in Skopje (Macedonia) to provide earthquake protection for a school. The Pestalozzi school was the first structure isolated with unreinforced rubber bearings so that the weight of the building caused the bearings to bulge sideways [57]. This was an important step in the development and implementation of the multilayered laminated rubber bearings.

In the 1970s in New Zealand, were introduced lead-rubber bearings, as a more dissipative energy alternative to laminated-rubber bearings [58]. They consist of traditional elastomeric bearings with the addition of a lead plug, a detailed description of the behavior of laminated elastomeric bearings can be found in [57]. Both lead-rubber bearings and laminated-rubber

bearings have been used for seismic isolation around the world due to their efficiency in protecting the buildings from the effects of earthquakes[52].

Victor Zayas conducted, in 1987, the first analytical and experimental studies on the Friction Pendulum system [59]. A Friction Pendulum system consists of an articulated friction slider that travels on a spherical concave sliding surface and uses gravity as the restoring force. Friction Pendulum systems have been extensively studied analytically and experimentally by many authors [60-67] and used for a variety of structures.

3.3. Types of base isolation systems

Base isolation systems are generally classified in elastomeric and sliding based types. The horizontal flexibility and the energy dissipative capacity are the common features that all base isolation systems have. The advantage of sliding-based systems is their capacity to slide freely over the foundation, thus reducing the forces transmitted to the structure. Many designs for base isolators have been suggested over time [68-79]. Here are briefly described only a few different types of base isolation systems that have been in use.

3.3.1. Elastomeric – based systems

Elastomeric bearings with steel reinforcement are the most commonly used for seismic isolation because their constructive shape is simple, cylindrical, or prismatic and can be made in a diverse range of sizes, depending on the structure to be seismically isolated. These systems can be easily produced and are resistant to atmospheric conditions, temperature differences, do not require maintenance during operation, with a lifespan of 50 years.

The main role of elastomeric based systems is to modify the fundamental period of the structure. Through increasing the fundamental period of the structure, beyond that of the earthquake, resonance is avoided and the seismic acceleration response and thus important stresses are reduced.

Elastomeric bearings are very stiff in the vertical direction because of steel reinforcements and very soft in the horizontal direction, because of the low stiffness of rubber, which guarantees an isolation effect. Elastomeric seismic isolation systems are considered to be low damping devices because they have relatively low damping values. Elastomeric bearings are classified into two types: low- and high-damping.

3.3.1.1. Low-Damping Rubber Bearings (LDRB)

The LDRB were initially made entirely of natural rubber, later their properties were improved by the addition of steel plates [80]. A bearing of this type consists of two thick steel endplates and many thin steel shims, which are vulcanized and bonded to the steel in a mold under heat and pressure. The steel shims prevent bulging of the rubber and provide the required vertical stiffness without increasing the horizontal stiffness significantly. This type of seismic isolation, made of natural or synthetic rubber, has been applied mainly in Japan, in combination with additional damping devices, like viscous dampers, lead bars, and steel bars. The elastomer used in Japan contains natural rubber, and neoprene has been used in projects in other countries, such as France [57].

The advantages of these bearings are: easy to design and manufacturing production process, and their mechanical response is unaffected by temperature, rate, history, or aging. The main disadvantage of this system is that must be used together with other additional energy dissipation systems because of a very low damping rate [57].

3.3.1.2. High-Damping Rubber Bearings (HDRB)

The HDRB are different from the low-damping rubber bearings presented above, in that they have a special composition that gives them effective damping between 0.1 ÷ 0.2. They have been developed to avoid additional devices required when using the LDRB. The damping of HDRB is improved by adding extra-fine carbon blocks, resins, oil, and some other fillers to the elastomer composition [81]. The addition of these materials increases the critical damping of the isolation system from 2 ÷ 3% to 10 ÷ 20% at 100% shear strain. The mechanical properties of high damping isolators are somewhat affected by the effect of rubber aging and temperature variations [80]. Changes in the horizontal characteristics of elastomeric isolators due to aging over the life of these are estimated to be less than 20% of the initial values [82]. The elements have higher stiffness and damping at the first loading cycle, after which the properties stabilize [83].

Among the advantages of HDRB systems is the lack of need to combine with other energy dissipation systems, as in the LDRB case, and the ease with which they are manufactured and designed. Another important characteristic of HDRB is that they provide vibration reduction by filtering high-frequency vibration caused by underground traffic[57].

3.3.2. Sliding – based systems

A natural and powerful energy dissipation device is based on friction force, which reduces the structure acceleration during an earthquake. The friction force depends on many factors: the sliding velocity, the contact pressure, the material of the rubbing surfaces, and the history of loading.

The pure friction isolation systems are the simplest base isolation systems of all, where the isolation mechanism is sliding friction. Because of numerous practical problems, this kind of base isolation system was accepted much later than other types, even if the initial isolation concepts were the sliding-based type.

Based on the same principle, a lot of different configurations were suggested [84-90]. In the coming section, few sliding-based systems will be shortly described.

3.3.2.1. Electricite-de-France system (EDF)

The Electricite-de-France system (EDF) is a combination of the elastomeric isolation with the sliding type one and was developed in the early 1970s.

The system combines the elastomeric bearings with two plates that allow sliding between them. One of the plates is made of an alloy of lead and bronze, and the other of stainless steel, the latter being connected to the superstructure. The friction surfaces are designed to have a coefficient of friction 0.2. The sliding elastomeric bearing pads consist of a block of elastomeric, reinforced by horizontal steel plates. The reinforced bearing pads have high vertical stiffness and a low stiffness to horizontal shear forces. The elastomeric bearing pads act as a filter between the structure and the ground, thus the forces transmitted to the structure are dependent on the characteristics of the filter itself [92].

While for low-intensity earthquakes the structure vibrates on the elastomeric bearings and returns to its original position, during severe earthquakes the structure vibrates on the elastomeric bearings as well as slides on the frictional surface. The lead-bronze alloy plate and the steel plate dissipate the energy induced by the earthquake by friction.

The EDF system is standardized for nuclear power plants in regions with high seismic activity and it has been successfully implemented in nuclear power plants in South Africa, Iran, and France.

3.3.2.2. Resilient-Friction Base Isolation system (R-FBI)

The R-FBI is made of concentric layers of Teflon coated plates, that are in friction contact, and to provide a restoring mechanism contains a central core of rubber, which carries no vertical load [89-91].

The lateral stiffness of the rubber and the coefficient of friction of the sliding elements are the parameters that characterize this isolation system. The friction damping is the main energy dissipater of the R-FBI system because the damping capability of the rubber is small. High friction coefficients produced by high sliding velocity between sliding layers are not ok for the isolation effect. Instead of one layer of sliding plate, can be used more plates, to reduce considerably the friction coefficients and the sliding velocity.

The R-FBI system is not a good isolator for the structures that are subjected to the vertical movements of the ground because of its rigidity in the vertical direction. It has been shown that this type of base isolation system is suitable for reducing the acceleration of light structures or equipment [93].

3.3.2.3. Friction Pendulum System (FPS)

The FPS is an isolation method that combines the sliding motion and returns force given by the geometric conformation of the system [57]. The FPS consists of an articulated slider on a spherical surface. The idea of using an articulated slider on a concave spherical shape was first proposed by Zayas [59].

Seismic isolation is obtained by changing the natural period of vibration of the supported structure. From the pendulum equation 3.1, it is determined the natural period of vibration (T) of a rigid structure isolated with FPS.

$$T = 2\pi\sqrt{\frac{R}{g}} \tag{3.1}$$

where g is the gravitational acceleration.

As can be observed from the pendulum equation the natural period is controlled by the selection of the radius (R) of the spherical sliding surface.

The intensity of the force at which the slip begins is controlled by selecting the material on which the friction is made. When the seismic forces are less than the friction force, the

isolated structure behaves like a normal, unisolated structure with a certain natural period of vibration. Once this friction force is exceeded, the dynamic response is controlled by the FPS system, and the isolated structure responds with another period of vibration [60].

The lateral stiffness of the activated FPS system is:

$$K = \frac{w}{R} \tag{3.2}$$

where *w* is the supported weight and R is the radius of the spherical surface.

3.3.2.4. Tuned Mass Damper system (TMD)

To reduce the dynamic response of a structure can be used a TMD device that is composed of a shock absorber, a mass, and a spring. The frequency of the damper is tuned to a certain frequency of the structure in such a way that when it is excited, the damper will vibrate out of phase with the movement of the structure. The energy is dissipated by the inertial force of the shock absorber acting on the structures.

Vibration control with the TMD's may be passive, semi-active, active, or hybrid. This depends on the control strategies that are adopted for the device. Damping, mass, and rigidity characterize the TMD device. The mass and stiffness of the damper with the given mass are chosen in such a way as to bring the own vibration frequency of the device closer to the resonant frequency of the structure to be protected [94].

The masses are made, in general, from steel or concrete blocks, mounted inside the buildings. These are moving in the opposite direction to the oscillations of the structure, in the resonance area, with the help of springs, fluids, or pendulums. The shock absorbers used in the system are of the viscous type.

3.4. Conclusions and contributions

There are various isolation systems that each have their own particularities. For example the elastomeric bearings can modify the fundamental period of the structure, but are very stiff in the vertical direction because of steel reinforcements. Elastomeric seismic isolation systems are considered to be low damping devices because they have relatively low damping values.

A natural and powerful energy dissipation devices are based on friction force, which reduces the structure acceleration during an earthquake. The friction isolation systems are the

simplest base isolation systems of all, where the isolation mechanism is sliding friction. The advantage of sliding-based systems is their capacity to slide freely over the foundation, thus reducing the forces transmitted to the structure.

From the isolation system it was chosen the study of the friction pendulum systems and tuned mass damper systems. Because friction pendulum systems with variable radii are little studied and used, the research was concentrated on the particularities of this systems compared to those with spherical or cylindrical surfaces.

Combinations of friction pendulums with various radii but also with the plan surface associated with tuned mass systems are not analyzed, therefore these types of systems will be studied in the next chapter.

4. DYNAMIC SIMULATIONS AND BEHAVIOUR OF STRUCTURES ISOLATED BY FRICTION PENDULUM

4.1. Description of the system

The structure was implemented in the Motion module of SolidWorks. The 3D model of the perfectly rigid structure was build with steel bars and wood plates. Because unidirectional displacement in X direction is considered in this study, for simplicity, instead of the real spherical devices, cylindrical friction pendulums with the same radius *R* are employed in the model.

The test structure, presented in Figure 4.1, is generated in SolidWorks as an assembly with three parts:

1 - the structure with the dimensions 1200x400x200 mm;

2 - the base plate with the dimensions 600x200x10 mm as a reference;

3 - the shaking plate with the dimensions 600x200x10 mm reproducing the ground motion.

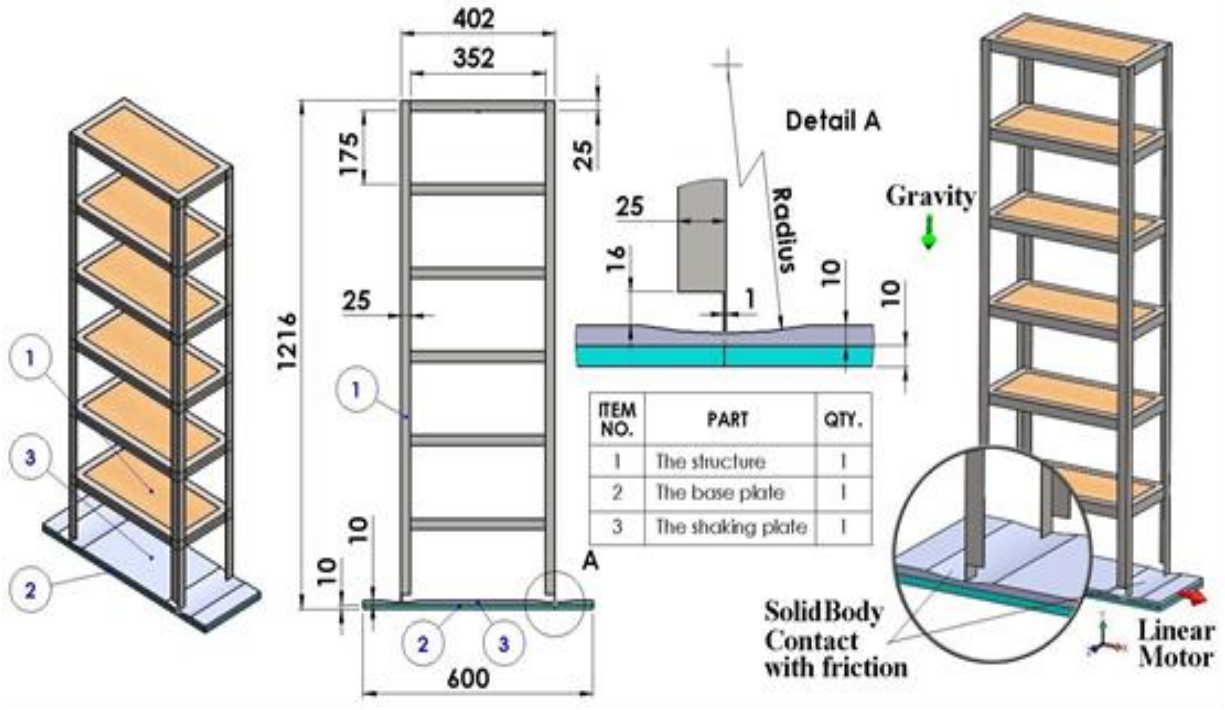

Figure 4.1 The test structure

The structure, as the part denoted with 1, has the geometry and essential dimensions described in Figure 4.1. The ground is conceived as an assembly consisting of two parts. One

of them is a base plate that is fixed, indicated as part 2 in the Figure 4.1, which is used as a reference. The second part is the shaking plate 3 that can shift along the base plate without friction. It reproduces the ground motion. The dimensions of the two plates are given also in Figure 4.1.

The shaking plate is moved in the X direction with a feature of the SolidWorks program called Linear Motor. It can impose a displacement after a harmonic function. A SolidBody Contact with friction is imposed between the bottoms side of the structure and cylindrical surface of the pendulums. The gravitational force oriented on Y direction is imposed for a 9806.65 mm/s^2 value of the gravitational acceleration.

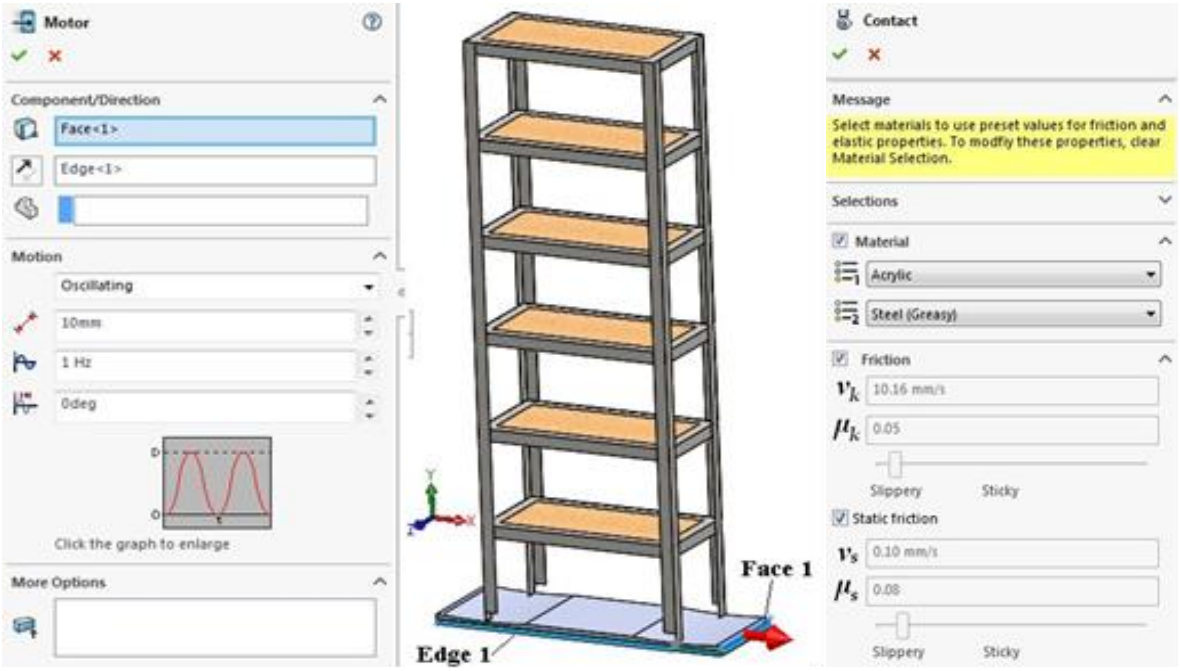

Figure 4.2 The Linear Motor and SolidBody Contact

4.2. Study on the effect of a simple friction pendulum radius on the response of isolated structures

The aim of the study is to identify the friction pendulum's radius which the natural frequencies ensures an efficient base isolation.

The model created in SolidWorks is employed in the research to find out the structural behavior. The excitation, ensured by a simulated shaking table, follows a harmonic displacement. The study revealed the frequency at which the chosen friction pendulums assure

efficient isolation. Also, it revealed the frequency domain in which the displacement of the structure is important.

The simulation was made in SolidWorks Motion, for the following conditions:

- the **base plate** is fixed;
- the **shaking plate** is moved on the X direction with a Linear Motor that imposes displacement with the following parameter: Oscillating motion, **Max Displacement 10 mm**, **Frequency f = 1 Hz**, **Shift 0 deg**;
- a SolidBody **Contact with friction** is imposed between the bottoms side of the structure made from acrylic material and cylindrical surface of the shaking plate made from steel (greasy) material. The following properties are imposed by SolidWorks Motion for the dynamic and **static friction coefficients** μ_D and μ_S, respectively the dynamic and **static velocity coefficient** v_D and v_S. These are: μ_D**=0.05** and v_D**=10.16 mm/s²** respectively μ_S**=0.08** and v_S**=0. 1 mm/s²**;
- the **gravitational acceleration** g=9806.65 mm/s^2 oriented in Y direction;
- the **time** of analyze is imposed as **30 s**;
- the **radius** of the sliding surface extruded from the shaking plate was modified in the range **110 ÷ 960 mm**, with a 50 mm step.

The system has a natural frequency f_n which can be calculated using the mathematical relation:

$$f_n = 2\pi\sqrt{\frac{g}{R}} \tag{4.1}$$

The structure's response in terms of displacements in X direction during the 30 seconds of forced excitation are presented in Figure 4.3, for the **18 analyzed cases**, corresponding to the radius modification in the 110 ÷ 960 range with a 50 mm step. From these time-histories one can observe that the structure's displacement amplitude becomes smaller and stable as value if the **R_{10} > 560 mm**. In addition, the system's frequency gets stable and takes the value of the pendulum. Table 4.1 show the minim and maxim values of the structure calculated by SolidWorks Motion for the linear displacement in X direction. These values are graphically presented in Figure 4.4.

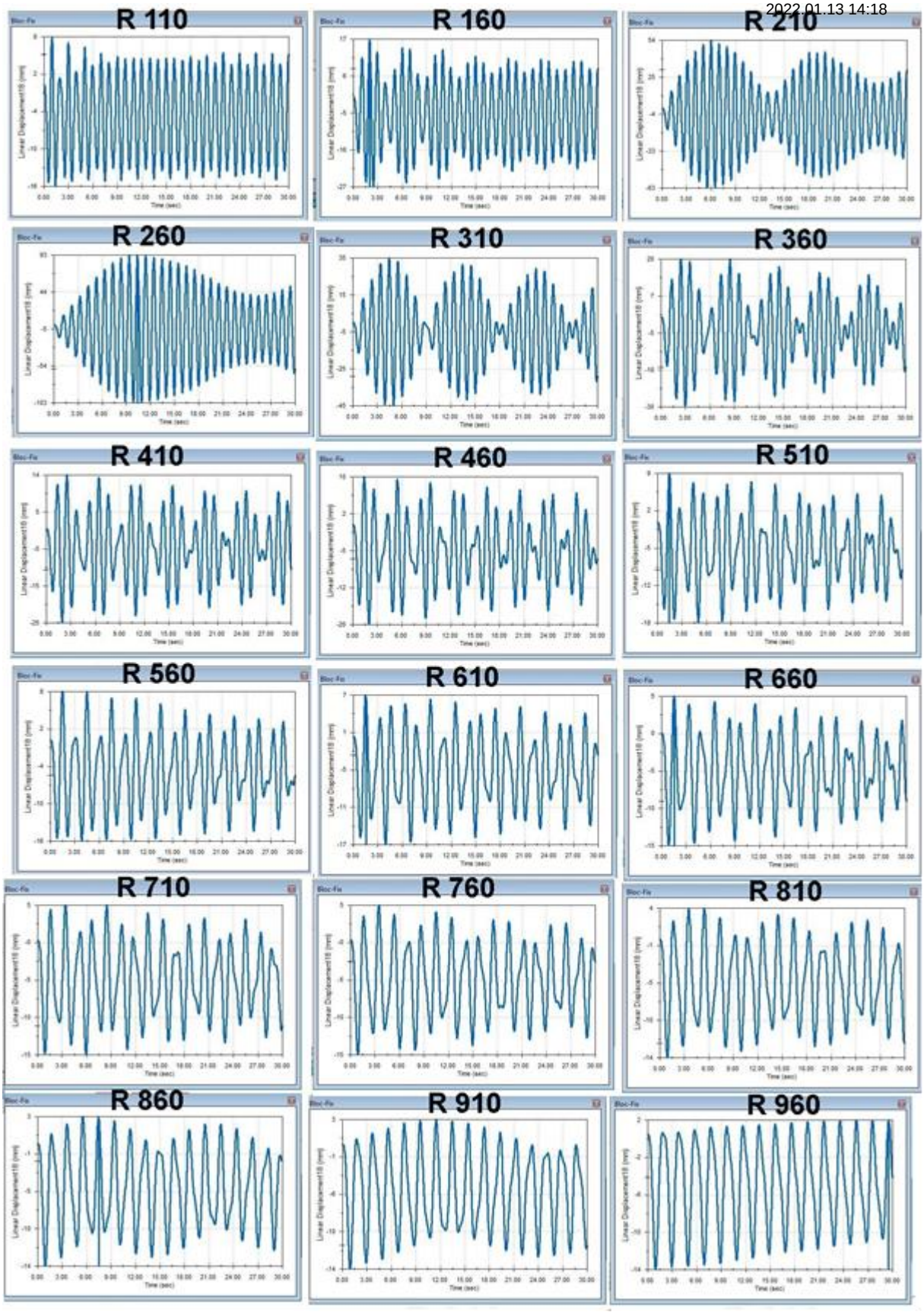

Figure 4.3 Response signal captured from the isolated structure for different friction pendulum radii

Table 4.1 Linear displacement in X direction

Radius [mm]	Bottom limit [mm]	Upper limit [mm]	Radius [mm]	Bottom limit [mm]	Upper limit [mm]
110	-15.92	7.54	**560**	-16.08	7.8
160	-26.53	17.26	**610**	-16.51	6.52
210	-62.57	53.79	**660**	-15.05	5.08
260	-103.29	93.35	**710**	-14.92	4.74
310	-45.31	35.47	**760**	-14.57	4.55
360	-30.36	19.61	**810**	-14.41	3.95
410	-24.63	14.23	**860**	-14.13	3.21
460	-19.88	9.69	**910**	-13.9	2.84
510	-18.46	9.11	**960**	-13.73	1.55

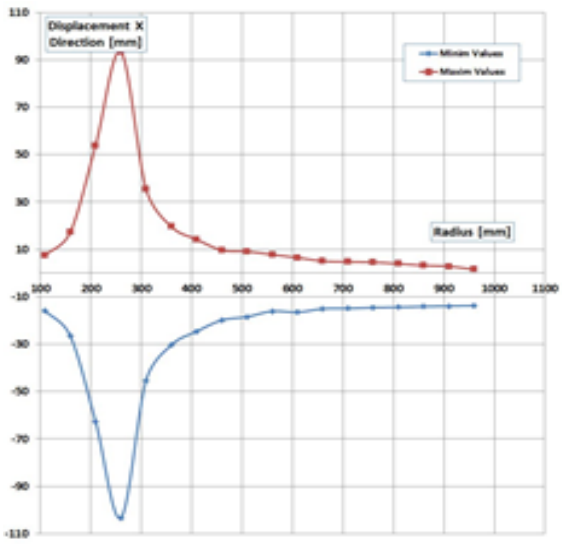

Figure 4.4 Bottom and upper displacement amplitudes

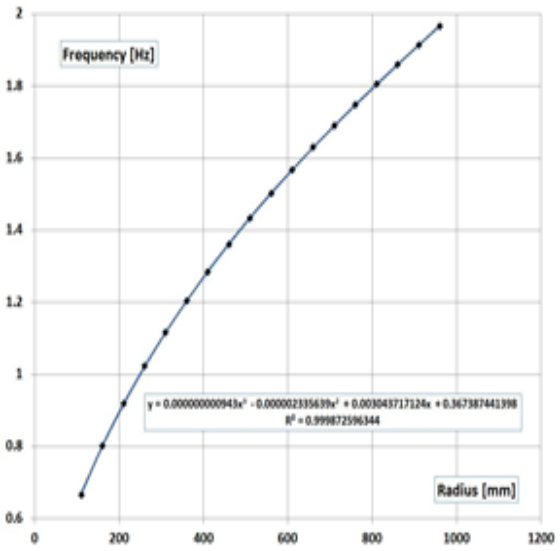

Figure 4.5 Frequency ratio f_n/f versus the sliding surface radius *R*

Figure 4.5 shows the evolution of the frequency ratio fn/f with respect to the sliding surface radius *R*. One can observe that for the ratio $fn/f > \sqrt{2}$ a reduced transmissibility is achieved and so the structure becomes isolated to the ground motion.

It was found efficient isolation is provided if the **radius** is bigger then **600 mm** in the case of exciting the structure with an oscillation having the **frequency** of **1 Hz** and the **amplitude** of **10 mm**. In addition, from the response signal's time history, an amplitude increase is observed if the excitation frequency is in a narrow band around pendulum's natural frequency.

4.3. Response of a structure isolated by friction pendulums with different radii

This study presents simulations that highlight the influence of the friction pendulum radius on the behavior of isolated structures. A model was created in SolidWorks, which is employed to find out the structural response. The excitation in term of displacements, ensured by a feature of the software program, follows a sine function. The study has shown the frequency evolution with the radius increase, along with the displacement of the isolated structure.

A schematic of the structure, reflecting the configuration and the component parts, the dimensions and details regarding the imposed contacts is given in Figure 4.1.

The sliding surface radius, modeled as an extrusion from the shaking plate, was stepwise modified in the range 110÷960 mm with a 50 mm step. Contact with friction (Table 4.2) is imposed between the bottom side of the structure and the cylindrical surface of the shaking plate. All the other simulation condition remained the same as in sub-chapter 4.2. Both components are made of steel. Frictionless contact was chosen between the fixed base plate and the shaking plate. The system has a natural frequency which is given by the relation 4.1.

Table 4.2 Contact condition based on friction coefficients

Contact case	Components	Contact type	μ_D [-]	v_D [mm/s^2]	μ_S [-]	v_S [mm/s^2]
1	Structure	Steel (dry)	0.25	10.16	0.3	0.1
	Shaking plate	Steel (dry)				

The simulation results are presented in Figures 4.6 to 4.9. One observe that for the frequency excitation **f_e=1 Hz**, if the SFP radius is low, for example 110 mm, the displacement of the structure follows the displacement of the ground, see Figure 4.6. If the radius of the sliding surface is increasing, the structure crosses through resonance. In this case, the amplitude of the structure's displacement increases as well. This is shown in Figure 4.7.

The biggest amplitude is achieved for the case R_4=260 mm, giving the natural frequency f_n=1.023 Hz, which is very close to the excitation frequency. An increase of the radius leads to an increase of f_n. After this frequency passes the excitation frequency, the amplitude of the structure's displacement decrease. The amplitudes for all cases in the resonance domain are presented in Table 4.3.

TIMIS GABRIELA-VASILICA
2022.01.13 14:18

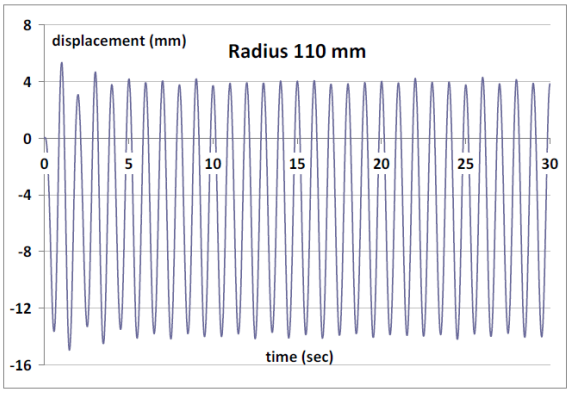

Figure 4.6 Under-resonant structural behavior

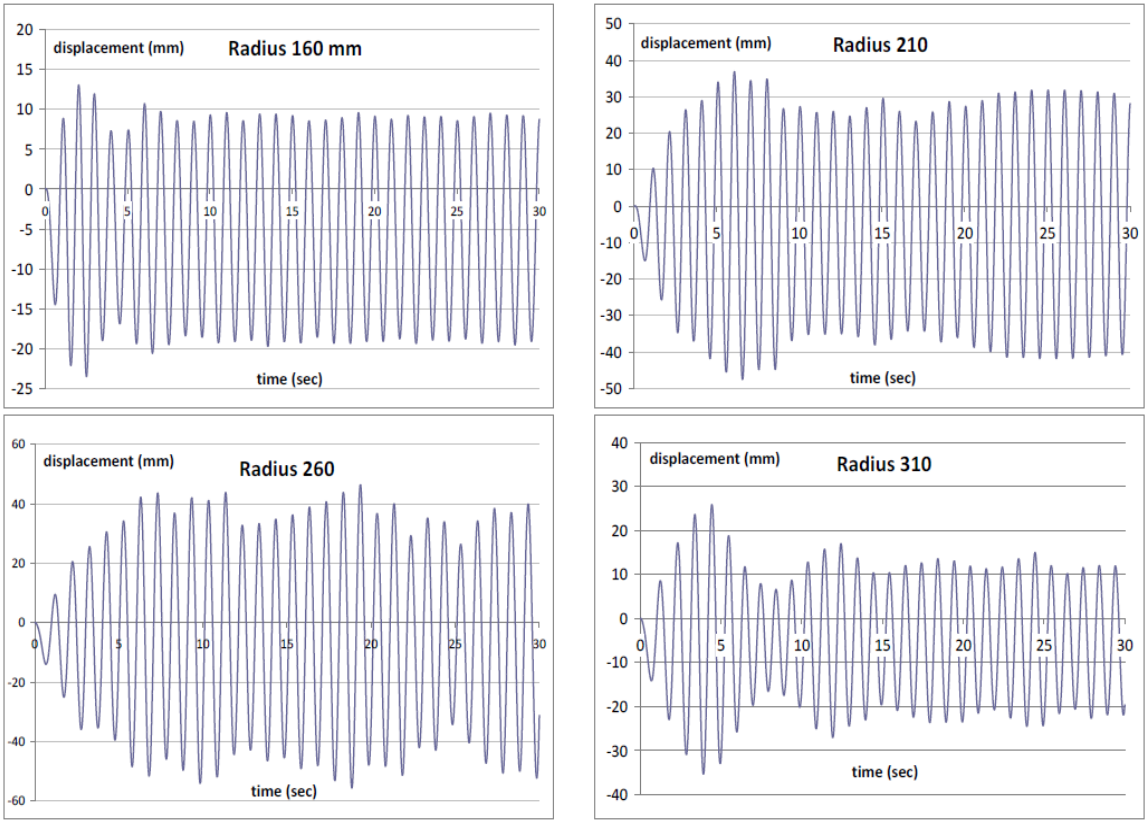

Figure 4.7 Structural behavior in the resonance domain

Table 4.3 Amplitudes achieved in the resonance domain

R_i [mm]	110	160	210	260	310	360	410	460	510
A_{min} [mm]	-14.95	-23.52	-47.54	-55.65	-35.31	-24.38	-19.09	-17.62	-15.09
Average [mm]	-4.81	-5.23	-5.32	-4.68	-4.74	-5.38	-5.06	-5.41	-4.70
A_{max} [mm]	5.34	13.07	36.90	46.30	25.83	13.62	8.98	6.80	5.70

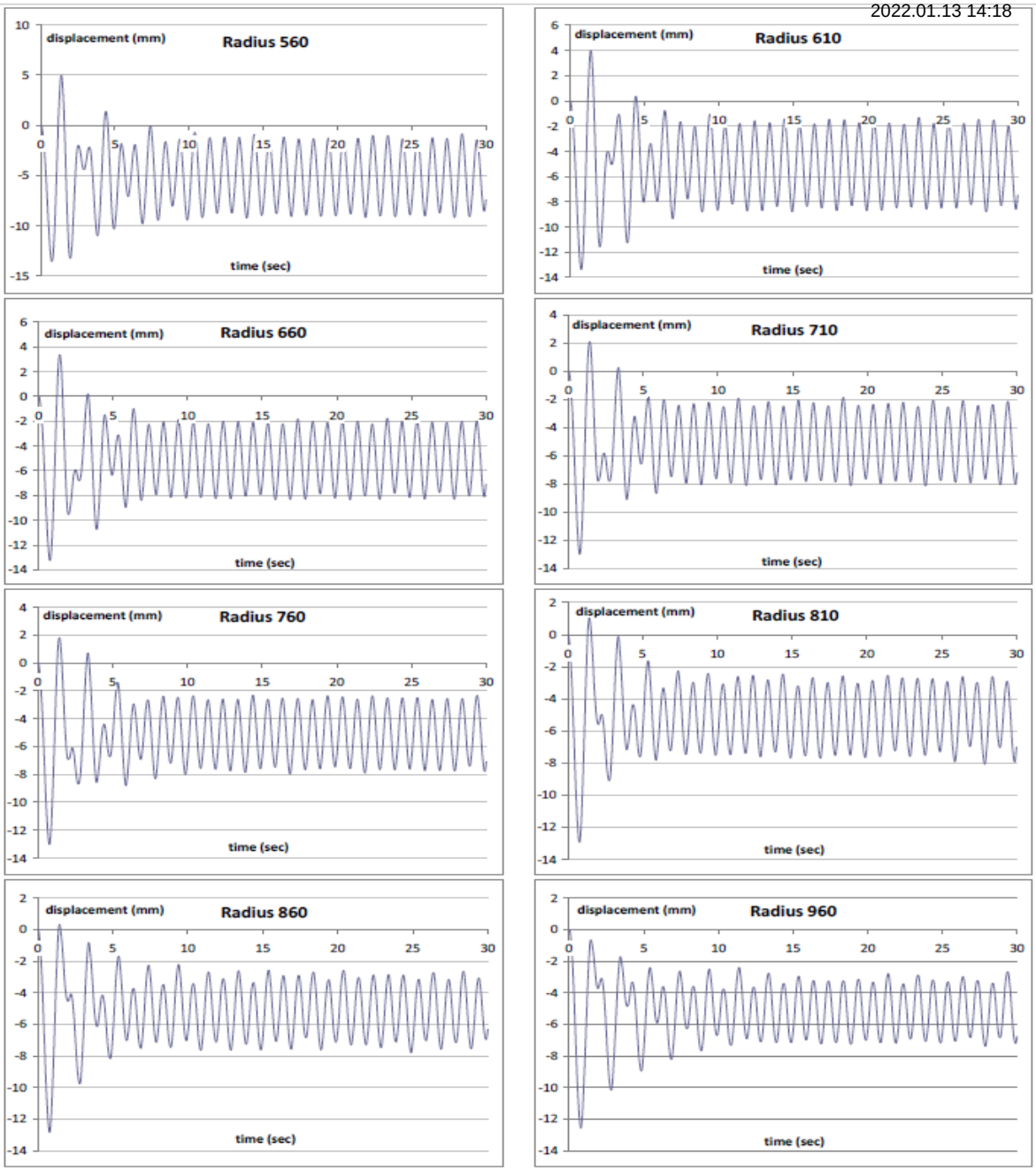

Figure 4.8 Structural behavior in post-resonance

For even bigger friction pendulum radii, the natural frequency increases and the amplitude of the structure's displacement decrease in consequence. The best results in isolating the structure are obtained for the frequency ratio $r = f_n/f_e > \sqrt{2}$ as stated in the theory. Not just the amplitudes in the transitory regime are in this domain the lowest, but also the evolution in the stabilized regime present low amplitudes. The highest amplitudes for the post-resonant regime are presented in Table 4.4, while Figure 4.9 shows the amplitudes for all the analyzed cases (sub-resonance, resonance and post-resonance domain).

Table 4.4 Amplitudes achieved in post-resonance

R_i [mm]	560	610	660	710	760	810	860	910	960
A_{min} [mm]	-13.52	-13.38	-13.24	-13.00	-13.01	-12.92	-12.83	-12.75	-12.55
Average [mm]	-4.29	-4.71	-4.95	-5.46	-5.61	-5.95	-6.27	-6.38	-6.28
A_{max} [mm]	4.94	3.96	3.35	2.08	1.80	1.02	0.30	0	0

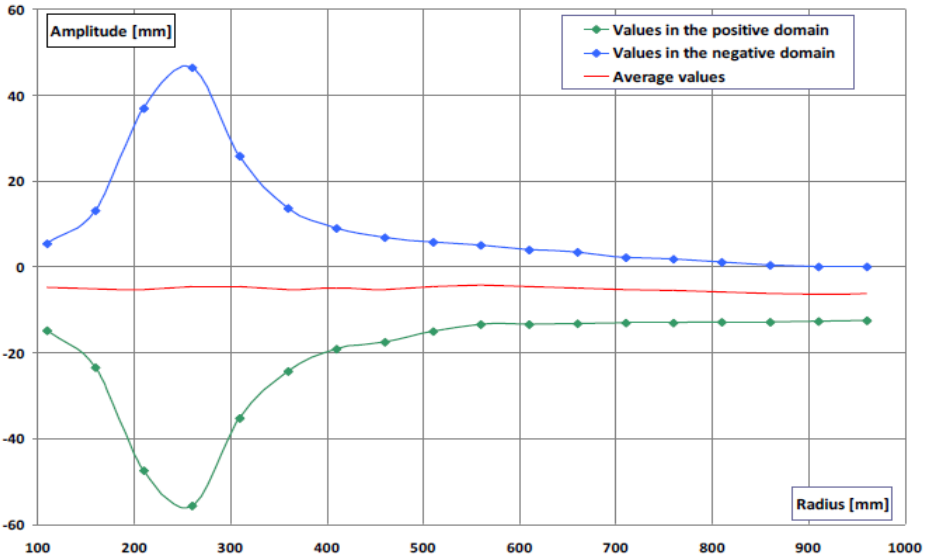

Figure 4.9 Amplitudes achieved for different friction pendulum radii (R = 110 ÷ 910 mm)

Having a look onto Figure 4.9 one can observe that an effective isolation is achieved for radii bigger then 610 mm. This means that, the friction pendulum must be designed to fulfill this condition, or, if the sub-resonant domain is chosen the radius must be small enough to avoid approaching the resonance. Obviously, design must consider the expected relevant period of the earthquake. Comparing the results with those of other simulations made for similar circumstances, but for different friction coefficients and excitation frequencies [98], it was noticed that the frequency ration r at which resonance is achieved moves to lower values for a bigger friction coefficient. Also, the amplitude in the resonance is smaller for the bigger friction coefficients.

It was found that the biggest amplitude is achieved for a natural frequency of the system that is similar with the excitation frequency. On the other hand, an effective isolation is obtained for frequency ratios r bigger then 1.4. For values of the friction pendulum radii ensuring this condition the amplitudes, in the transitory as well as that in the stabilized regime, accomplishes smallest values. In the stabilized regime, the structural displacement is half of the excitation amplitude.

4.4. The effect of the friction coefficient and the pendulum radius on the behaviour of structures isolated with simple friction pendulums

A rigid structure isolated with simple friction pendulums (SFP) behave in respect to the radius of the sliding surface. The friction coefficient of the involved materials has a limited, but clear influence. The frequency of the ground trepidation has also to be considered.

For calculating the natural frequency f_n of the isolated system one can involve the relation 4.1. One can observe that the friction coefficient μ and the weight of the structure G do not influence the natural frequency.

The frequency and the amplitude resulted for a given excitation depends on the excitation parameters, which are the amplitude A_e and the frequency f_e. The task of the SFP is to maintain the amplitude of the displacement A_{max} achieved in the transitory regime as well as the amplitude in the stabilized regime A_{stab} as small as possible, in order to avoid dangerous acceleration.

During ground shacking, the inertial forces belonging to the structure push it in horizontal direction. The force caused by friction opposes to this action, being a reaction force. Note that the friction coefficient μ varies with the speed. If the inertia exceeds the friction force, a relative displacement between the structure and the friction pendulum takes place and the structure attains another frequency f_{struc} as the excitation. This is lower as f_e and supplementary contribute to the reduction of the structure's acceleration.

This study shows the results of simulation made on a rigid structure isolated with four simple friction pendulums. A model in SolidWorks was created that was used to find out how the pendulum radii and friction coefficients respectively the frequency of the excitation influences the structural response. It has also been found that the frequency of the structure does not increase with the frequency of excitation if the latter exceeds the natural frequency of the pendulum, but in the post-resonance domain, it remains constant taking the value of the natural frequency of the system.

Description of the system composed by the structure and the friction pendulum has the geometry and essential dimensions described in [43].

The **shaking plate** is moved in the X direction with a feature of the SolidWorks program called Linear Motor. It can impose a displacement after a harmonic function.

Case 1 - for the **first simulations** following parameters were used: $\boldsymbol{A_{e1}}$**=5 mm** ensured by the command **Max Displacement** and nine frequencies $\boldsymbol{f_{e1}}$**=0.75 Hz;** $\boldsymbol{f_{e2}}$**=1 Hz;** $\boldsymbol{f_{e3}}$**=1.5 Hz;**

f_{e4}=2 Hz; f_{e5}=2.5 Hz; f_{e6}=3 Hz; f_{e7}=3.5 Hz; f_{e8}=4.5 Hz and **f_{e9}=6 Hz**, ensured by the command **Frequency**.

The pendulum's sliding surface is realized as a cylindrical material extrusion applied to the shaking plate. In this stage of the research the **radius R=260 mm** was selected and the analysis **time** was set for **10 seconds**. The contact between the structure and the shaking plate was simulated considering the **static and dynamic friction coefficients μ_D and μ_S** presented in Table 4.5.

Table 4.5 Contact condition - friction coefficients

Contact case	Components	Contact type	μ_D [-]	v_D [mm/s^2]	μ_S [-]	v_S [mm/s^2]
1	Structure	Steel (dry)	0.25	10.16	0.3	0.1
	Shaking plate	Steel (dry)				
2	Structure	Acrylic	0.05	10.16	0.08	0.1
	Shaking plate	Steel (greasy)				
3	Structure	Custom	0.03	10.16	0.05	0.1
	Shaking plate					

Case 2 - the analyses in the **second stage** are made for a **time** length of **30 seconds** and an excitation with **A_{e2}= 10 mm** and **f_{e2}=1 Hz**. Several radii of the sliding surface were selected for this stage of the study.

The initial **radius** was R_1=110 mm and afterwards it was step-by-step modified by increasing it with 50 mm until the radius value R_{18}=960 mm was achieved. The three considered contact conditions are indicated in Table 4.5.

The simulation **results for the first study (Case 1)** are presented in Figure 4.10, where the **acrylic/steel contact** is considered. The **FP** with **R_4=260 mm** has $f_{n4} = 2\pi\sqrt{R_4/g} = 0.9774\ Hz$, determining the occurrence of resonance at this excitation frequency. The largest displacement is expected at this excitation and it is really achieved, Figure 4.11 confirming it. Estimating the response frequencies f_{struc} from Figure 4.10, one can observe that this frequency increases until the natural frequency f_n of the system is achieved and stop increasing if $f_e > f_n$. In the post-resonance domain $f_{struc} = f_n$.

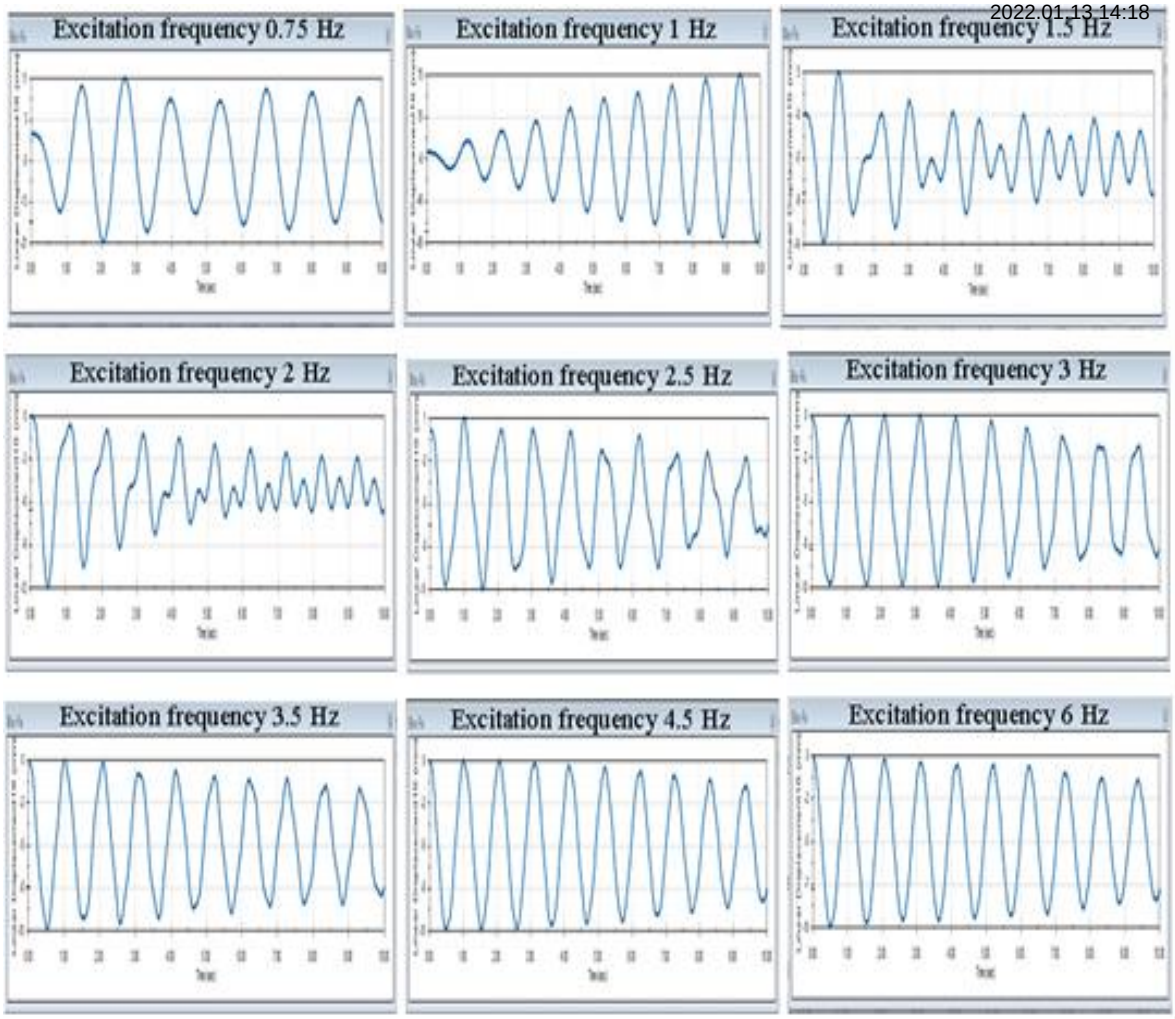

Figure 4.10 Elongation achieved in X direction for the structure isolated by SFPs with acrylic pivots and stainless steel sliding surfaces

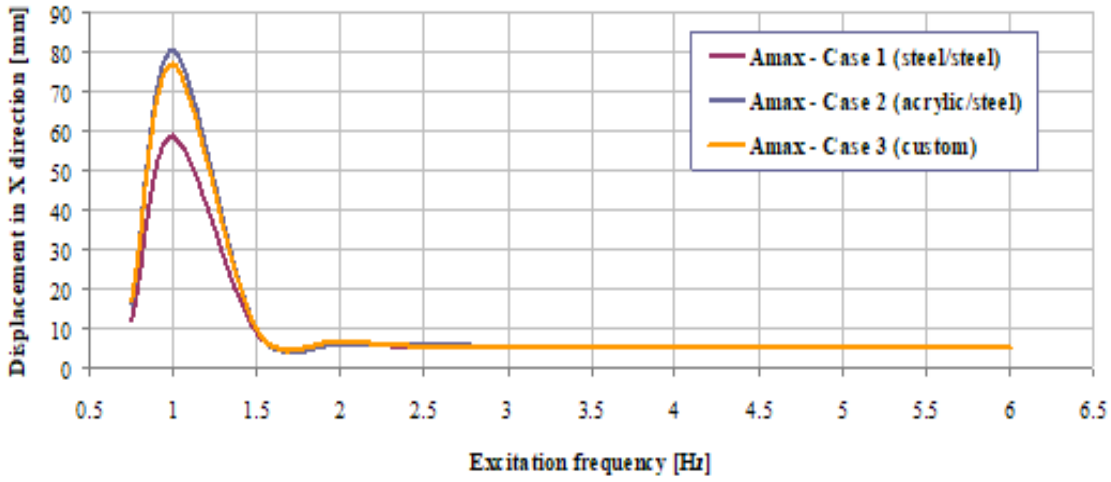

Figure 4.11 Elongation achieved in X direction for different frequencies of the excitation

If $f_e > \sqrt{2} f_n$, the displacement of the structure A_{max} is smaller as the ground motion A_e and so a good isolation is accomplished. Moreover, because the frequency of the isolated structure does not increase if f_e exceeds f_n clearly results that the acceleration amplitude do not change. In consequence, the best seismic isolation is ensured by the analyzed SFP for excitation **frequencies** above **3 Hz**, but an acceptable level of isolation is ensured also if f_e is in the range **1-3 Hz**.

Next results reflect the research made by considering **different friction coefficients and pendulum radii** in the condition that the excitation **frequency is maintained unchanged**. The responses of the structure in terms of displacements in the horizontal direction X are given in Figure 4.12 for the resonance was passed, while the Figure 4.13 shows the behavior in the post-resonance domain.

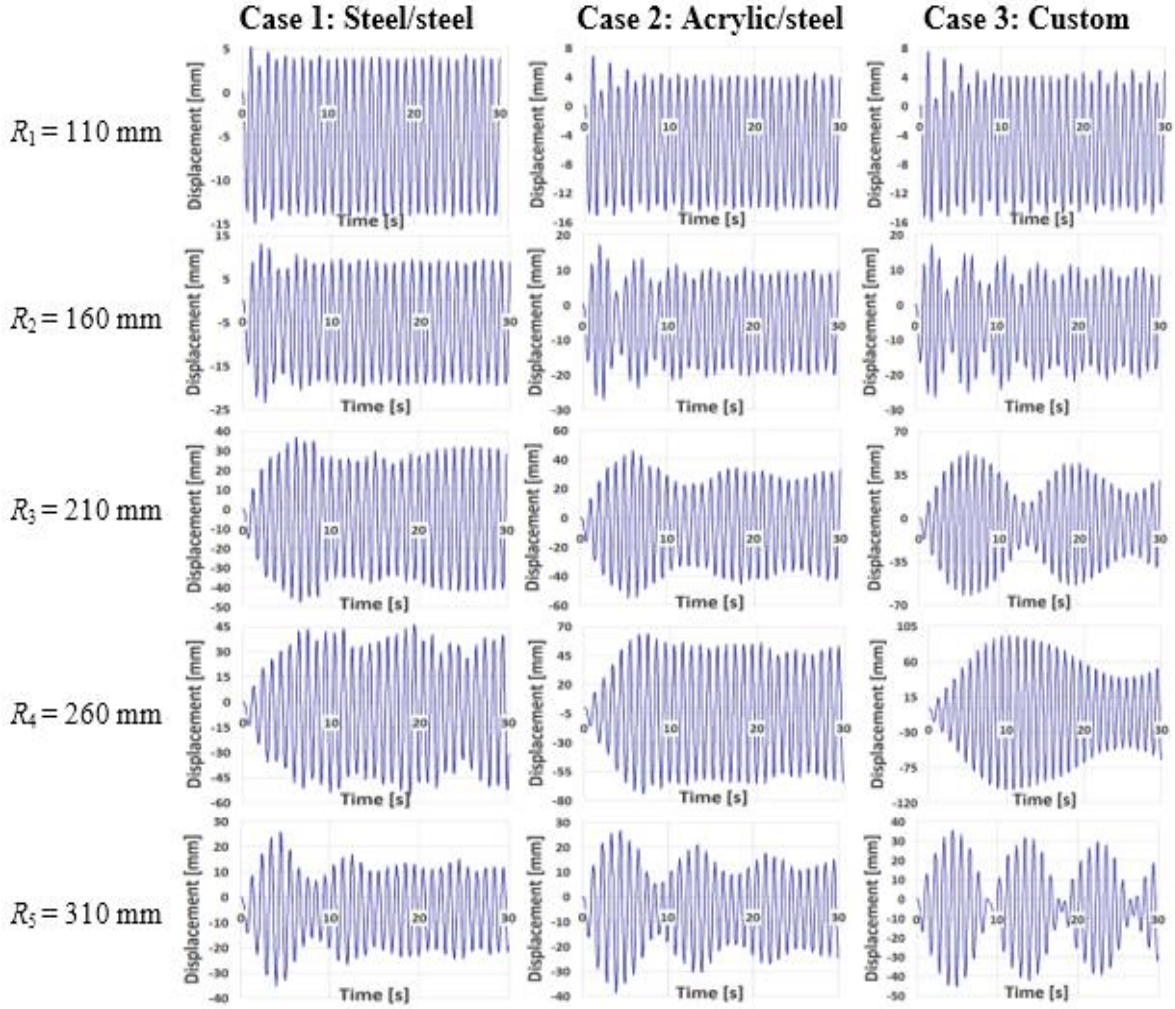

Figure 4.12 Structural displacement evolution with the pendulum radii increase until the resonance is passed

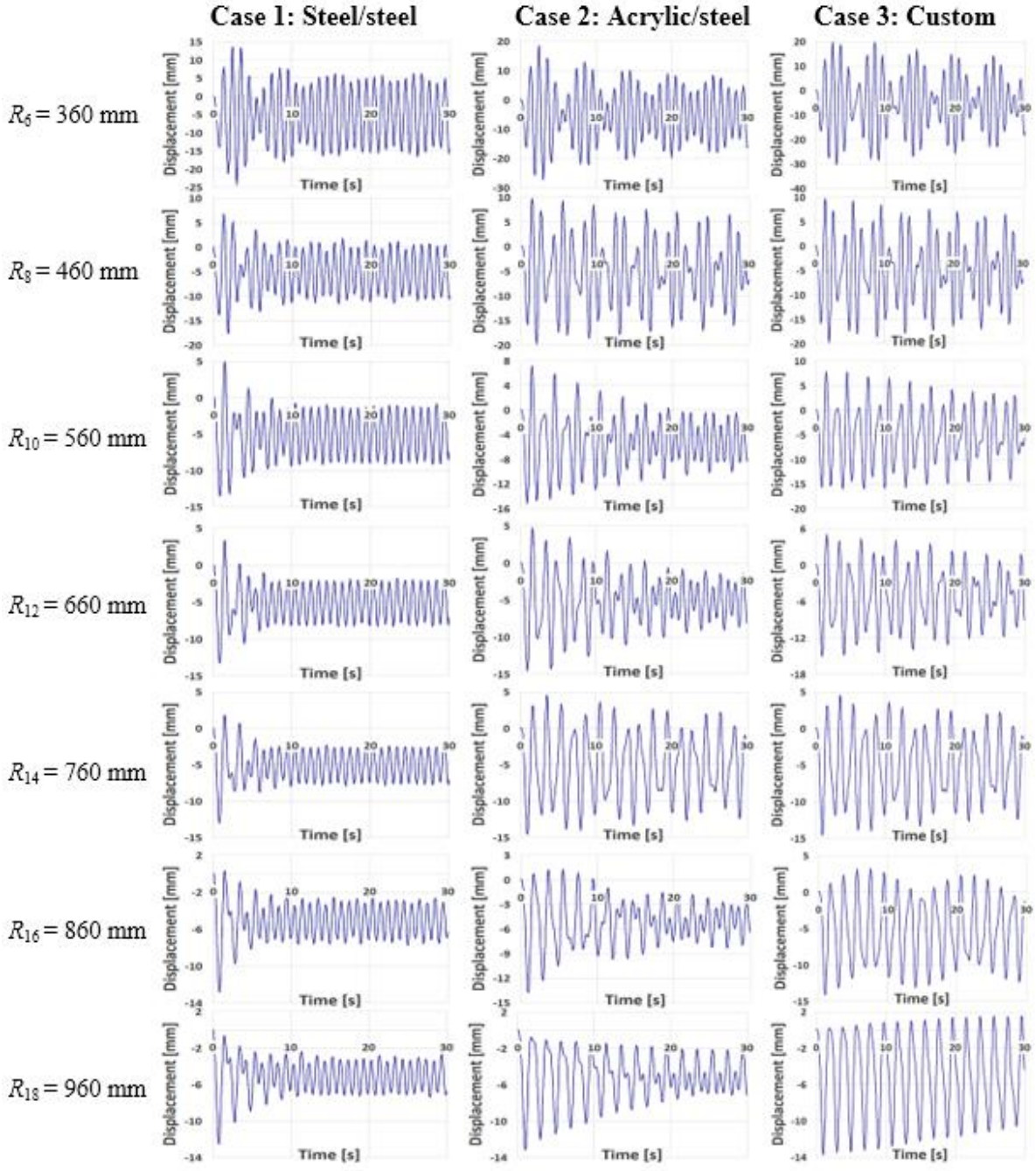

Figure 4.13 Structural displacement evolution with the pendulum radii increase in the post-resonance domain

From Figure 4.14 it can be observed that the effective isolation is assured for **radii** bigger then **610 mm** for all the three friction coefficients. In consequence, for the excitation frequency f_{e2}**=1 Hz** considered in the second stage of the study, the friction pendulum should fulfill this condition. Evidently, for friction pendulums working in real conditions, their design must consider the significant earthquake period *T* that is expected in the region of the isolated

structure. Another conclusion rising from Figure 4.14 refers to the amplitude achieved in resonance; the higher the friction coefficient, the lower the amplitude is. Also, it ca be observed here that the friction coefficient does not affect the resonance frequency.

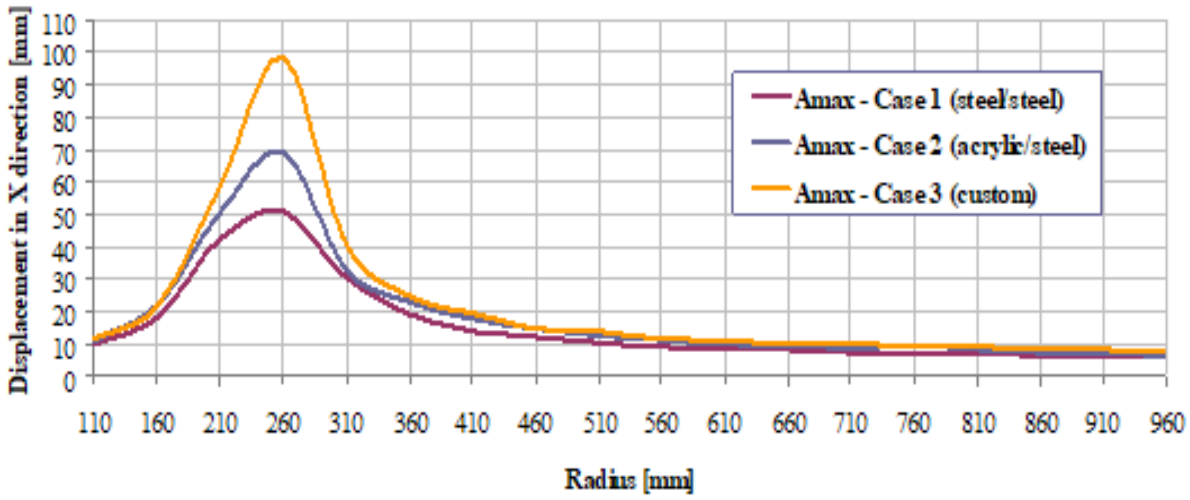

Figure 4.14 Maximum amplitudes for the different pendulum radii
and the three friction coefficients

It was found that the best isolation is achieved if the excitation frequency exceeds 1.5 times the natural frequency of the friction pendulum. This natural frequency is not influenced by the weight of the structure and the friction coefficient has also a low influence, but if it has higher values the amplitude of the oscillation decrease. Hence, these two parameters have a low influence on the dynamic behavior of the isolated structure. On the other hand, the pendulum radius has a significant influence on this behavior, since it is the parameter controlling the natural frequency of the pendulum.

It was finally concluded that isolation can be made either by dissipating energy by ensuring a certain significant friction coefficient or by permitting a large relative displacement between the ground and the structure and avoiding in this way significant acceleration of the structure. The two constructive parameters, namely the friction coefficient and the pendulum radius, must be carefully adapted in both design cases.

4.5. Comparison of the performance of friction pendulums with uniform and variable radii

The study described in the following aimed to find the influence of the curvature of the sliding surface on the response of the isolated structure under harmonic excitations.

To this aim, friction pendulums were designed which differ by the shape and dimension of the cylindrical sliding surface, respectively by the friction coefficients. Our target was to find out how the structure responds to a given excitation when the structure is equipped with diverse friction pendulums. A sinusoidal excitation with the frequency of 1 Hz is applied and the response in terms of displacements is captured. It was found that the frequency of the structure does not change with the FP radius but the amplitude of the displacement is strongly dependent on this parameter. Because the circular and elliptical sections of the FP provide the structure with different natural frequencies, the resonance is achieved at other radii.

To obtain the response of a rigid structure isolated with diverse FPs, SolidWorks simulations were performed, in particular by using the Motion module. The isolated structure's 3D geometrical model is described in [44].

Simulations are made in the following conditions:

- The **base plate**, which is set as a reference, is fixed;
- The **shaking plate** simulating the horizontal trepidation of the earth is harmonically moved in the X direction. This is made with the help of the Linear Motor, a feature of SolidWorks Motion module. It imposes a **Max Displacement A=10mm** by a **Frequency f_{exc} = 1 Hz**.
- The **gravitational acceleration** is set by default as g=9806.65 mm/s^2 and is oriented in the Y direction;
- The **time** for this study is imposed as **30 seconds**;

In this study, the mentioned parameters are maintained unchanged, but the **radii** of the sliding surfaces are modified by each simulation. However, for all simulations these are modeled as an extrusion applied to the shaking plate.

Case 1 - for the **first set of simulations**, the base of the cylinder used for extrusion is a **circle**, the **radius** being modified in the range **R = 110 ÷ 960 mm** by a 50 mm pitch. The depth of the **extrusion** is **4 mm**, therefore the minimum **thickness** of the **shaking plate** under the

pendulum is **6 mm**. A suggestive image showing all radii used to create of the FP is given in Figure 4.15.

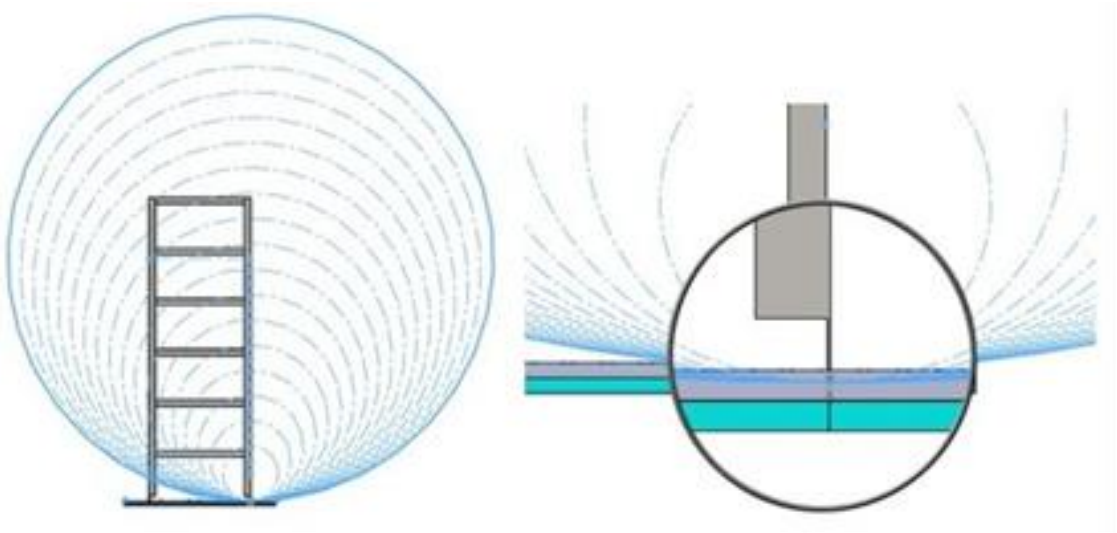

Figure 4.15 The extrusions made with a circular shape

The contact condition between the structure and the sliding surface is bounded contact with friction, the friction coefficient μ being dependent of the chosen materials. Note that the friction coefficient depend on the relative speed beteen the two components in contact. The values for the first two cases presented in Table 4.6 were taken from the SolidWorks library, while for the third case the values were defined to achieve a lower damping.

Table 4.6 Contact condition

Contact case	Components	Contact type	μ_D [-]	v_D [mm/s^2]	μ_S [-]	v_S [mm/s^2]
1	Structure	Steel (dry)	0.25	10.16	0.3	0.1
	Shaking plate	Steel (dry)				
2	Structure	Steel (greasy)	0.05	10.16	0.08	0.1
	Shaking plate	Steel (greasy)				
3	Structure	Teflon	0.03	10.16	0.05	0.1
	Shaking plate	Steel (greasy)				

In the absence of friction between the structure and the sliding surface, the natural frequency f_n of a rigid structure isolated with a FP is found from the mathematical relation 4.1. From relation 4.1 clearly results that f_n is independent of the weight of the structure.

If subjected to a harmonic excitation f_{exc}, the structure oscillates in respect to the two mentioned frequencies. When the relation between the two frequencies is $f_n < f_{exc}$, the frequency of the structure is the frequency of the excitation. If $f_n > f_{exc}$, the system maintain its natural frequency no matter how big the frequency of the excitation is. When the two amplitudes achieve close values, the amplitude of the oscillation increases dramatically, and for equal frequencies the resonance is attained. The amplitude resulted in resonance depends on the friction coefficient; the smaller the friction coefficient, the bigger the amplitude is.

Case 2 - for the **second set of simulations**, for extrusion were used cylinders that have **elipses** at the base. The **semi-major axis** of the **ellipse** is allways $\boldsymbol{R_V}$**= 960 mm**, while the **semi-minor axis** is modified in the range $\boldsymbol{R_H}$ **= 110 ÷ 960 mm** by a 50 mm pitch, as shown in Figure 4.16. Because the slope of the sliding surface is significantly bigger for the case ellipse 110-960 than for the case radius 110, it was expected in the case of the sliding surface having constructed with an eliptical cylinder to get no relative displacement between the structure and the shaking plate. It was also anticipated to achieve the resonance at higher values of the semi-minor axis of the ellipse as the radius of the cylinder.

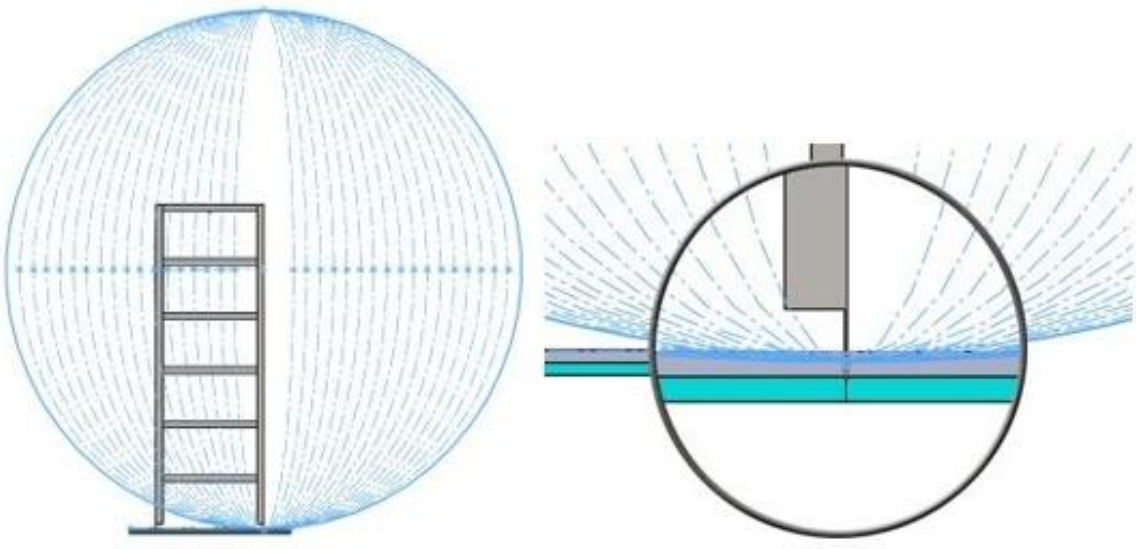

Figure 4.16 The extrusions made with an elliptical shape

It is no relation presented in the literature for determining the natural frequency of the elliptical FP, thus the behavior in terms of frequencies and amplitudes of the oscillation of the

isolated structure cannot be predicted. In order to clarify this aspect, simulations were performed with elliptical FPs.

Figure 4.17 presents the signals in the time domain and the frequency domain (by FFT representation) for three typical behaviors of both the FPs. In the left column in this figure it is represented the analysis for a pre-resonance behavior, in the central column the behavior in resonance and in the right column the behavior in post-resonance. The **friction coefficient** is chosen for the contact **case 1** (steel dry – steel dry).

***R* = R_H = 160 mm; R_V=960 mm** ***R* = 260 mm; R_H = 460 mm; R_V=960 mm** ***R* = R_H = 910 mm; R_V=960 mm**

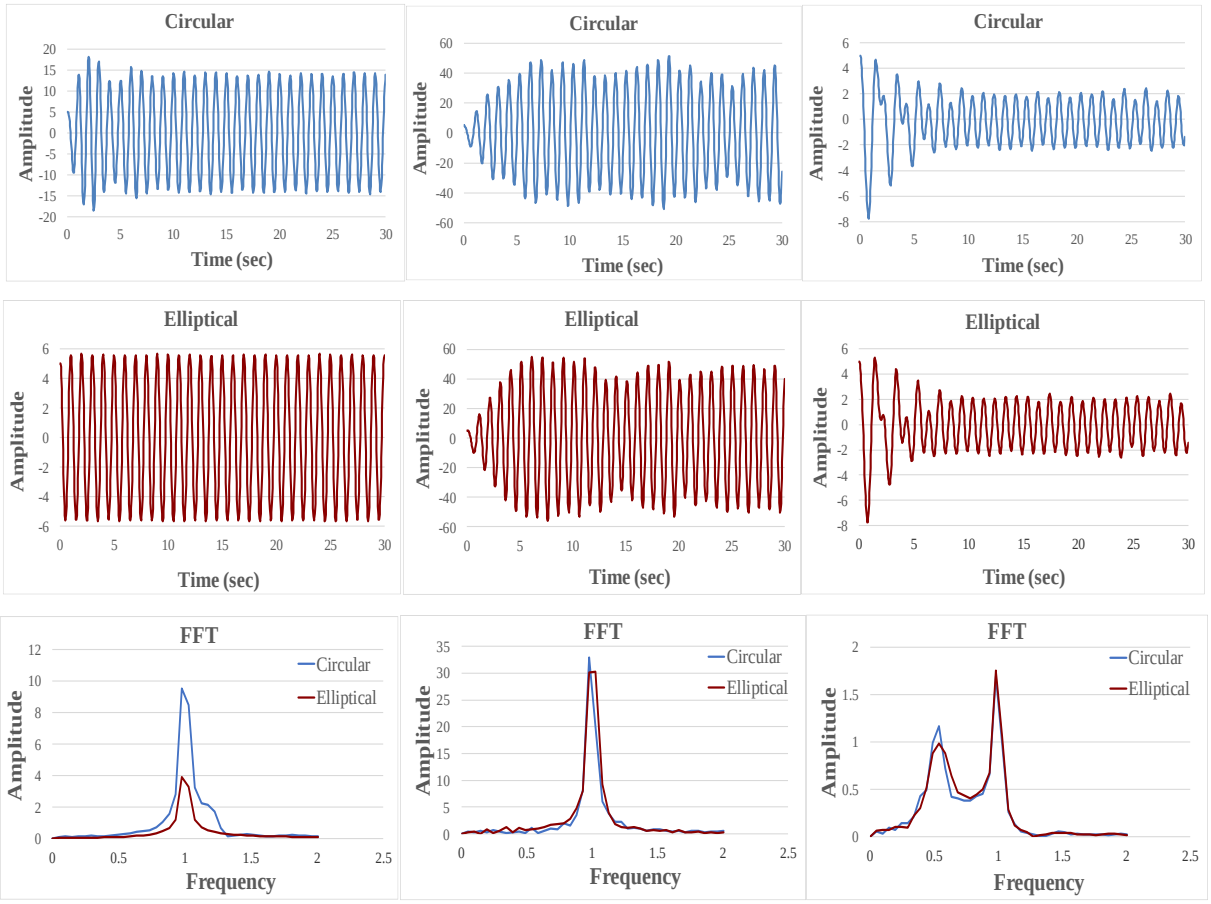

Figure 4.17 Response signal captured from the isolated structure
for different friction pendulum radii

Figure 4.18 offers a comprehensive image on the behavior of the structures when it is isolated with FPs that have all considered radii and both circular and elliptic cylindrical shapes. In this figure, the minim and maxim values of the structure's displacements in the X direction are indicated in order to show for which horizontal radii the resonance is achieved.

One can observe in Figure 4.18 that, as expected, the resonance is achieved for smaller values of R in comparison with R_H. This determines a bigger pre-resonance domain for the elliptical FP, while the post-resonance is earlier achieved by the FP constructed with a circular cylindrical sliding surface. The magnitudes of the curves represented in Figure 4.18 are quite similar for similar friction coefficients. Because the magnitudes are extracted from the signals by involving the FFT, just coarse values are obtained. To precisely estimate the magnitudes an advanced signal processing algorithm is requested [95].

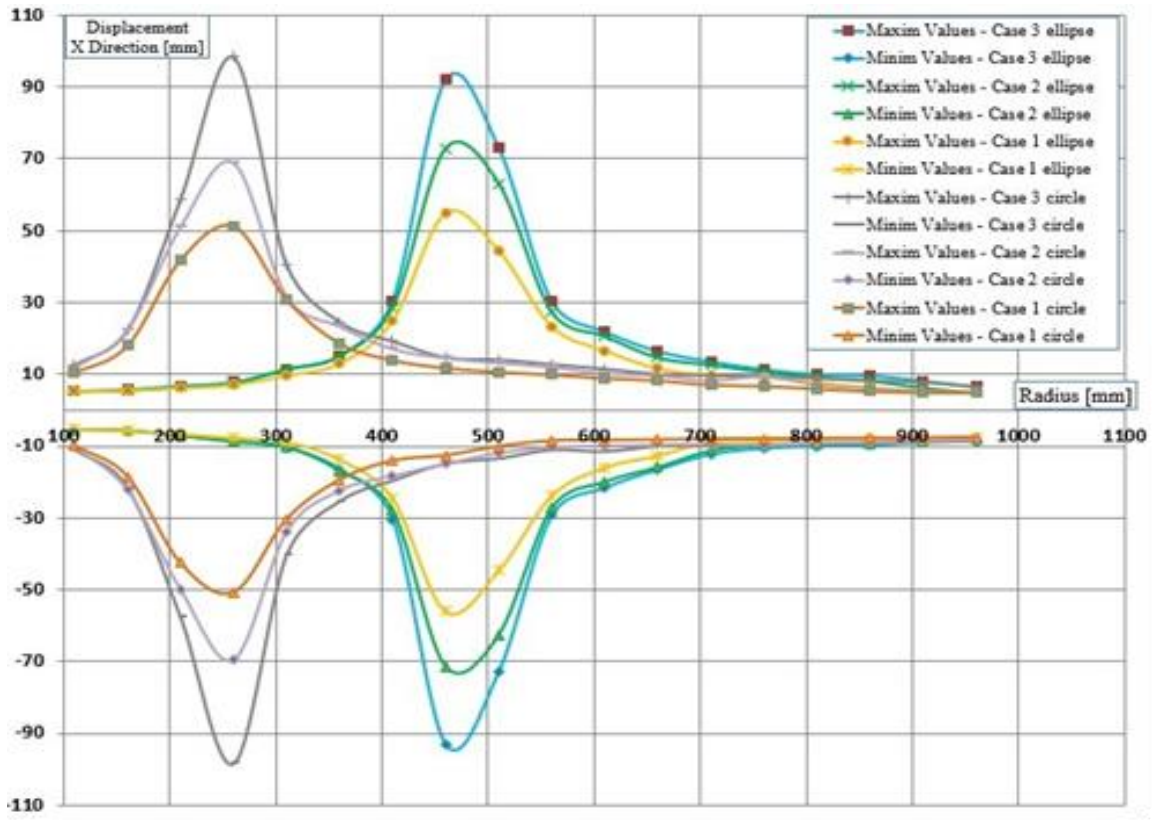

Figure 4.18 Maximum and minimum displacement amplitudes

It is possible to control the occurrence of resonance by changing the semi-minor axis of the ellipse, therefore it is possible to design the FP in order to work in pre- or post-resonance depending on the parameters (frequency and amplitude) expected for the ground excitation. For both sets of pendulums, it was concluded that the best isolation of the structure is achieved when the natural frequency of the pendulum is at least 1.5 times lower than the ground excitation.

It was also found that the friction coefficient has the same influence on the amplitudes of the structure's response if the FP has the same natural frequency. This is best visualized at resonance, the curves in Figure 4.18 achieving approximately the same magnitude.

4.6. Study on the behaviour of the isolated structures with friction pendulums and a counterweight

The aim of the study is to identify the behavior of the isolated structures with a friction pendulum and a counterweight, as well as the influence of the spring constant k to assure efficient isolation.

To determine the structural behavior, a model of a six-story building was created in SolidWorks software with the help of which the simulations were made [96]. In Figure 4.19 is presented the test structure generated in SolidWorks as an assembly with four parts: 1 – the **rigid structure**, made of steel bars with the dimensions 1200x400x200 mm; 2 – the **base plate** that is fixed and is used as a reference, with the dimensions 600x200x10 mm; 3 – the **shaking plate** reproducing the horizontal trepidation of the ground and has the same dimensions as the base plate; 4 – the **counterweight**, with the dimensions 100x150 mm and with the weight of **17.784 kg**, which is fastened with **2 springs** in the upper part of the structure and has the role of stabilizing the structure subjected to the horizontal trepidation of the earth.

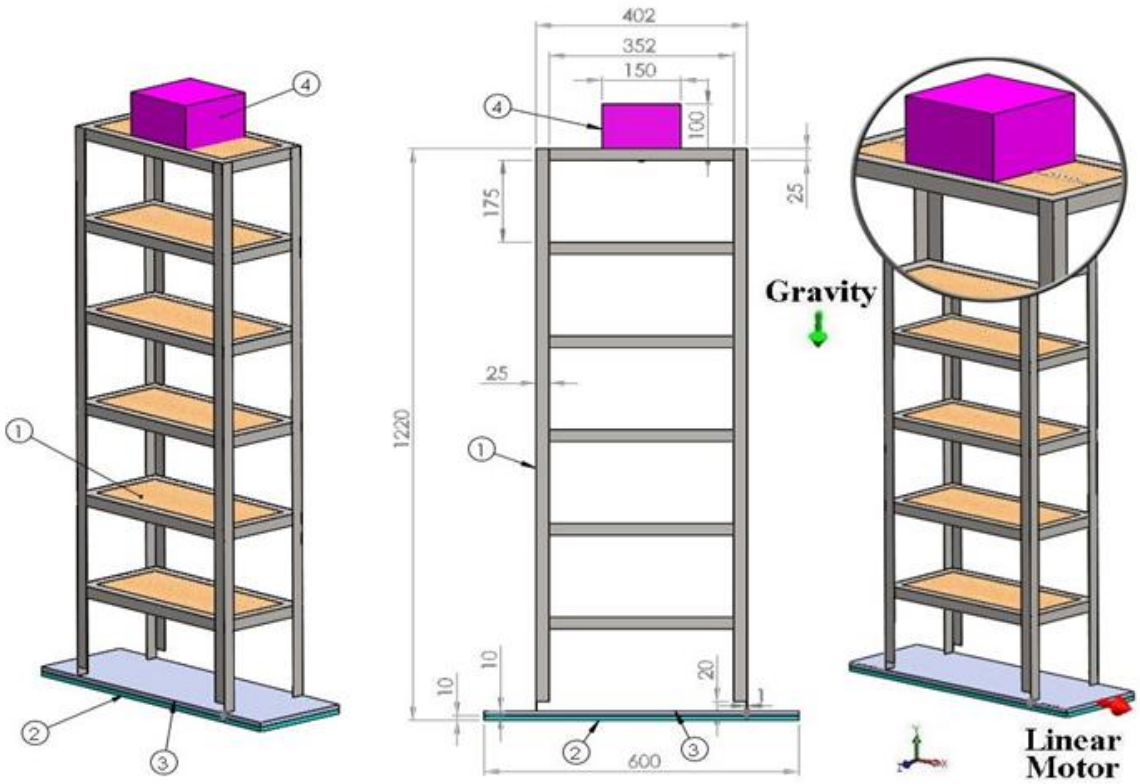

Figure 4.19 The test structure designed in SolidWorks

The simulations were performed in the SolidWorks Motion module, for the follow-ing conditions:

- The **base plate** is fixed and is used as a reference;
- The **shaking plate**, simulating the horizontal trepidation of the earth, is moved in the X direction with the help of the Linear Motor, a feature of the SolidWorks Motion module. It imposes displacement with the following parameters: Oscillating motion, **Max Displacement A=20mm**, **Frequency f = 1 Hz**, and **Shift=0 deg**;
- The **gravitational acceleration** is g=9806.65 mm/s2 and is oriented in the Y direction;
- A SolidBody **Contact with friction** is imposed between the structure and the sliding surface, the **friction coefficient μ** being dependent on the chosen materials. The contact between the structure and the shaking plate was simulated considering the static and **dynamic friction coefficients μ_D** and **μ_S**, respectively the **dynamic** and **static velocity coefficient v_D** and **v_S** presented in Table 4.7.
- For this study the **time** of analysis is imposed as **30 s**;
- The **counterweight** and the **structure** are caught by the edge of the steel bars, respectively the edge of the shaking plate by four springs. The **spring parameters** (k –spring constant, coil diameter, number of coils, wire diameter) are presented in Figure 4.20.

Table 4.7 Friction coefficients

Contact case	**Components**	**Contact type**	**μ_D [-]**	**v_D [mm/s^2]**	**μ_S [-]**	**v_S [mm/s^2]**
1	Structure	Steel (Greasy)	0.05	10.16	0.08	0.1
	Shaking plate	Steel (Greasy)				

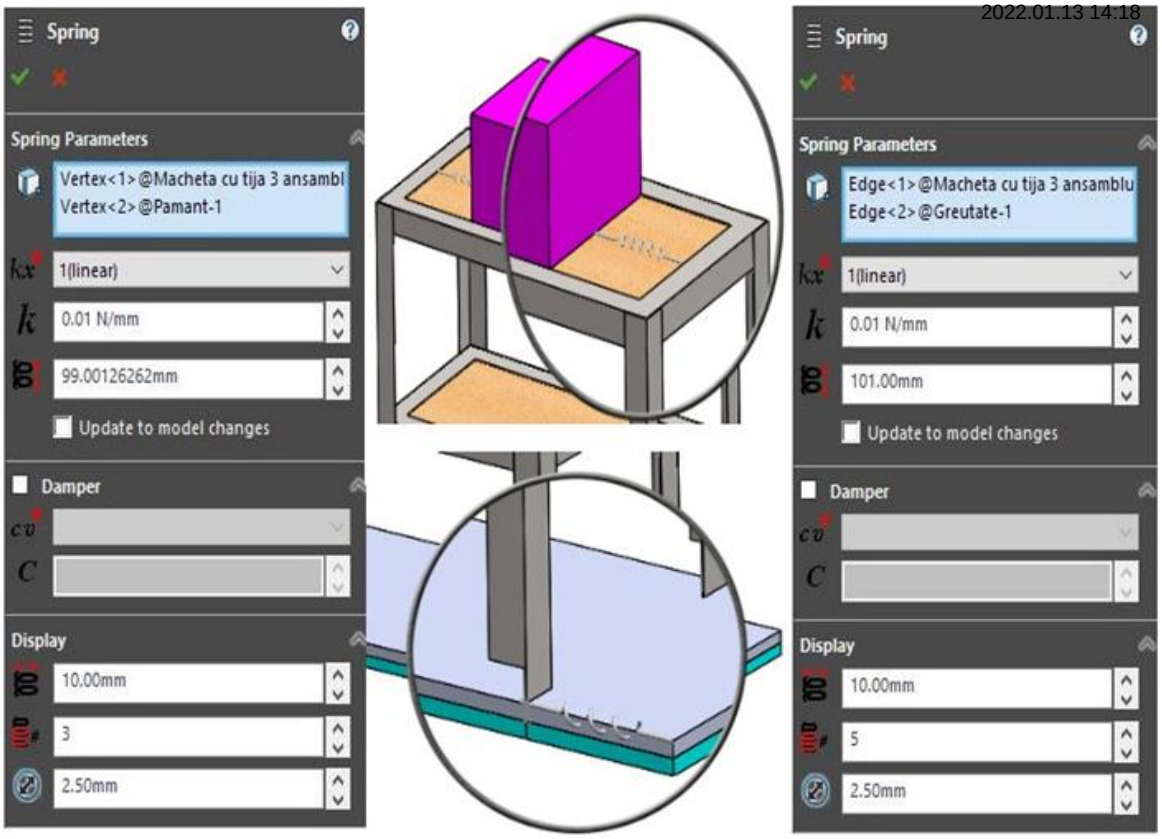

Figure 4.20 The springs position and parameters

Case 1 - in the first case of the research the contact between the structure and **the shaking plate** was simulated considering **the friction coefficients** presented in Table 4.7, but **without friction between the structure and the counterweight**. In this case, the **constant *k* of the springs** with which the structure is caught with the shaking plate it **remains unchanged (*k*=0.01 N/mm)**, while **the constant *k* of the spring** with which **the counterweight is caught is modified with each simulation (*k*=0.004÷0.01 N/mm).**

Case 2 - the simulations in the second case are made with **the same spring parameters and conditions from the first case**, both for the structure and the counterweight, but in this case, a **contact with friction between the structure and the counterweight** was also added. The contact between the structure – shaking plate and the structure – counterweight was simulated considering the static (μ_S) and the dynamic (μ_D) friction coefficients presented in Table 4.7.

The simulation results for the first case are presented in Figure 4.21 and Figure 4.22, where contact with friction is considered only between the structure and the shaking plate.

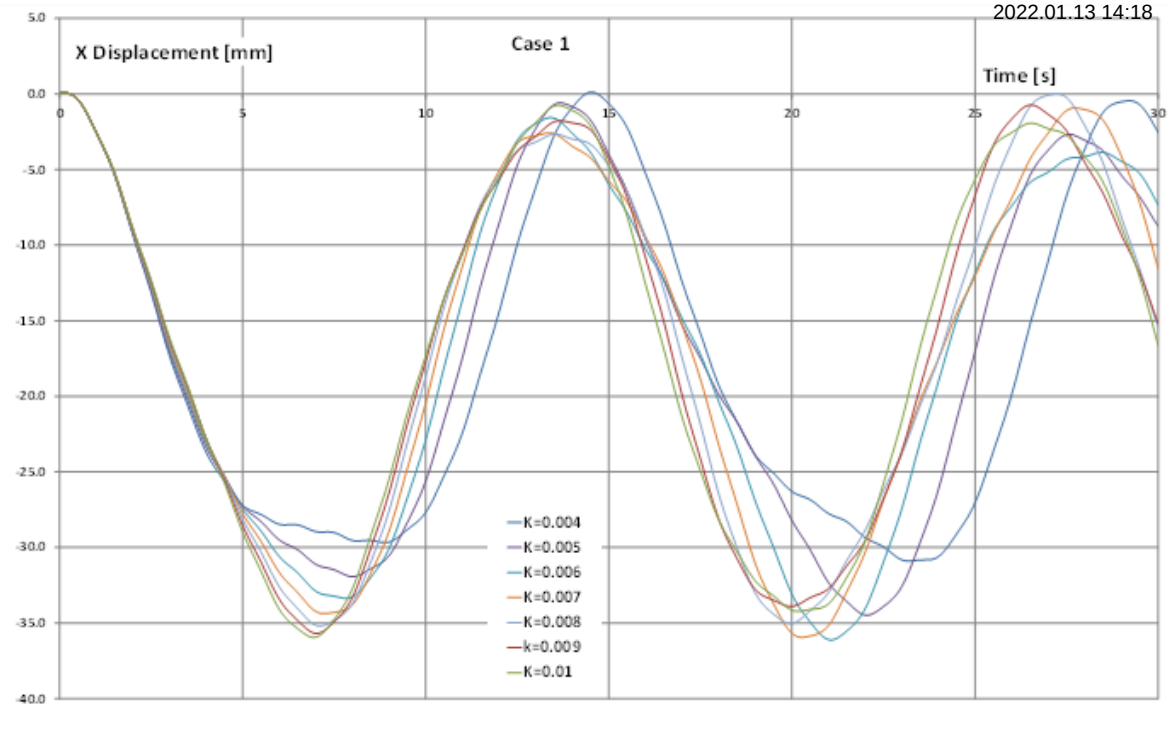

Figure 4.21 **Case 1** – Displacement between the structure and the base plate

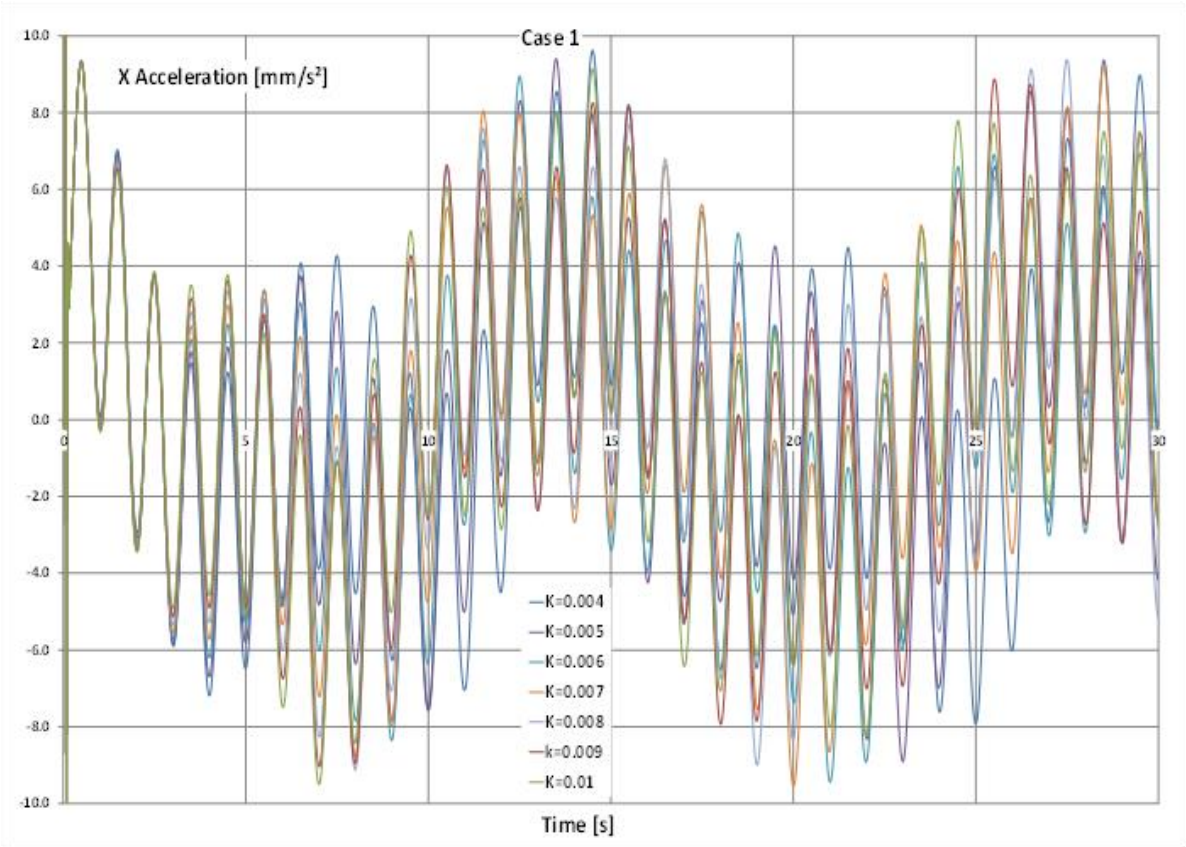

Figure 4.22 **Case 1** – The acceleration of the structure

One can observe that the acceleration and the displacement of the structure have been decreased as the spring constant *k* increased.

In the Figure 4.23 and Figure 4.24 are presented the results for the second case, considering contact with friction between the structure – base plate and the structure – counterweight.

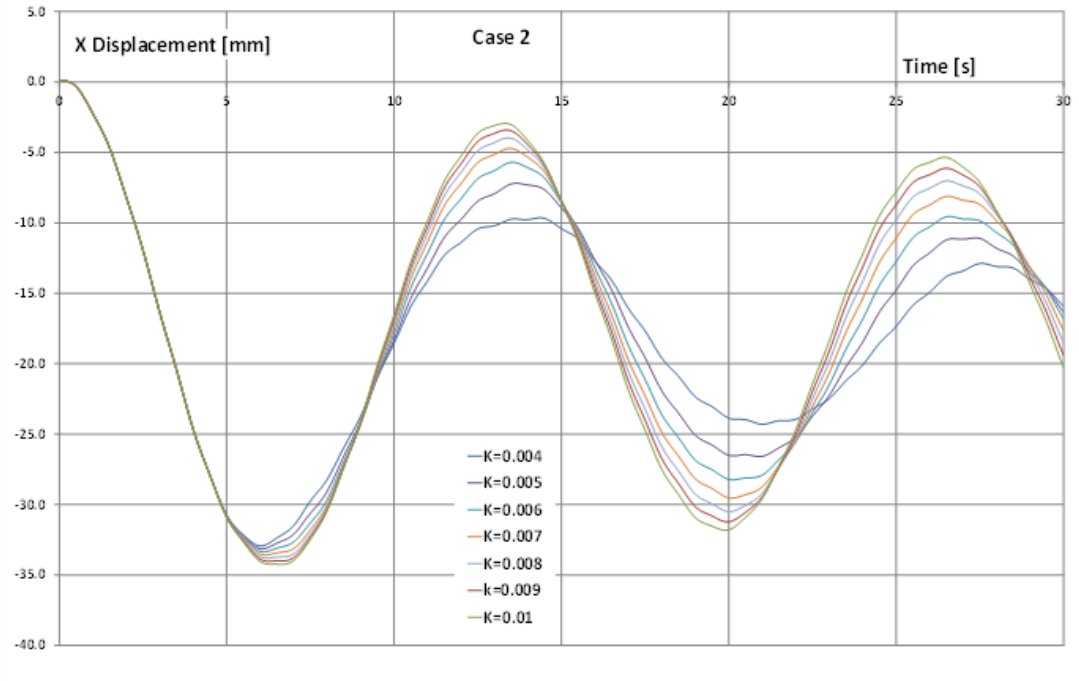

Figure 4.23 **Case 2** – Displacement between the structure and the base plate

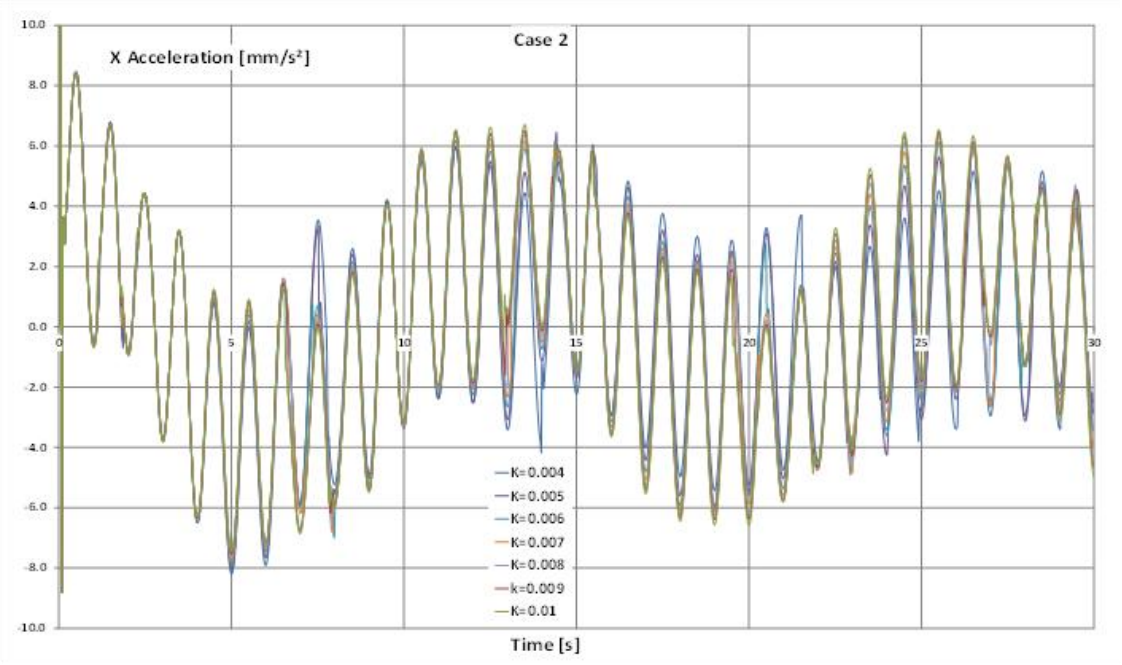

Figure 4.24 **Case 2** – The acceleration of the structure

From Figure 4.23 and Figure 4.24, one can observe that the acceleration and the displacement of the structure decreased, even more than in the first case, when the second friction contact between the structure and the counterweight was added. This means that to have better isolation, both contacts with friction (structure - base plate and structure - counterweight) must be considered.

The next two figures present a comparison between the results from the **Case 1** and the **Case 2**. The analysis is made to find the best constructive solution in regard to the surface and mass.

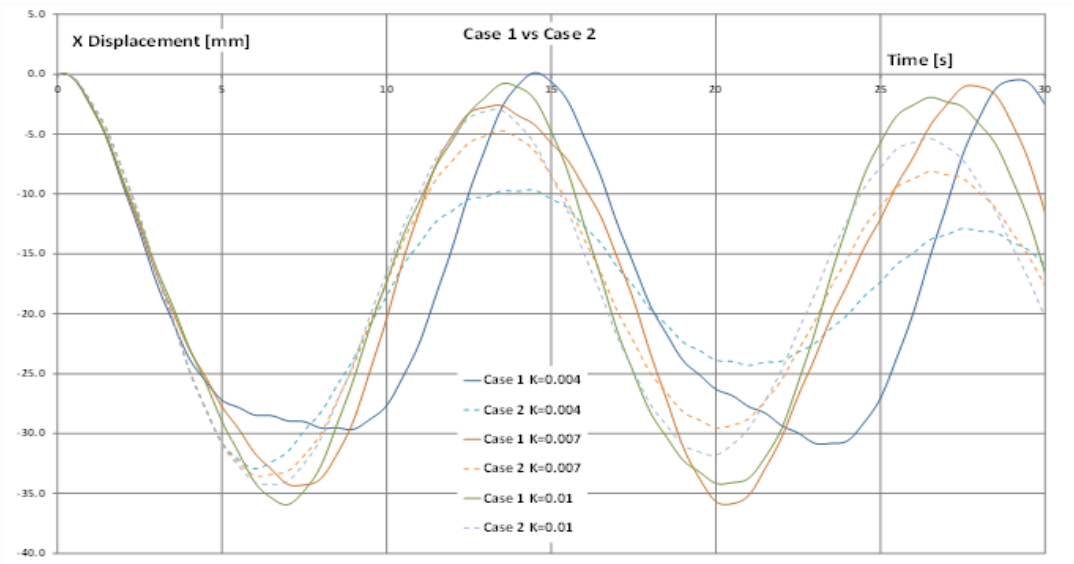

Figure 4.25 Displacement - **Case 1 vs Case 2**

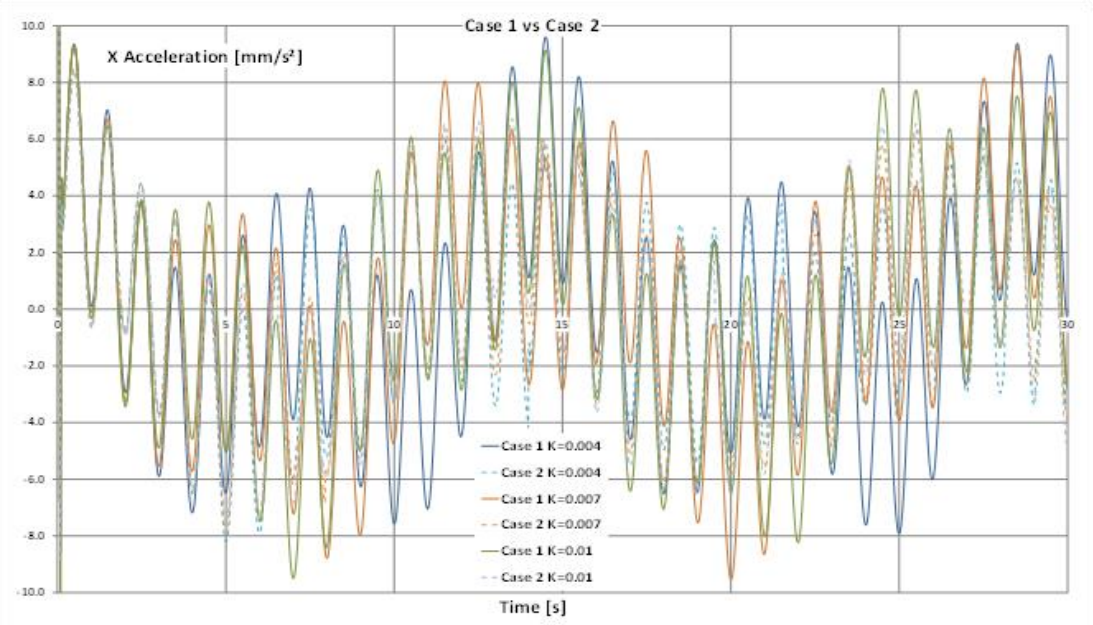

Figure 4.26 Acceleration - **Case 1 vs Case 2**

4.7. Conclusions and contributions

The studies presented in this chapter show the results of simulation made on a rigid structure isolated with four simple friction pendulums. A model in SolidWorks was designed and used to find out how the pendulum radii and friction coefficients, respectively the frequency of the excitation, influences the structural response.

The study regarding ***the effect of a simple friction pendulum radius on the response of isolated structures*** revealed the frequency at which the chosen friction pendulums ensure efficient isolation. Also, it revealed the frequency domain in which the displacement of the structure is important. It was found that efficient isolation is provided if the radius is bigger than 600 mm in the case of exciting the structure with an oscillation having the frequency of 1 Hz and the amplitude of 10 mm. In addition, from the response signal's time history, an amplitude increase is observed if the excitation frequency is in a narrow band around pendulum's natural frequency.

In the research regarding the ***response of a structure isolated by friction pendulums with different radii*** was found that an effective isolation is achieved for radii bigger then 610 mm. This means that, the friction pendulum must be designed to fulfill this condition, or, if the sub-resonant domain is chosen the radius must be small enough to avoid approaching the resonance. Obviously, design must consider the expected relevant period of the earthquake. Comparing the results with those of other simulations made for similar circumstances, but for different friction coefficients and excitation frequencies, it was noticed that the frequency ration *r* at which resonance is achieved moves to lower values for a bigger friction coefficient. Also, the amplitude in the resonance is smaller for the bigger friction coefficients.

Also, it was found that the biggest amplitude is achieved for a natural frequency of the system that is similar with the excitation frequency. On the other hand, an effective isolation is obtained for frequency ratios *r* bigger then 1.4. For values of the friction pendulum radii ensuring this condition the amplitudes, in the transitory as well as that in the stabilized regime, accomplishes smallest values. In the stabilized regime, the structural displacement is half of the excitation amplitude.

In the study regarding ***the effect of the friction coefficient and the pendulum radius on the behavior of structures isolated with simple friction pendulums*** it has been found that the frequency of the structure does not increase with the frequency of excitation if the latter exceeds the natural frequency of the pendulum, but in the post-resonance domain, it remains constant taking the value of the natural frequency of the system. The results of simulation made

for this study show that the best isolation is achieved if the excitation frequency exceeds 1.5 times the natural frequency of the friction pendulum. The natural frequency is not influenced by the weight of the structure and the friction coefficient has also a low influence, but if it has higher values the amplitude of the oscillation decrease. Hence, these two parameters have a low influence on the dynamic behavior of the isolated structure. On the other hand, the pendulum radius has a significant influence on this behavior, since it is the parameter controlling the natural frequency of the pendulum. It was finally concluded that isolation can be made either by dissipating energy by ensuring a certain significant friction coefficient or by permitting a large relative displacement between the ground and the structure and avoiding in this way significant acceleration of the structure. The two constructive parameters, namely the friction coefficient and the pendulum radius, must be carefully adapted to ensure efficient isolation.

In the research regarding the ***comparison of the performance of friction pendulums with uniform and variable radii*** a friction pendulum was developed which differs by the shape and dimension of the cylindrical sliding surface, respectively, by the friction coefficients, to find out how the structure responds. It has been found that the frequency of the structure does not change with the FP radius but the amplitude of the displacement is strongly dependent on this parameter. Because the circular and elliptical sections of the FP provide the structure with different natural frequencies, the resonance is achieved at other radii. Also, it was observed that it is possible to control the occurrence of resonance by changing the semi-minor axis of the ellipse, therefore it is possible to design the FP in order to work in pre- or post-resonance depending on the parameters (frequency and amplitude) expected for the ground excitation. For both sets of pendulums, it was concluded that the best isolation of the structure is achieved when the natural frequency of the pendulum is at least 1.5 times lower than the ground excitation. It was also established that the friction coefficient has the same influence on the amplitudes of the structure's response if the FP has the same natural frequency.

The last study regarding ***the behavior of the isolated structures with friction pendulums and a counterweight*** is made on a combination of isolation systems consisting of sliding surface and tuned mass at which the connection between the structure and the ground is ensured by springs. For this system it was found that the best isolation is achieved if the spring constant *k*, with which the mass is caught, is higher and if there are two surface contacts with friction. The two constructive parameters, namely the spring constant and the friction coefficient, must be carefully adapted to achieve efficient isolation.

5. EXPERIMENTAL RESEARCH

5.1. Description of the experimental stand

To validate the results obtained by dynamic simulations, experimental tests were designed and performed on a small-scale model. The experimental tests were realized on a shaking table (Figure 5.2) designed in the Laboratory for studying the seismic actions of the Babeş-Bolyai University.

The experimental stand is composed of the elements described below, where the position number corresponds to the number in Figure 5.1:

1. shaking plate;
2. sliding supports;
3. chassis;
4. control box;
5. control box support;
6. electric motor;
7. electric motor support;
8. crank mechanism;
9. linear rolling bearings;

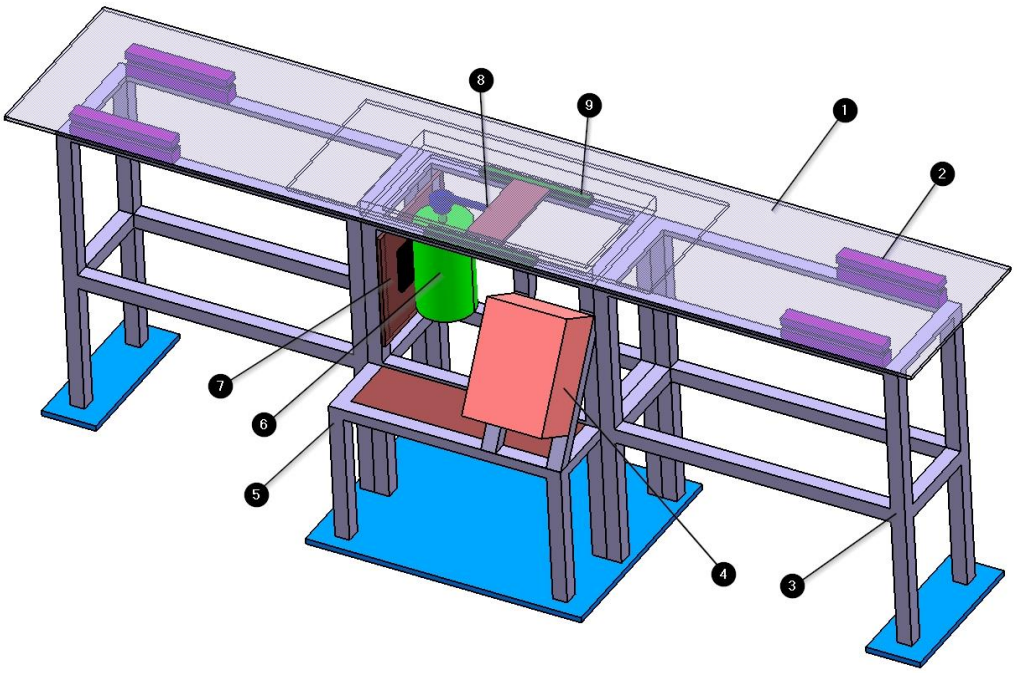

Figure 5.1 Experimental stand

The electric motor (6), the 2 linear rolling bearings (9), and the 4 sliding supports form the actuation system. With the help of the electric motor (6) and the crank mechanism (8), the rotational movement is transformed into a translational movement. During operation, the shaking plate (1) executes a linear reversible displacement. The automatic control system (4) commands the frequency of the shaking plate (1) and the speed of the electric motor (6). The shaking plate (1) has the dimensions 2500x500 mm and, together with the sliding supports (2), is mounted on the chassis (3).

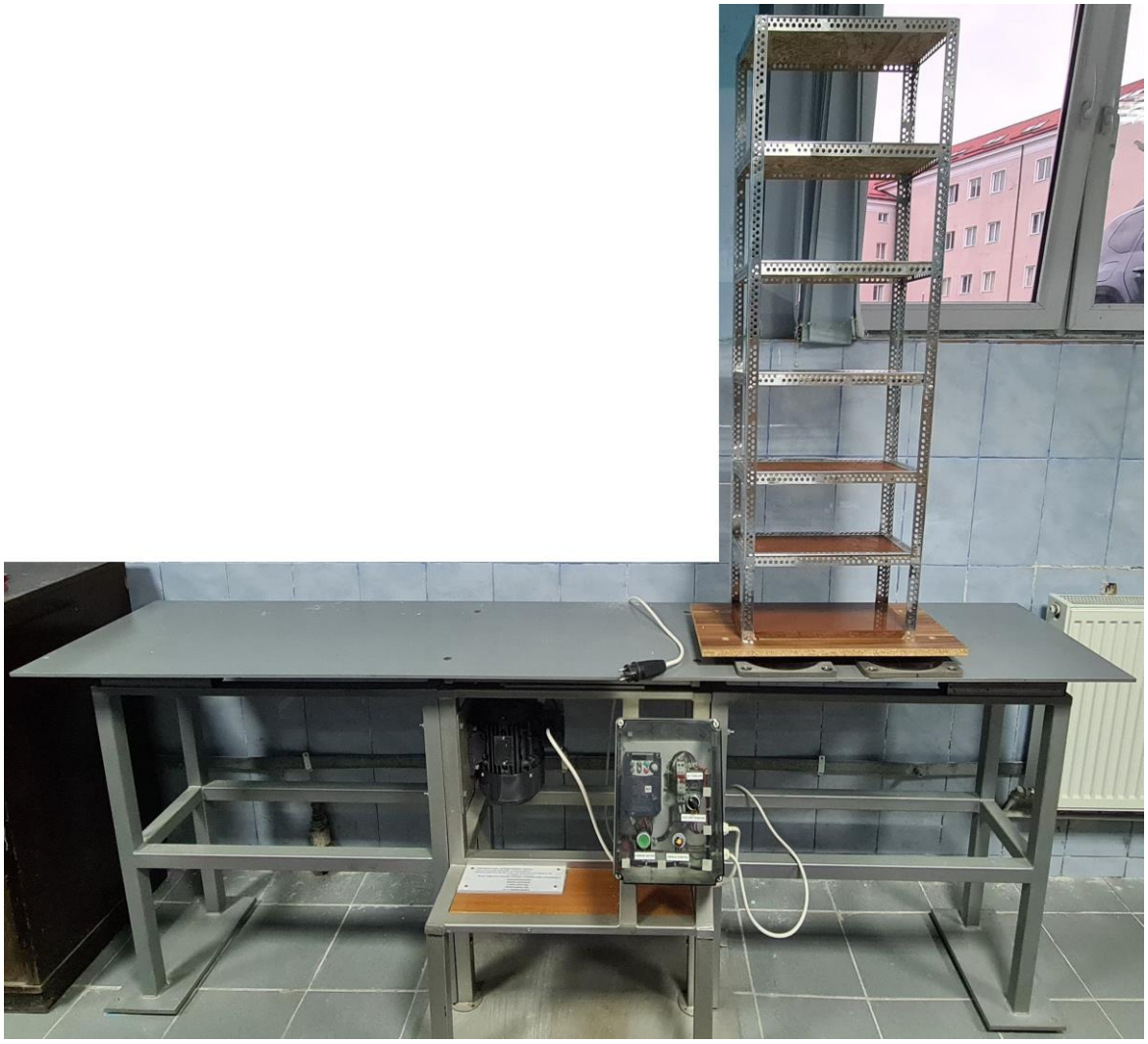

Figure 5.2 Experimental stand for determining the dynamic characteristics of a rigid structure isolated with friction pendulums

A FRENIC-Mini frequency converter was used for the electric drive of the motor, presented in Figure 5.3.

Figure 5.3 FRENIC-Mini frequency converter

The characteristics of the frequency converter are:

- power range: - 0.1kW - 2.2kW (200V single-phase power supply);
  - 0.4kW - 4.0kW (400V three-phase power supply);
- frequency: max. 400 Hz;
- energy saving function;
- built-in PID control;
- potentiometer included on the console for setting the reference;
- simplified torque control algorithm;
- braking unit included, accepts external braking resistance;

Among the most important advantages of this type of converter are voltage-frequency control, an increase of safety and precision in the operation of the machine, smooth starting and stopping of motors and mechanisms, and elimination of the shocks induced to the resistance structure, being eliminated the sudden starts / stops.

Besides the FRENIC-Mini frequency converter, the control box contains the following components:

- a start button (Figure 5.4);
- a direct on-off switch (Figure 5.5);
- a control potentiometer (Figure 5.6);
- a PLN4-C10 / 1N bipolar modular automatic fuse (Figure 5.7).

All these components are mounted in a PCT 121609 EURONORD box.

Figure 5.4 Start button

Figure 5.5 Direct on-off switch

Figure 5.6 Control potentiometer

Figure 5.7 Automatic fuse

The electric motor (Figure 5.8) is from the TechTop company, model T1A 90S-6, they are ideal for any kind of general purpose application in which the starting torque performance and low weight are key factors.

Figure 5.8 The electric motor (model T1A 90S-6)
used to drive the table

The technical data sheet of the electric motor is presented in the Table 5.1.

Table 5.1 Technical data sheet of the electric motor (model T1A 90S-6)

General data		
Frame size	90	
Housing material	Aluminum	
Install model	According to the standard	
Type of feet	Removable feet	
Net weight	11.8 kg	
Insulation class	F *H*	(Standard) *(Optional)*
Protection degree	IP 55 *IP 56*	(Standard) *(Optional)*
Thermal protection	Without *Customizable*	(Standard) *(Optional)*
Rotation direction	Clockwise *Counter clockwise*	(Standard) *(Optional)*
Service duty	S1	
Vibration level	A	
Balance	Half-key balanced	
Cable glands	1 - M20 × 1.5	
Cooling	IC 411	
Painting color	RAL 7024 *Customizable*	(Standard) *(Optional)*
Regulations	IEC / DIN / ISO / VDE / EN	
Standard	IEC 60034	

Environmental conditions	
Ambient temperature	From -20°C to +40°C
Maximum altitute	1000 m above sea level

Electrical data		
Output	0.75	kW
Frequency	50	Hz
Voltage (±5%)	230 400 276 480	V Δ @ 50Hz V Y @ 50Hz V Δ @ 60Hz V Y @ 60Hz
Rotation speed	940 1130	RPM @ 50Hz RPM @ 60Hz
Rated current	3.86 2.23	A (In) @ Δ 50Hz A (In) @ Y 50Hz
Starting current	4.1	×In
Rated torque	7.62	Nm (Mn)
Starting torque	1.8	×Mn
Breakdown torque	2.2	×Mn
Efficiency	IE1 71.5 70.9 65.8	 @ 100% load @ 75% load @ 50% load
Power factor cosφ	0.68	@ 100% load

Mechanical data		
Bearings brand	C&U *Customizable*	(Standard) *(Optional)*
Bearings type	6205 2RZ C3 6205 2RZ C3	(DE) (NDE)
Lifetime of bearings		20000 hours
Allowed radial load Allowed axial load		921 N 801 N
Grease type		
Lubrication interval of NDE bearing Lubrication interval of DE bearing		h h
Moment of inertia	0.003266	Kg*m²
Noise level	59	dB(A)

(www.techtop.com)

The mechanical drive of the vibrating table - the movement is transmitted from the electric motor to the vibrating table through a pulley mounted on the motor shaft and a connecting rod connecting the pulley and the vibrating table through a screw T. The three components pulley, screw T and connecting rod set the vibrating table plate in motion.

In Figure 5.9 is presented the experimental stand electrical diagram:

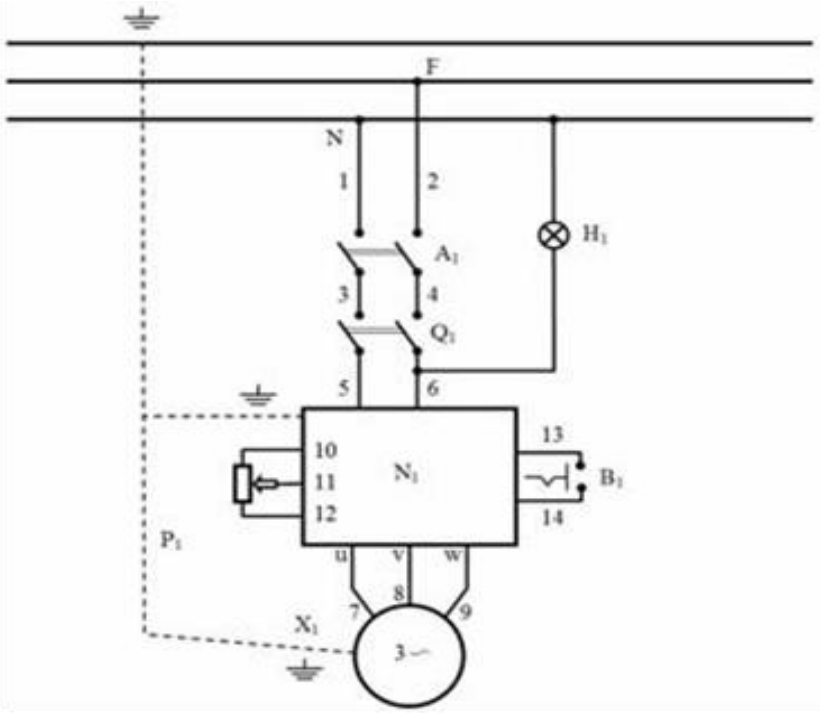

Figure 5.9 The experimental stand electrical diagram

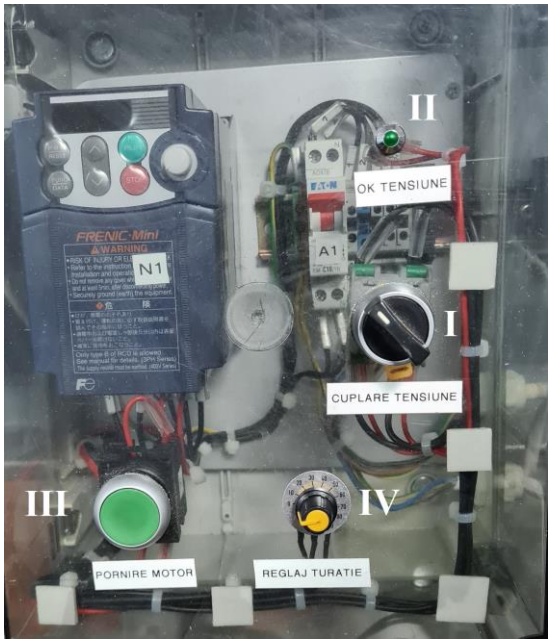

Figure 5.10 Vibrating table control box

Vibrating table control box is presented in the Figure 5.10 and contains the following elements:

- I - main on / off function switch;
- II - green LED that signal the connection to the electrical network;
- III - motor on / off button;
- IV - potentiometer for adjusting the motor speed.

Vibrating table involves performing the following operation mode:

1. the vibrating table is connected to the 220 V AC mains through of a plug;
2. by turning the switch I from left to right and turning on the green LED II, the system is switched on;
3. by pressing button III, the electric motor is supplied with voltage;
4. from potentiometer IV, by a fine rotation from left to right, the motor speed is gradually started from 60 rpm to about 400 rpm;
5. to stop the gearing, potentiometer IV is brought to the initial position 0;
6. press button III, switching off the power supply to the electric motor;
7. by turning switch I from right to left and turning off LED II, the system is disconnected from the power supply;

The base isolation system is located on the shaking plate and is composed of 2 types of FPs (with spherical and elliptical sliding surface):

- 4 spherical friction pendulums (made of stainless steel). The radius of the sliding surface of the FPs is R=810 mm.

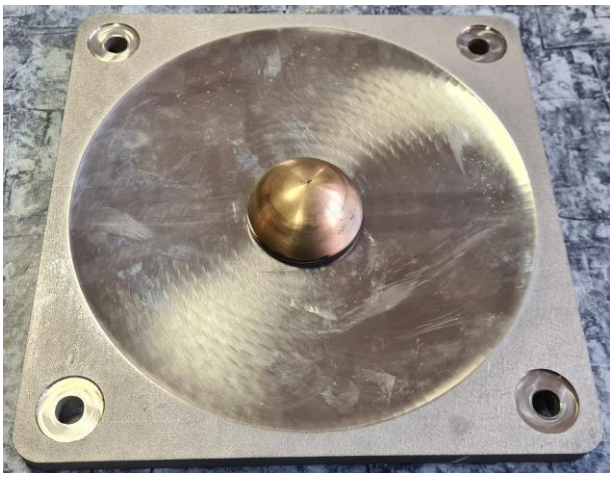

Figure 5.11 Spherical friction pendulum with radius of R=810 mm.

- 4 elliptical friction pendulums (made of stainless steel). The radius of the sliding surface of the FPs is measured with a digital radius gauge from 5 to 5 mm distance, and the values are presented in the Table 5.2.

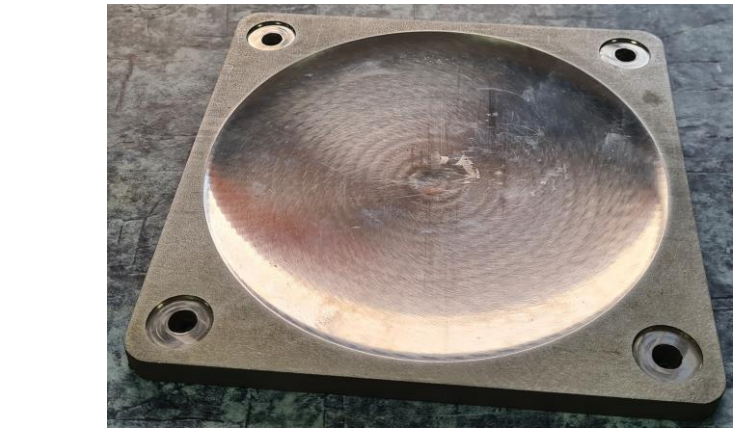

Figure 5.12 Elliptical friction pendulum with variable radius.

Table 5.2 Measured radius of the sliding surface of the elliptical FPs

Reference	X [mm]	Y [mm]
A	5	0.01
B	10	0.05
C	15	0.10
D	20	0.20
E	25	0.30
F	30	0.45
G	35	0.60
H	40	0.8
I	45	1.00
J	50	1.30
K	55	1.60
L	60	1.90
M	65	2.30
N	70	2.70
O	75	3.15
P	80	3.70
Q	85	4.30
R	90	5.00
S	95	6.00
T	100	7
U	105	8.50

- 4 pivots composed of a hemispherical bronze cap, under which the elastomeric layer with a thickness of 2.5 mm is fixed by vulcanization. The sole intended for frictional contact is made of polyethylene with a thickness of 0.4 mm.

Figure 5.13 The pivot that slide on the surfaces of the FPs.

The test structure, presented in Figure 5.14, has the dimensions 1200x400x200 mm and simulates a 6 storey building. The structure is made of a lightly drilled profile, made of galvanized sheet metal with an L-shaped section 20x20 mm, assembled with screws. Its mass can be modified by adding additional masses of known value.

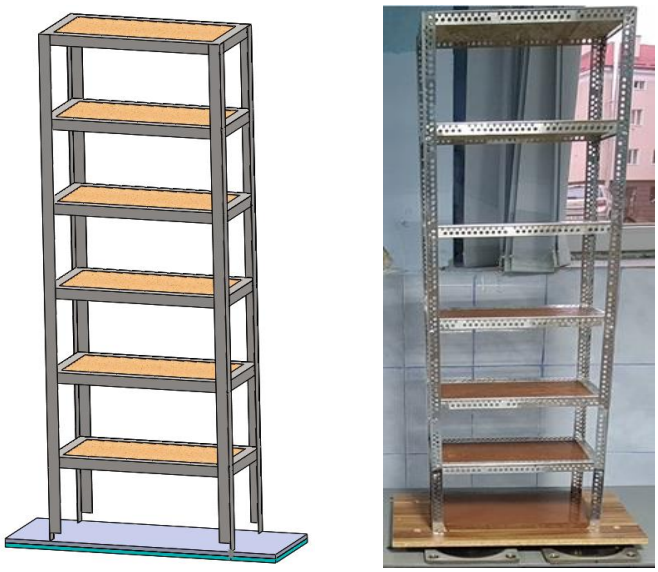

Figure 5.14 Laboratory test structure

It was used for measurements a seismic accelerometers PCB Piezotronics, model 393B05 presented in the Figure 5.15. The accelerometer was placed on the shaking table and on the structure. The technical data sheet of the seismic accelerometer is presented in the Figure 5.16.

Figure 5.15 Seismic accelerometer

Model Number 393B05	SEISMIC ICP® ACCELEROMETER		
Performance	**ENGLISH**	**SI**	
Sensitivity(± 10 %)	10 V/g	1.02 V/(m/s²)	
Measurement Range	0.5 g pk	4.9 m/s² pk	
Frequency Range(± 5 %)	0.7 to 450 Hz	0.7 to 450 Hz	
Frequency Range(± 10 %)	0.5 to 750 Hz	0.5 to 750 Hz	
Frequency Range(± 3 dB)	0.2 to 1700 Hz	0.2 to 1700 Hz	
Resonant Frequency	≥ 2.5 kHz	≥ 2.5 kHz	
Broadband Resolution(1 to 10,000 Hz)	0.000004 g rms	0.00004 m/s² rms	[1]
Non-Linearity	≤ 1 %	≤ 1 %	[2]
Transverse Sensitivity	≤ 5 %	≤ 5 %	
Environmental			
Overload Limit(Shock)	± 300 g pk	± 2950 m/s² pk	
Temperature Range	-15 to +176 °F	-26 to +80 °C	
Temperature Response	See Graph	See Graph	
Base Strain Sensitivity	≤ 0.0005 g/με	≤ 0.005 (m/s²)/με	[1]
Electrical			
Excitation Voltage	18 to 30 VDC	18 to 30 VDC	
Constant Current Excitation	2 to 10 mA	2 to 10 mA	
Output Impedance	<500 Ohm	<500 Ohm	
Output Bias Voltage	7 to 12 VDC	7 to 12 VDC	
Discharge Time Constant	0.5 to 2.0 sec	0.5 to 2.0 sec	
Settling Time	<100 sec	<100 sec	
Spectral Noise(1 Hz)	0.50 μg/√Hz	4.9 (μm/sec²)/√Hz	[1]
Spectral Noise(10 Hz)	0.10 μg/√Hz	1.0 (μm/sec²)/√Hz	[1]
Spectral Noise(100 Hz)	0.07 μg/√Hz	0.7 (μm/sec²)/√Hz	[1]
Spectral Noise(1 kHz)	0.05 μg/√Hz	0.5 (μm/sec²)/√Hz	[1]
Physical			
Sensing Element	Ceramic	Ceramic	
Sensing Geometry	Flexural	Flexural	
Housing Material	Titanium	Titanium	
Sealing	Hermetic	Hermetic	
Size (Diameter x Height)	0.99 in x 1.22 in	25 mm x 31 mm	
Weight	1.8 oz	50 gm	[1]
Electrical Connector	10-32 Coaxial Jack	10-32 Coaxial Jack	
Electrical Connection Position	Top	Top	
Mounting Thread	10-32 Female	10-32 Female	

Typical Sensitivity Deviation vs Temperature

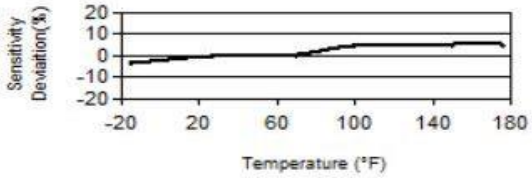

CE [3]

All specifications are at room temperature unless otherwise specified.
In the interest of constant product improvement, we reserve the right to change specifications without notice.

ICP® is a registered trademark of PCB Group, Inc.

Figure 5.16 Technical data sheet of the seismic accelerometer (model 393B05) (www.pcb.com)

The data is retrieved via a four-channel NI 9234 acquisition module coupled to a compact NI ENET-9163 chassis with Ethernet data transmission. Finally, they are downloaded and processed in LabVIEW software from a laptop.

Figure 5.17 Data acquisition and processing system

5.2. Description of the virtual instrumentation

The program in which the data was processed and the input-output applications were developed is **"LabVIEW"** [97]. The program uses the visual programming language being developed by the company "National Instruments".

A virtual tool created in the LabVIEW programming environment consists of a front panel, block diagram, and graphic symbol/connector. The front panel is an interactive interface to control inputs and observe outputs, which is basically the graphical user interface. It is displayed on the computer screen and has the same role as the front panel of a physical instrument, containing both controls and indicator and display elements.

For data acquisition a virtual tool capable of acquiring the signal was used, presenting its evolution in time and frequency, and saving it in a file (Figure 5.18). The connection between the virtual instrument and the physical acquisition system is made through the **"DAQ Assistant"** module, which allows the control of the number of samples and sampling rates. With the help of DAQ, several signal channels can be read simultaneously, which are viewed in the **"WaveForm Graph"** oscilloscope.

By processing the signal, with the help of the **"Spectral Measurements"** icon calculates the Discrete Fourier Transfor (DFT) which is represented in Figure 5.20. In this way, it is possible to roughly identify the frequencies for the signal acquired with the accelerometer placed on the two levels: ground (mobile plate of the shaking table) and structure. The data is saved using the **"Write to Measurements"** icon.

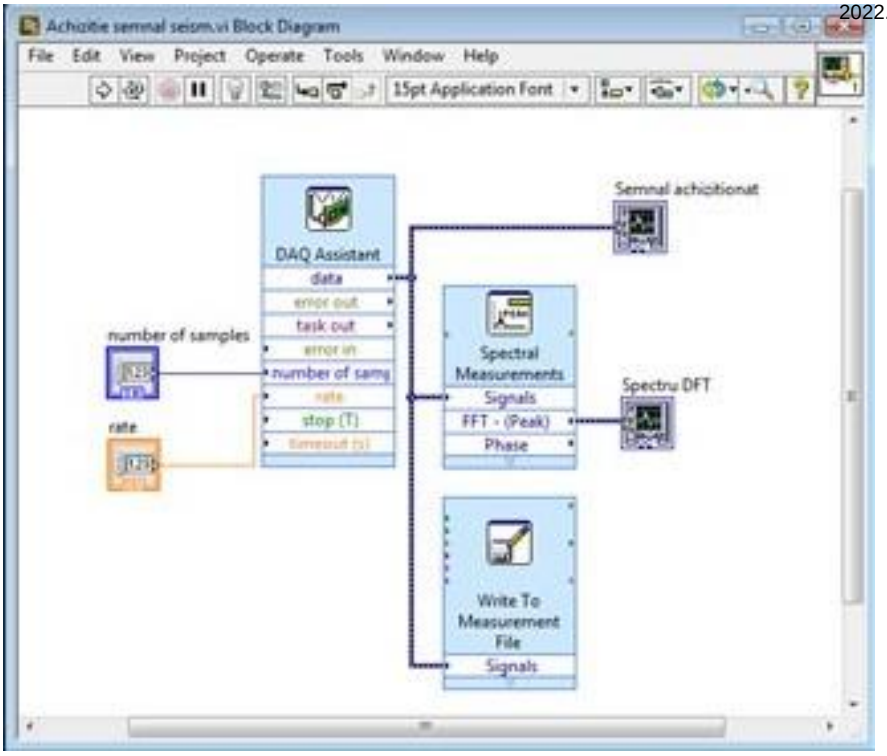

Figure 5.18 Front panel for writing data

An example of a signal acquired is presented in Figure 5.19.

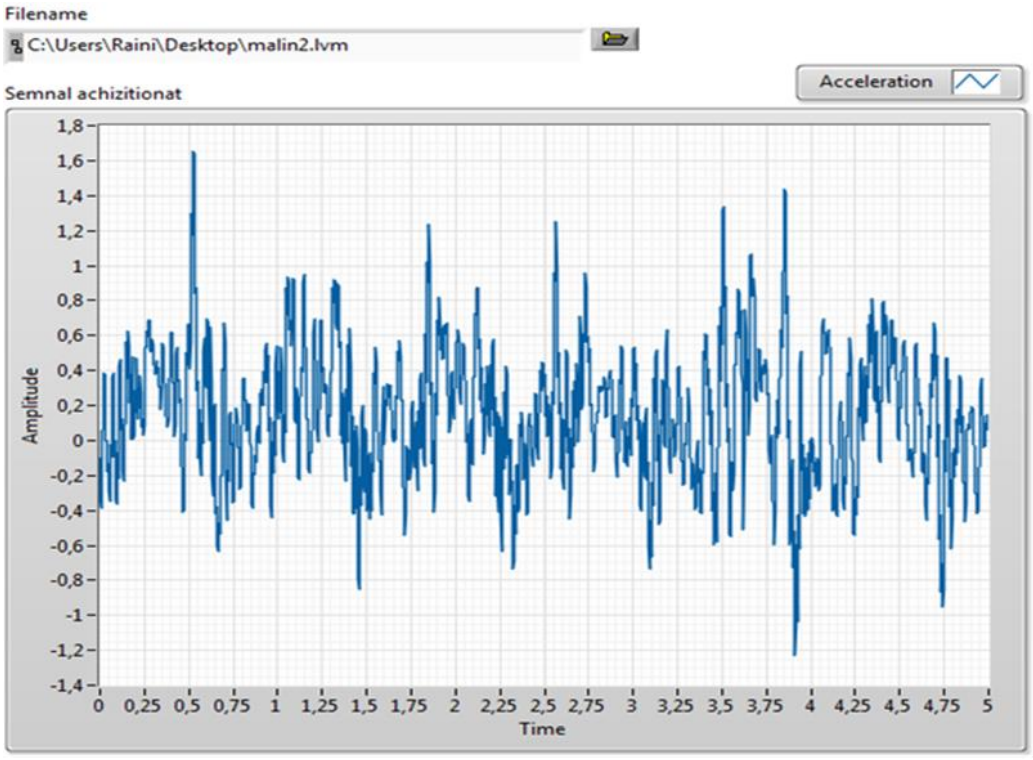

Figure 5.19 The acquired signal

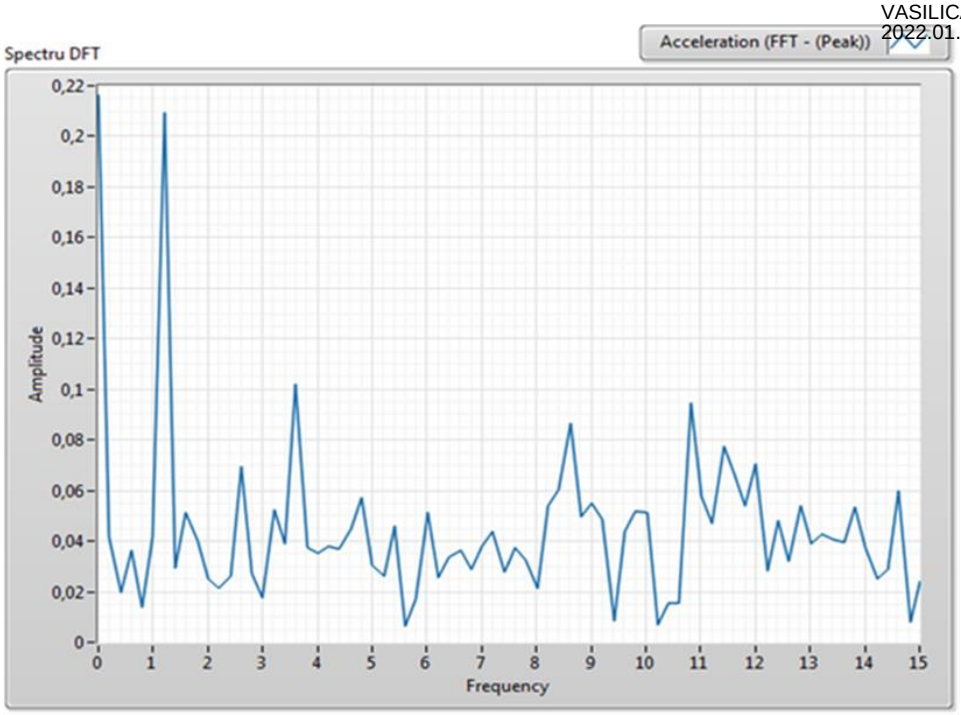

Figure 5.20 DFT spectrum for the acquired signal

The second virtual instrument, represented in Figure 5.21 permits the visualization and analysis of the stored signals, a front panel was built that can read (**"Read from Measurements File"**) the saved data. The same signal as that presented in Figure 5.19 is displayed.

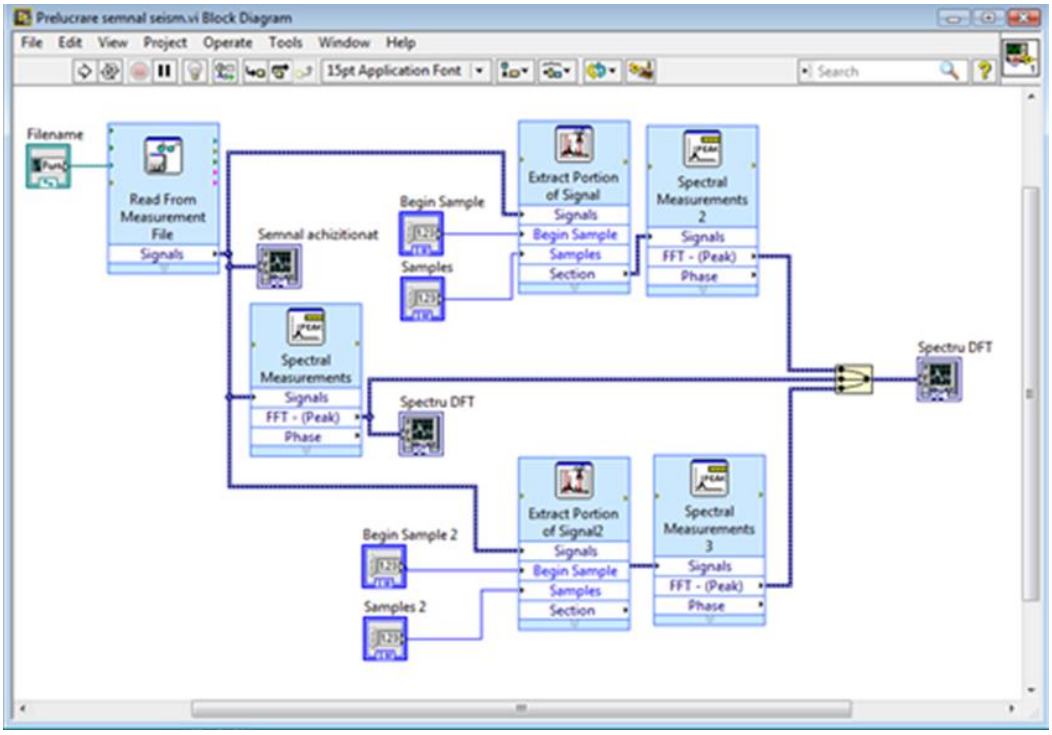

Figure 5.21 Front panel for signal visualization and analysis

With this virtual instrument, 3 DFTs are made overlaped in a single chart. One DFT is for the entire acquired signal (25600 samples), and the other 2 have a smaller number of samples. This number of samples is chosen after several attempts so as to obtain the highest amplitude value. This method ensures the obtaining of the correct frequency which is placed next to the highest amplitude [99]. This is explained by the fact that the frequencies are displayed on spectral lines that depend on the signal length, the distance between two spectral lines being the inverse of time:

$$\Delta f = \frac{1}{t} = \frac{r}{N} - 1 \tag{5.1}$$

where Δf is the frequency resolution, t – signal length in the time domain, N - number of samples, r - frequency rate.

By changing the sample number N, Δf is modified until the spectral line is brought to the real frequency; here the maximum amplitude of the spectrum is obtained. The three spectra are observed in Figure 5.22.

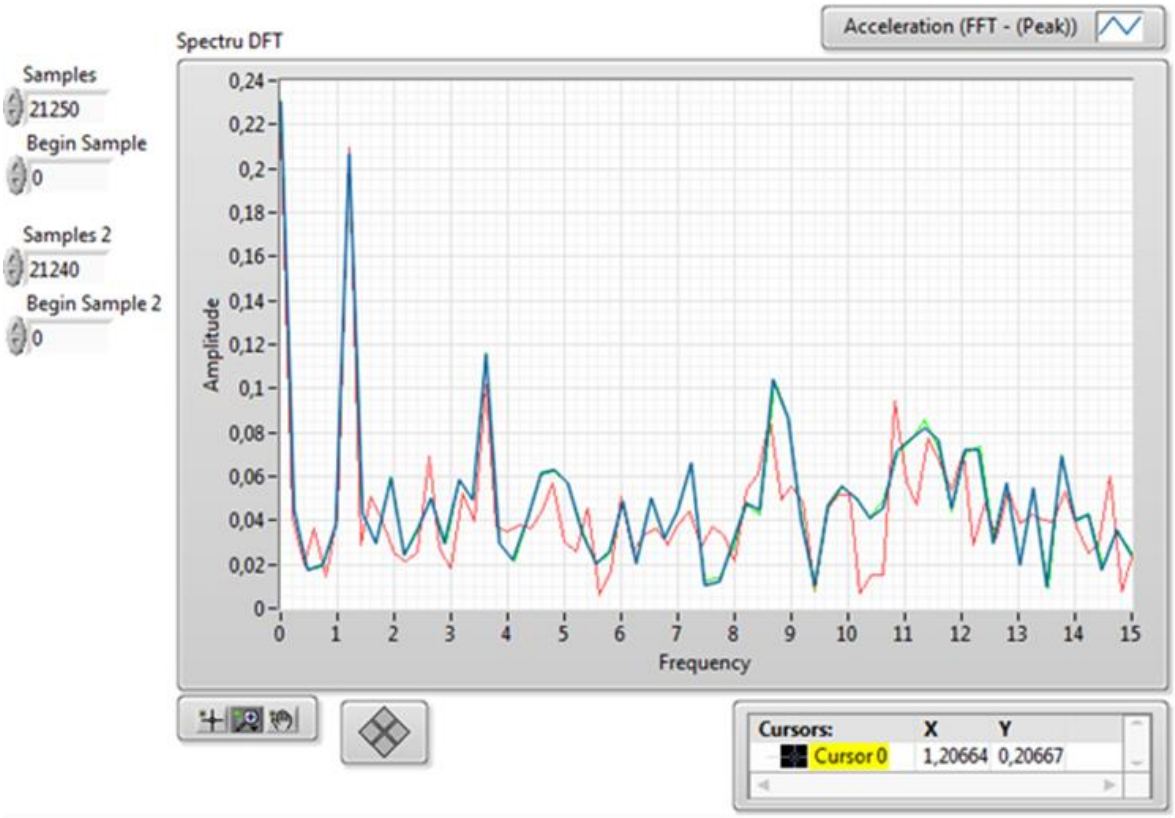

Figure 5.22 Overlaped DFTs spectrum for the acquired signal

A zoom on the peak of the signal in the frequency range, marked in the Figure 5.22, is represented in the Figure 5.23. Frequencies and amplitudes were read using the gray line cursor in the below figure.

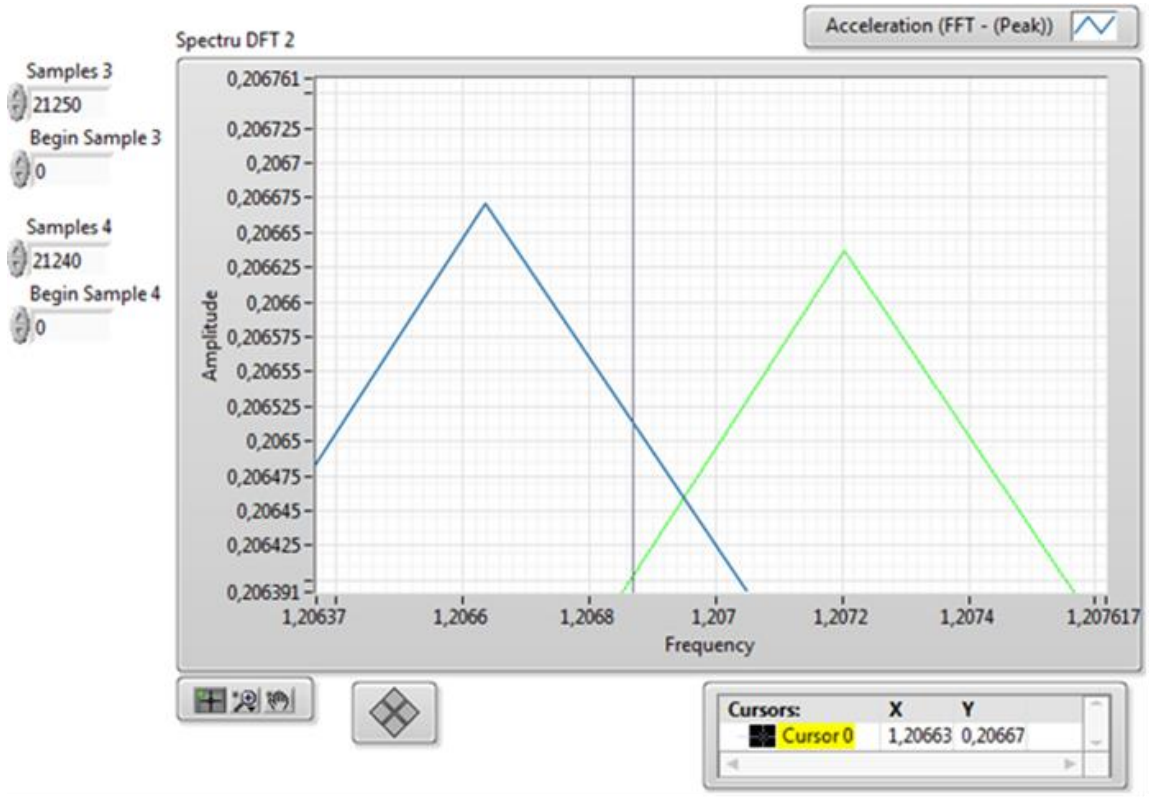

Figure 5.23 Zoom on the peak of the signal

5.3. Results

Experimental measurements were performed for the frequency obtained by setting the potentiometer between 1.55 – 5 Hz, which were read from the frequency converter display. The dependence between the potentiometer setting and the frequency are determined by 5 measurements, the values being presented in the Table 5.3. The accelerometer is placed on the oscillating table and the settings of the acquisition system are: sampling rate 5120 Hz and sample number 25600, resulting in an acquisition time of 5 seconds.

Table 5.3 Frequncy - electronic panel display correlation

No.	Control panel frequency [Hz]	File name	DFT Amplitude [g]	Average Amplitude [g]	Measured frequency [Hz]	Average frequency Hz
1	1.55	calib 1.55_1.lvm	0.1595	0.154418	0.40026	0.40065
		calib 1.55_2.lvm	0.15483		0.4007	
		calib 1.55_3.lvm	0.15483		0.4007	
		calib 1.55_4.lvm	0.15531		0.40089	
		calib 1.55_5.lvm	0.14762		0.4007	
2	2.0	calib2_1.lvm	0.36788	0.367814	0.60515	0.603726
		calib2_2.lvm	0.36075		0.60515	
		calib2_3.lvm	0.37144		0.59803	
		calib2_4.lvm	0.37468		0.60515	
		calib2_5.lvm	0.36432		0.60515	
3	2.5	calib2.5_1.lvm	0.66455	0.674298	0.80392	0.80392
		calib2.5_2.lvm	0.6867		0.80392	
		calib2.5_3.lvm	0.68006		0.80392	
		calib2.5_4.lvm	0.66898		0.80392	
		calib2.5_5.lvm	0.6712		0.80392	
4	3.0	calib3_1.lvm	1.01297	0.9874	0.98006	0.99446
		calib3_2.lvm	1.00949		0.99806	
		calib3_3.lvm	1.00949		0.99806	
		calib3_4.lvm	0.92721		0.99806	
		calib3_5.lvm	0.97784		0.99806	
5	3.5	calib3.5_1.lvm	1.35582	1.357462	1.17031	1.168462
		calib3.5_2.lvm	1.36544		1.17006	
		calib3.5_3.lvm	1.35556		1.16084	
		calib3.5_4.lvm	1.35924		1.17055	
		calib3.5_5.lvm	1.35125		1.17055	
6	4.0	calib4_1.lvm	1.74236	1.738344	1.29204	1.292102
		calib4_2.lvm	1.72594		1.29165	
		calib4_3.lvm	1.73452		1.29192	
		calib4_4.lvm	1.73661		1.29155	
		calib4_5.lvm	1.75229		1.29335	
7	4.5	calib4.5_1.lvm	2.46013	2.556708	1.40503	1.40503
		calib4.5_2.lvm	2.43544		1.40503	
		calib4.5_3.lvm	2.64051		1.40503	
		calib4.5_4.lvm	2.62468		1.40503	
		calib4.5_5.lvm	2.62278		1.40503	
8	5.0	calib5_1.lvm	3.08544	3.09367	1.59803	1.59803
		calib5_2.lvm	3.09573		1.59803	
		calib5_3.lvm	3.10601		1.59803	
		calib5_4.lvm	3.09573		1.59803	
		calib5_5.lvm	3.08544		1.59803	

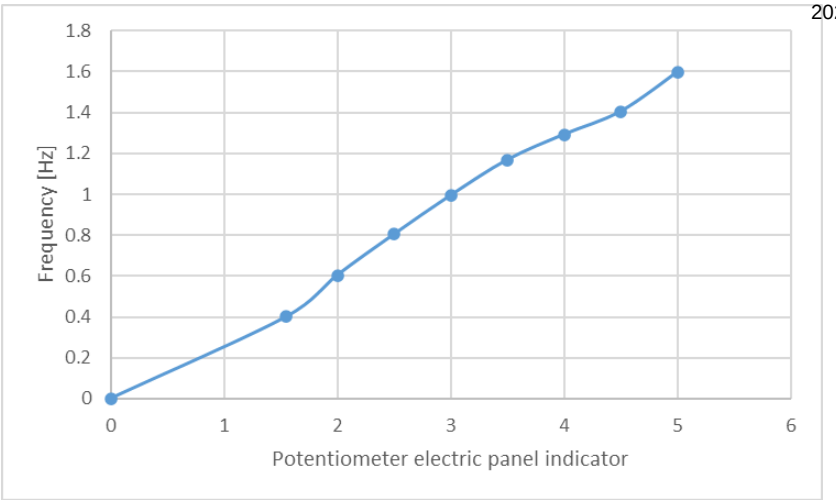

Figure 5.24 Frequency evolution with motor speed

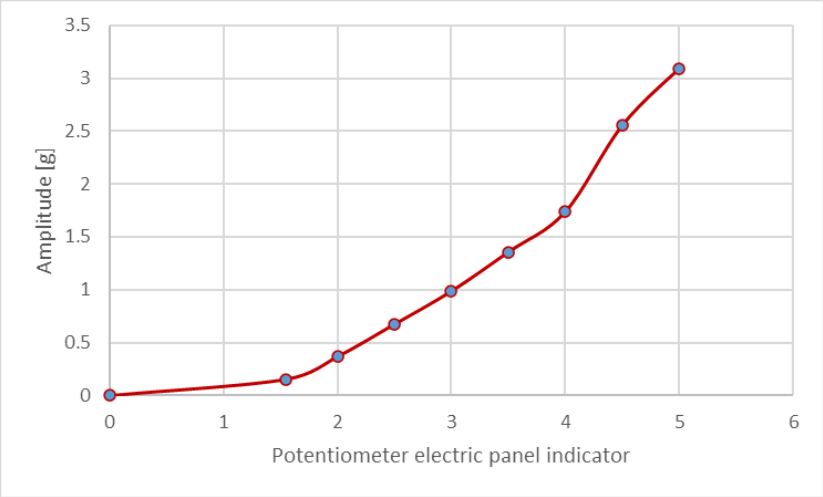

Figure 5.25 Amplitude evolution with motor speed

Based on the correlation between the frequencies and the adjustment in the control panel, the accelerometer was moved to the first level structure and measurements were made again. The settings from the previous measurements were maintained: sampling rate 5120 Hz and sample number 25600, resulting in an acquisition time of 5 seconds. Measurements were performed under the same conditions for the 2 types of friction pendulums.

An overview with all measurements, for both types of friction pendulums, are presented in Table 5.4 - Table 5.7. Also from the experimental results were plotted the frequencies and amplitudes in Figure 5.26 - Figure 5.31.

Case 1 - Spherical friction pendulums

Table 5.4 Frequncy – spherical friction pendulums

No.	Control panel frequency [Hz]	File name	Average exitacion frequency [Hz]	Structure measured frequency [Hz]	Structure average frequency [Hz]
1	1.55	calib 1.55_1.lvm	0.40065	0.40026	0.40065
		calib 1.55_2.lvm		0.4007	
		calib 1.55_3.lvm		0.4007	
		calib 1.55_4.lvm		0.40089	
		calib 1.55_5.lvm		0.4007	
2	2.0	calib2_1.lvm	0.603726	0.665665	0.6640986
		calib2_2.lvm		0.665665	
		calib2_3.lvm		0.657833	
		calib2_4.lvm		0.665665	
		calib2_5.lvm		0.665665	
3	2.5	calib2.5_1.lvm	0.80392	0.80392	0.80392
		calib2.5_2.lvm		0.80392	
		calib2.5_3.lvm		0.80392	
		calib2.5_4.lvm		0.80392	
		calib2.5_5.lvm		0.80392	
4	3.0	calib3_1.lvm	0.99446	0.8918546	0.9049586
		calib3_2.lvm		0.9082346	
		calib3_3.lvm		0.9082346	
		calib3_4.lvm		0.9082346	
		calib3_5.lvm		0.9082346	
5	3.5	calib3.5_1.lvm	1.168462	0.9947635	0.9931927
		calib3.5_2.lvm		0.994551	
		calib3.5_3.lvm		0.986714	
		calib3.5_4.lvm		0.9949675	
		calib3.5_5.lvm		0.9949675	
6	4.0	calib4_1.lvm	1.292102	1.0723932	1.07244466
		calib4_2.lvm		1.0720695	
		calib4_3.lvm		1.0722936	
		calib4_4.lvm		1.0719865	
		calib4_5.lvm		1.0734805	
7	4.5	calib4.5_1.lvm	1.40503	1.1521246	1.1521246
		calib4.5_2.lvm		1.1521246	
		calib4.5_3.lvm		1.1521246	
		calib4.5_4.lvm		1.1521246	
		calib4.5_5.lvm		1.1521246	
8	5.0	calib5_1.lvm	1.59803	1.2944043	1.2944043
		calib5_2.lvm		1.2944043	
		calib5_3.lvm		1.2944043	
		calib5_4.lvm		1.2944043	
		calib5_5.lvm		1.2944043	

Table 5.5 Amplitude – spherical friction pendulums

No.	Control panel frequency [Hz]	File name	Average amplitude [g]	Structure measured amplitude [g]	Structure average amplitude [g]
1	1.55	calib 1.55_1.lvm	0.154418	0.1595	0.154418
		calib 1.55_2.lvm		0.15483	
		calib 1.55_3.lvm		0.15483	
		calib 1.55_4.lvm		0.15531	
		calib 1.55_5.lvm		0.14762	
2	2.0	calib2_1.lvm	0.367814	0.36788	0.367814
		calib2_2.lvm		0.36075	
		calib2_3.lvm		0.37144	
		calib2_4.lvm		0.37468	
		calib2_5.lvm		0.36432	
3	2.5	calib2.5_1.lvm	0.674298	0.731005	0.7417278
		calib2.5_2.lvm		0.75537	
		calib2.5_3.lvm		0.748066	
		calib2.5_4.lvm		0.735878	
		calib2.5_5.lvm		0.73832	
4	3.0	calib3_1.lvm	0.9874	0.9218027	0.898534
		calib3_2.lvm		0.9186359	
		calib3_3.lvm		0.9186359	
		calib3_4.lvm		0.8437611	
		calib3_5.lvm		0.8898344	
5	3.5	calib3.5_1.lvm	1.357462	1.152447	1.1538427
		calib3.5_2.lvm		1.160624	
		calib3.5_3.lvm		1.152226	
		calib3.5_4.lvm		1.155354	
		calib3.5_5.lvm		1.1485625	
6	4.0	calib4_1.lvm	1.738344	1.4461588	1.44282552
		calib4_2.lvm		1.4325302	
		calib4_3.lvm		1.4396516	
		calib4_4.lvm		1.4413863	
		calib4_5.lvm		1.4544007	
7	4.5	calib4.5_1.lvm	2.556708	1.7958949	1.86639684
		calib4.5_2.lvm		1.7778712	
		calib4.5_3.lvm		1.9275723	
		calib4.5_4.lvm		1.9160164	
		calib4.5_5.lvm		1.9146294	
8	5.0	calib5_1.lvm	3.09367	2.1906624	2.1965057
		calib5_2.lvm		2.1979683	
		calib5_3.lvm		2.2052671	
		calib5_4.lvm		2.1979683	
		calib5_5.lvm		2.1906624	

TIMIS GABRIELA-VASILICA
2022.01.13 14:18

Case 2 - Elliptical friction pendulums

Table 5.6 Frequncy – elliptical friction pendulums

No.	Control panel frequency [Hz]	File name	Average exitacion frequency [Hz]	Structure measured frequency [Hz]	Structure average frequency [Hz]
1	1.55	calib 1.55_1.lvm	0.40065	0.40026	0.40065
		calib 1.55_2.lvm		0.4007	
		calib 1.55_3.lvm		0.4007	
		calib 1.55_4.lvm		0.40089	
		calib 1.55_5.lvm		0.4007	
2	2.0	calib2_1.lvm	0.603726	0.60515	0.603726
		calib2_2.lvm		0.60515	
		calib2_3.lvm		0.59803	
		calib2_4.lvm		0.60515	
		calib2_5.lvm		0.60515	
3	2.5	calib2.5_1.lvm	0.80392	0.80392	0.80392
		calib2.5_2.lvm		0.80392	
		calib2.5_3.lvm		0.80392	
		calib2.5_4.lvm		0.80392	
		calib2.5_5.lvm		0.80392	
4	3.0	calib3_1.lvm	0.99446	0.8232504	0.8353464
		calib3_2.lvm		0.8383704	
		calib3_3.lvm		0.8383704	
		calib3_4.lvm		0.8383704	
		calib3_5.lvm		0.8383704	
5	3.5	calib3.5_1.lvm	1.168462	0.9128418	0.91140036
		calib3.5_2.lvm		0.9126468	
		calib3.5_3.lvm		0.9054552	
		calib3.5_4.lvm		0.913029	
		calib3.5_5.lvm		0.913029	
6	4.0	calib4_1.lvm	1.292102	0.9431892	0.94323446
		calib4_2.lvm		0.9429045	
		calib4_3.lvm		0.9431016	
		calib4_4.lvm		0.9428315	
		calib4_5.lvm		0.9441455	
7	4.5	calib4.5_1.lvm	1.40503	0.983521	0.983521
		calib4.5_2.lvm		0.983521	
		calib4.5_3.lvm		0.983521	
		calib4.5_4.lvm		0.983521	
		calib4.5_5.lvm		0.983521	
8	5.0	calib5_1.lvm	1.59803	1.0227392	1.0227392
		calib5_2.lvm		1.0227392	
		calib5_3.lvm		1.0227392	
		calib5_4.lvm		1.0227392	
		calib5_5.lvm		1.0227392	

Table 5.7 Amplitude – elliptical friction pendulums

No.	Control panel frequency [Hz]	File name	Average amplitude [g]	Structure measured amplitude [g]	Structure average amplitude [g]
1	1.55	calib 1.55_1.lvm	0.154418	0.1595	0.154418
		calib 1.55_2.lvm		0.15483	
		calib 1.55_3.lvm		0.15483	
		calib 1.55_4.lvm		0.15531	
		calib 1.55_5.lvm		0.14762	
2	2.0	calib2_1.lvm	0.367814	0.36788	0.367814
		calib2_2.lvm		0.36075	
		calib2_3.lvm		0.37144	
		calib2_4.lvm		0.37468	
		calib2_5.lvm		0.36432	
3	2.5	calib2.5_1.lvm	0.674298	0.731005	0.7417278
		calib2.5_2.lvm		0.75537	
		calib2.5_3.lvm		0.748066	
		calib2.5_4.lvm		0.735878	
		calib2.5_5.lvm		0.73832	
4	3.0	calib3_1.lvm	0.9874	0.774314268	0.75476856
		calib3_2.lvm		0.771654156	
		calib3_3.lvm		0.771654156	
		calib3_4.lvm		0.708759324	
		calib3_5.lvm		0.747460896	
5	3.5	calib3.5_1.lvm	1.357462	0.89890866	0.899997306
		calib3.5_2.lvm		0.90528672	
		calib3.5_3.lvm		0.89873628	
		calib3.5_4.lvm		0.90117612	
		calib3.5_5.lvm		0.89587875	
6	4.0	calib4_1.lvm	1.738344	1.055695924	1.05326263
		calib4_2.lvm		1.045747046	
		calib4_3.lvm		1.050945668	
		calib4_4.lvm		1.052211999	
		calib4_5.lvm		1.061712511	
7	4.5	calib4.5_1.lvm	2.556708	1.185290634	1.231821914
		calib4.5_2.lvm		1.173394992	
		calib4.5_3.lvm		1.272197718	
		calib4.5_4.lvm		1.264570824	
		calib4.5_5.lvm		1.263655404	
8	5.0	calib5_1.lvm	3.09367	1.380117312	1.383798591
		calib5_2.lvm		1.384720029	
		calib5_3.lvm		1.389318273	
		calib5_4.lvm		1.384720029	
		calib5_5.lvm		1.380117312	

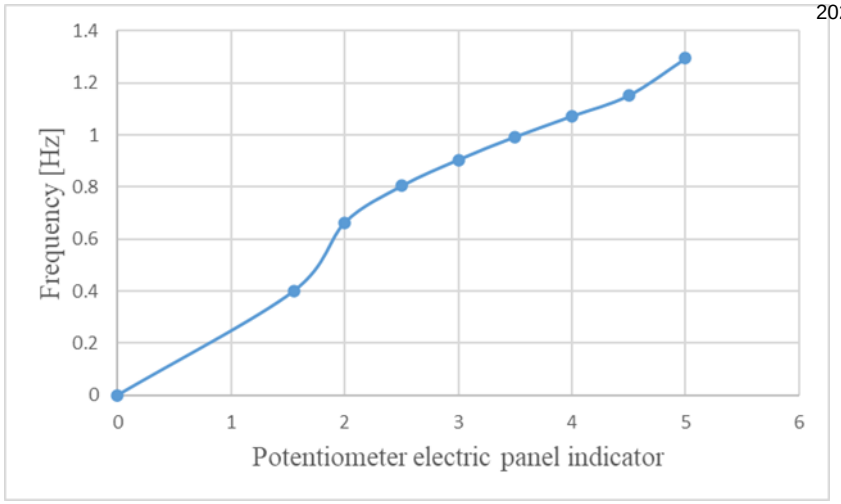

Figure 5.26 Frequency – spherical friction pendulums

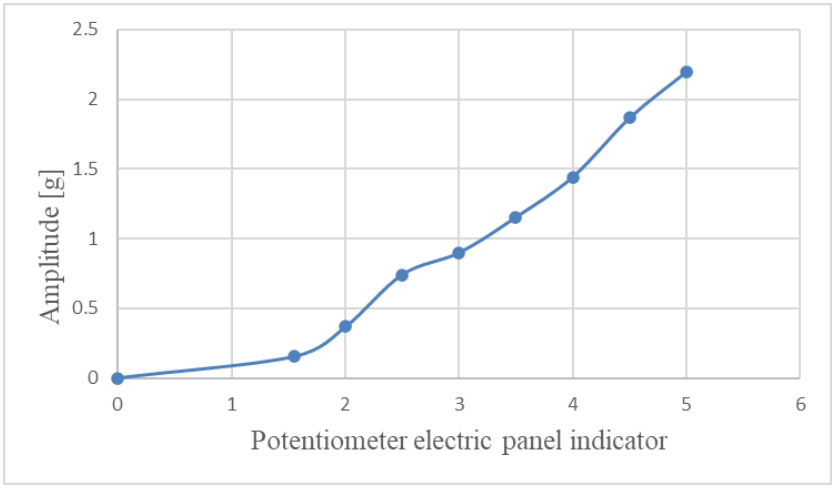

Figure 5.27 Amplitude - spherical friction pendulums

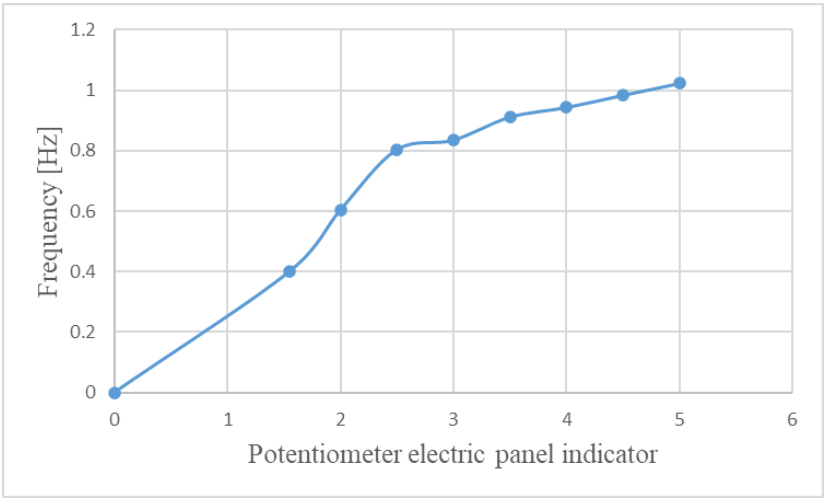

Figure 5.28 Frequency – elliptical friction pendulums

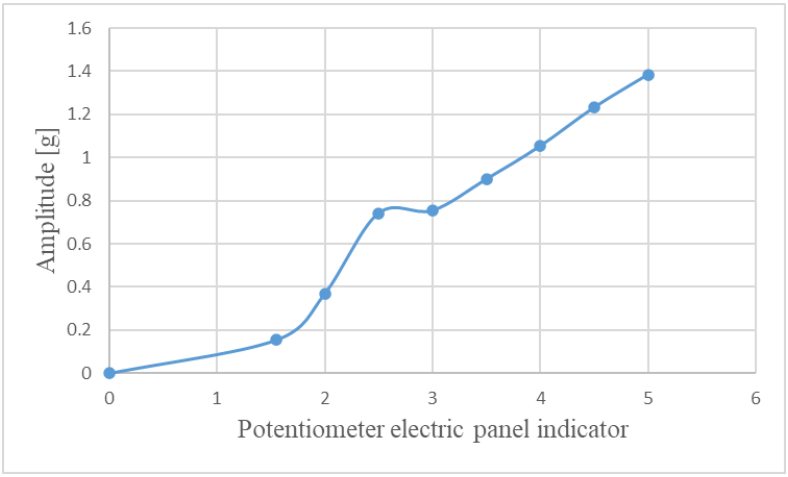

Figure 5.29 Amplitude - elliptical friction pendulums

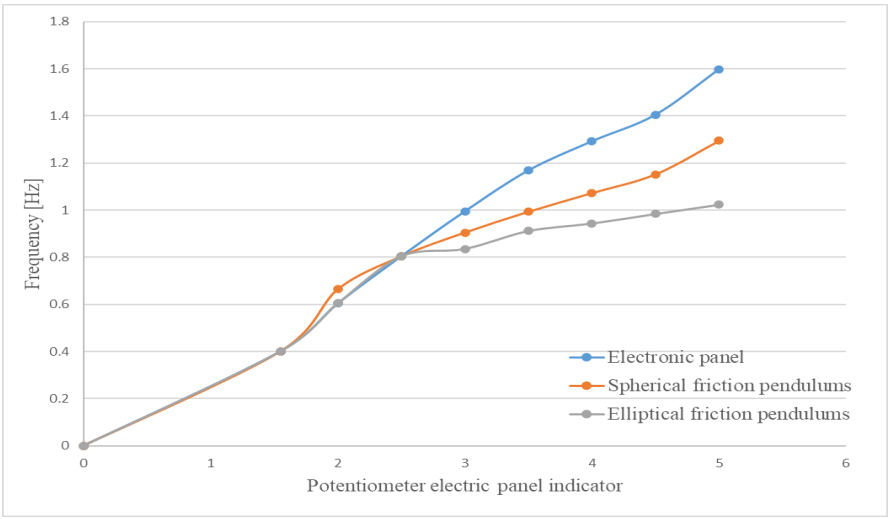

Figure 5.30 Frequency comparison between spherical and elliptical friction pendulums

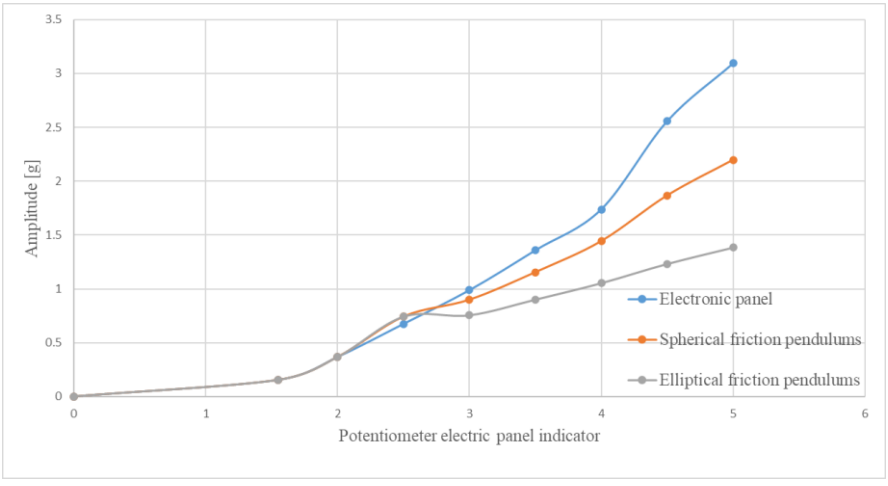

Figure 5.31 Amplitude comparison between spherical and elliptical friction pendulums

5.4. Conclusions and contributions

The tests were performed on a structure very similar to the one modeled and used for simulations in SolidWorks. In the real case, to read the frequencies, a post-processing of the signal is needed in order to find the maximum amplitude obtained when the signal is repeatedly shortened. This amplitude is found on the spectral line that indicates the real frequency. This operation was performed manually using 3 DFT spectra obtained for different signal lengths.

It was observed that the friction pendulums with small radii has a reduced effect on the isolation of the structure with either spherical or elliptical surface. This is explained by the fact that by reducing the size of the structure a proportional reduction of the radius of the friction pendulum cannot be applied. In the case of the experiment, a relatively high frequency of shaking table was needed to ensure the sliding of the pivots on the surface of the pendulum.

The detachment was not performed at low frequencies because the static coefficient of friction does not ensure slipping. In the case of high speeds, the dynamic friction coefficient comes into action, which has lower values than the static one, thus allowing slipping. One problem with the experiment was the alignment of the pendulums and pivots. If they were not perfectly aligned the relative movement between the structure and the pendulum, respectively the moving plate of the oscillating table took place at higher frequencies of the oscillating table because it was necessary to overcome higher resistance forces. Therefore, during experiments to ensure good isolation it is necessary that the systems with sliding surfaces and pivots must be perfectly aligned to ensure the relative movement between the pendulum and the structure at low lateral forces.

6. CONCLUSIONS AND ORIGINAL CONTRIBUTIONS

6.1. Conclusions

The main goal of the researches regarding the behavior of structures isolated by friction pendulum systems was to find out how different parameters of the isolation devices (radii, friction coefficients, spring stiffness, etc), respectively the frequency of the excitation, influences the structural response.

For this research, it was important to know the digital signals describing various earthquake movements. The digital format allowed to re-analyze the past earthquakes and to use digital data as input for dynamic simulation made for base-isolated structures. An algorithm was developed to extract the signals and the numerical values from an image with the help of the WebPlotDigitizer software.

Also, another algorithm was developed to estimate the velocity and displacement of the earthquake signals with known acceleration. The algorithm, nominated as PySEMO, was implemented in the Python programming language and was used to find the velocity and the displacement evolution for earthquake signals acquired with accelerometers.

An application in the Python programming language was created that generates digital signals with known parameters (frequency, amplitude, phase, damping coefficient, existence of noise). These digital signals, since have known parameters, can be used to create benchmarks for test and dynamic simulations.

A model (with steel bars and wood plates) was designed in SolidWorks software, used to perform the dynamic simulations in the Motion module of SolidWorks. The dynamic simulations with SolidWorks also gave incorrect points in the case of the transformation from accelerations to displacement solved by the solver. To eliminate them, it was necessary to compare the results from SolidWorks with those obtained by direct integration with the PySemo application.

It was found that efficient isolation is provided if the pendulum radius is bigger than 600 mm in the case of exciting the structure with an oscillation having the frequency of 1 Hz. It has also been established that the frequency of the structure does not increase with the frequency of excitation if the latter exceeds the natural frequency of the pendulum, but in the post-resonance domain, it remains constant taking the value of the natural frequency of the system.

The results of simulation shows that the best isolation is achieved if the excitation frequency exceeds 1.5 times the natural frequency of the friction pendulum. The natural frequency is not influenced by the weight of the structure and the friction coefficient has also a low influence, but if it has higher values the amplitude of the oscillation decrease. Hence, these two parameters have a low influence on the dynamic behavior of the isolated structure. On the other hand, the pendulum radius has a significant influence on this behavior, since it is the parameter controlling the natural frequency of the pendulum.

It was concluded that isolation can be made either by dissipating energy by ensuring a certain significant friction coefficient or by permitting a large relative displacement between the ground and the structure and avoiding in this way significant acceleration of the structure. The two constructive parameters, namely the friction coefficient and the pendulum radius, must be carefully adapted to ensure efficient isolation.

A friction pendulum system was constructed which differs by the shape and dimension of the cylindrical sliding surface, respectively, by the friction coefficients, to find out how the structure responds. It has been found that the frequency of the structure does not change with the FP radius but the amplitude of the displacement is strongly dependent on this parameter. Because the circular and elliptical sections of the FP provide the structure with different natural frequencies, the resonance is achieved at other radii. This determines a bigger pre-resonance domain for the elliptical FP, while the post-resonance is earlier achieved by the FP constructed with a circular cylindrical sliding surface.

It is possible to control the occurrence of resonance by changing the semi-minor axis of the ellipse, therefore it is possible to design the FP in order to work in pre- or post-resonance depending on the parameters (frequency and amplitude) expected for the ground excitation. For both sets of pendulums, it was concluded that the best isolation of the structure is achieved when the natural frequency of the pendulum is at least 1.5 times lower than the ground excitation. Another conclusion was that the friction coefficient has the same influence on the amplitudes of the structure’s response if the FP has the same natural frequency.

Finally, an isolation system with a plan sliding surface restrained by springs and with a counterweight on the top of the structure was designed to find the best constructive solution regarding the surface and mass. For this system it was found that the best isolation is achieved if the spring constant k, with which the mass is caught, is higher and if there are two surface contacts with friction. The two constructive parameters, namely the spring constant and the friction coefficient, must be carefully adapted to achieve efficient isolation.

The results obtained from dynamic simulations have been confirmed by the experimental tests performed on a small-scale model in the laboratory.

In all cases, after a higher amplitude is observed at the beginning, it decreases and remains constant in a relatively short time. Even if the experiments were done with precision machined systems to ensure the best possible isolation, this goal could only be obtained at higher frequencies of the vibrating table.

It was observed that the friction pendulums with small radii has a reduced effect on the isolation of the structure with either spherical or elliptical surface. This is explained by the fact that by reducing the size of the structure a proportional reduction of the radius of the friction pendulum cannot be applied.

To ensure better isolation at low frequencies, very large radii should be applied to the sliding surface. If it is possible in a balanced position, when the structure is centered, this surface should be flat for easy detachment at a force as low as possible.

6.2. Personal contributions

Based on the researches regarding the behaviour of structures isolated by friction pendulum, the following personal contributions can be retained as original methods and concepts:

a) an algorithm was designed to extract the signals and the numerical values from an image with the help of the WebPlotDigitizer software;

b) an application was developed in the Python programming language that generates digital signals with known parameters (frequency, amplitude, phase, damping coefficient, existence of noise);

c) an algorithm was developed to estimate the velocity and displacement of the earthquake signals with known acceleration;

d) Python Seismic Motion (PySEMO) application was developed to perform fast simulation and prove it works for signals with one or more components, in the absence or presence of damping, and with or without noise;

e) a model for isolated structure (with steel bars and wood plates) was implemented in SolidWorks software, used to perform the dynamic simulations in the Motion module of SolidWorks;

f) the connection between the different parameters of the isolation devices (variable radii, friction coefficients, frequency of the excitation, and spring stiffness) and the structural response was established;

g) a friction pendulum system with variable radius was designed and compared from performance point of view with current friction pendulums (uniform radii);

h) development of an isolation system with a plan sliding surface restrained by springs and with a counterweight on the top of the structure;

i) validate the results obtained from dynamic simulations through experimental tests performed on a small-scale model;

j) dissemination of research results in the relevant publication for the earthquake engineering domain.

6.3. Dissemination of research results

The studies conducted during the doctoral research period had materialized in the following materials published in specialized journals and national and international conferences of profile.

Journal articles:

1. Gillich G R, Nedelcu D, **Mălin T C**, Iancu V, Hamat C A and Gillich N (2019), *"The effect of the friction coefficient and the pendulum radius on the behavior of structures isolated with simple friction pendulums"*, Romanian Journal of Acoustics and Vibration 15(2) pp 130-135. (**ISI**)

2. Gillich Gilbert-Rainer, Nedelcu Dorian, **Mălin Tatian-Cristian**, Gillich Nicoleta, Iancu Vasile, *"Response of a structure isolated by friction pendulums with different radii"*, Annals of the "Constantin Brancusi" University of Targu Jiu, Engineering Series, No.3/2018. (**BDI**)

3. **T. C. Mălin**, G. R. Gillich, D. Nedelcu, V. Iancu, *"Earthquake registration databases"*, Annals of the "Eftimie Murgu" University of Resita, No. 1, 2019. (**BDI**)

4. **Tatian-Cristian Mălin**, Dorian Nedelcu, Gilbert-Rainer Gillich, *"A Python application to generate digital signals"*, Studia Universitatis Babeș-Bolyai, Engineering 65(1) 2020. (**BDI**)

Conference proceedings papers:

1. D Nedelcu, G-R Gillich and **C Mălin Tatian**, *"A comparative study about some application packages used in Photogrammetry",* The 23rd edition of Innovative Manufacturing Engineering & Energy International Conference, Pitesti, Romania, 22-24 May 2019. (**ISI**)

2. **Mălin T C**, Nedelcu D, Gillich G R, Petrica A and Padurean I (2019), *"Comparison of the performance of friction pendulums with uniform and variable radii"*, 37th International JVE Conference in Bratislava, Slovakia, April 24-26th 2019, Vibroengineering Procedia 23 pp 81-86. (**Scopus**)

3. Gilbert-Rainer Gillich, Dorian Nedelcu, **Cristian-Tatian Mălin**, Istvan Biro and Magd Abdel Wahab, *"Efficient algorithm for frequency estimation used in structural damage detection"*, 13th International Conference on Damage Assessment of Structures DAMAS 2019, 9-10 July 2019, Porto, Portugal. In: Wahab M. (eds) Proceedings of the 13th International Conference on Damage Assessment of Structures. Lecture Notes in Mechanical Engineering. Springer, Singapore. (**Scopus**)

4. D. Nedelcu, **T. C. Mălin**, G. R. Gillich, C. I. Barbinta and V. Iancu, *"Displacement and velocity estimation of the earthquake response signals measured with accelerometers"*, The 9th International Conference on Advanced Concepts in Mechanical Engineering - ACME 2020, June 04-05, 2020, Iasi, Romania. (**Scopus**)

5. **Tatian-Cristian Mălin**, Gilbert-Rainer Gillich, Dorian Nedelcu, *"Study on the behavior of the isolated structures with friction pendulums and a counterweight "*, AVMS 2021, Timisoara, Romania. (**Scopus**)

6. Nedelcu, D., Gillich, G.R., Iancu, V., **Mălin. C.T.,** *"Study on the effect of a simple friction pendulum radius on the response of isolated structures"*, ICMSAV 2018 & COMAT 2018 & Emech 2018, Brasov, Romania, 25-26 October 2018. (**BDI**)

7. **T. C. Mălin**, G. R. Gillich, D. Nedelcu, V. Iancu, *"Digitization of earthquake signals stored as images"*, 43rd International Conference on mechanics of Solids, Brasov, Romania, 21-22 November 2019. (**BDI**)

6.4. Future research directions

The research presented in this thesis opens new research directions, on the one hand in the field of dynamic simulations of structures isolated by friction pendulum, as well as the development of new devices based on the history of the place on the other hand. For example, the structure can be considered as elastic, in this case certain modes of vibration of the structure can overlap with the natural frequency of the friction pendulum or excitation. It is also possible to study systems that have incorporated in the pivot structure an elastomeric component that manifests itself at low lateral forces induced by small accelerations of the ground.

REFERENCES

1. Aurel Stratan. Dinamica Structurilor şi Inginerie Seismică. [v.2014]
2. "M 8.3 - Sea of Okhotsk". USGS. 2013-05-25. Retrieved 2013-05-25.
3. "M 4.2 - Vanuatu region". earthquake.usgs.gov. Retrieved 2018-01-22.
4. Chopra A. K., Dynamics of structures theory and applications to earthquake engineering, Ediţia a 2-a, Prentice Hall, New Jersey, 2001.
5. Collier C.J., Elnashai A. S., A procedure for combining vertical and horizontal seismic action effects, Journal of Earthquake Engineering, pp. 521-539, 2001.
6. Girard A., Nicolas R., Structural dynamics in industry, Editura ISTE, Londra, 2010.
7. Hauser F., Răileanu V., Fielitz W., Dinu C., Landes M., Bălă A., Prodehl C., Seismic crustal structure between the Transylvanian Basin and the Black Sea, Editura Tectonophysics, România, 2007.
8. Ionescu C., Inginerie seismică, Lucrări, I.P. Iaşi, 1997.
9. Ionescu C., Seisme, poduri şi avarii, I.P. Iaşi, 1995.
10. Ionescu C., Stabilitatea şi Dinamica construcţiilor, Editura Societăţii Academice „Matei-Teiu Botez”, Iaşi, 2004.
11. “M 7.9 April 18, 1906 San Francisco Earthquake”. earthquake.usgs.gov.
12. "Imperial Valley Earthquake". Southern California Earthquake Data Center. Retrieved July 30, 2010.
13. "Historic World Earthquakes". U.S. Geological Survey Earthquake Hazards Program. Archived from the original on November 8, 2010. Retrieved July 30, 2010.
14. Stover, C.W.; Coffman, J.L. (1993), Seismicity of the United States, 1568–1989 (Revised), U.S. Geological Survey professional paper, 1527, United States Government Printing Office.
15. "Quake Zone Acts to Solve Water Crisis; Imperial Valley Rationed as Crews Start Repairs on Nine Canal Breaks", Los Angeles Times, May 21, 1940.

16. Sieh, K. (1996). "The repetition of large-earthquake ruptures". Proceedings of the National Academy of Sciences. 93 (9): 3764–3771. Bibcode:1996PNAS...93.3764S. doi:10.1073/pnas.93.9.3764. PMC 39434.

17. Bolt, B.; Johnston, R. G.; Lefter, J.; Sozen, M. A. (1975), "The study of earthquake questions related to Veterans Administration hospital facilities", Bulletin of the Seismological Society of America, 65 (4): 937, 938, 943–945.

18. California Division of Highways (1975), "Highway damage in the San Fernando earthquake", San Fernando, California, earthquake of 9 February 1971, Bulletin 196, California Division of Mines and Geology, p. 369.

19. Pandea, Razvan-Adrian (4 March 2014). "March 4, 1977 Earthquake". Agerpres.

20. Emil-Sever Georgescu; Antonios Pomonis (October 2008). "The Romanian earthquake of March 4, 1977 revisited: new insights into its territorial, economic and social impacts and their bearing on the preparedness for the future" (PDF). Indian Institute of Technology, Kanpur.

21. Charles Scawthorn, "Earthquakes: A Historical Perspective," in Earthquake Engeneering Handbook. Boca Raton, FL, USA: CRC Press, 2002, ch. 2, pp. 22-88.

22. "Preliminary reconnaissance report of the 1995 Hyogoken-Nanbu earthquake," Architectural Institute of Japan, Tokyo, 1995.

23. https://ngawest2.berkeley.edu ,downloaded at October 30, 2019.

24. https://www.strongmotioncenter.org ,downloaded at October 30, 2019.

25. http://www.kyoshin.bosai.go.jp ,downloaded at October 30, 2019.

26. Kanamori H., Importance of historical seismograms for geophysical research, in: Historical Seismograms and earthquakes of the world, Ed. W.H.K. Lee, Meyers H. and Shimazaki K., Academic Press, 1988, pp. 16-33.

27. Michelini A., De Simoni B., Amato A., & Boschi E., Collecting, Digitizing and Distributing Historical Seismological Data, EOS TRANSACTIONS AGU, Vol.86, No.28, 2005.

28. Rohatgi A., WebPlotDigitizer, https://automeris.io/WebPlotDigitizer ,Version 4.2, April 2019, email: ankitrohatgi@hotmail.com, San Francisco, California, USA.

29. Robert K. Dueck, Digital Design with CPLD Applications and VHDL, Cengage Learning, 2nd edition, 2011.

30. John G. Proakis, Dimitris G. Manolakis, Digital Signal Processing, Pearson Prentice Hall, 2007.

31. Grahame Smillie, Analogue and Digital Communication Techniques, Newnes, 1999.

32. D. Nedelcu, T. C. Malin, G. R. Gillich, C. I. Barbinta and V. Iancu, Displacement and velocity estimation of the earthquake response signals measured with accelerometers, The 9th International Conference on Advanced Concepts in Mechanical Engineering - ACME 2020, June 04-05, 2020, Iasi, Romania.

33. T. C. Malin, G. R. Gillich, D. Nedelcu, V. Iancu, Earthquake registrations database, Annals of the "Eftimie Murgu" University of Resita, No. 1, 2019.

34. T. C. Malin, G. R. Gillich, D. Nedelcu, V. Iancu, Digitization of earthquake signals stored as images, 43rd International Conference on mechanics of Solids, 2019.

35. Gillich G R, Gillich N, Chioncel C P, Cziple F 2008, Legal aspects concerning the evaluation of pollution effects due to vibrations in urban areas Journal of Environmental Protection and Ecology 9 (2) pp 465-473.

36. González-Martín A, Hernandes-Gomes G (2019), How engineers use integrals: the cases of Mechanics of Materials and Electromagnetism Proceedings of the 43rd Conference of the International group for the Psychology of Mathematics Education 2 pp 280-287.

37. Jones S R (2015) Areas, anti-derivatives, and adding up pieces: Definite integrals in pure mathematics and applied science contexts The Journal of Mathematical Behavior 38 pp 9-28.

38. Chioncel C, Chioncel P and Gillich N (2008), Scalar control structure of an asyncronous motor at maximum torque Annals of DAAAM and Proceedings of the International DAAAM Symposium pp 233-234.

39. Minda A, Gillich G R, Budai A and Vasile O (2019), The study of vibration transmission using virtual instruments Romanian Journal of Acoustics and Vibration 15(2) pp 143-148.

40. Chioncel C, Babescu M, Chioncel P, Gillich N and Gillich G R (2007), Speed control method for asynchronous motor Annals of DAAAM and Proceedings of the International DAAAM Symposium pp 137-138.

41. Gillich G R, Frunzaverde D, Gillich N and Amariei D (2010), The use of virtual instruments in engineering education Procedia - Social and Behavioral Sciences 2(2) pp 3806-3810.

42. Nedelcu D., Iancu V., Gillich G.R., Bogdan S.L., Study on the effect of the friction coefficient on the response of structures isolated with friction pendulums, Vibroengineering Procedia, Vol. 19, 2018, pp. 6-11.

43. Gillich G R, Nedelcu D, Malin T C, Iancu V, Hamat C A and Gillich N (2019), The effect of the friction coefficient and the pendulum radius on the behavior of structures isolated with simple friction pendulums Romanian Journal of Acoustics and Vibration 15(2) pp 130-135.

44. Malin T C, Nedelcu D, Gillich G R, Petrica A and Padurean I (2019), Comparison of the performance of friction pendulums with uniform and variable radii Vibroengineering Procedia 23 pp 81-86.

45. Iancu V., Gillich G.R., Iavornic C.M., Gillich N., Some models of elastomeric seismic isolation devices, Applied Mechanics and Materials, Vol. 430, 2013, pp. 356-361.

46. Iancu V., Vasile O., Gillich G.R., Modelling and Characterization of Hybrid Rubber-Based Earthquake Isolation Systems, Materiale Plastice, 49(4), 2012, pp. 237-241.

47. Kelly M J 1993, Earthquake-Resistant Design with Rubber (London: Springer-Verlag).

48. Gillich G R, Samoilescu G, Berinde F, Chioncel C P 2007, Experimental determination of the rubber dynamic rigidity and elasticity module by time-frequency measurements Materiale Plastice 44 (1) pp 18-21.

49. https://www.ngdc.noaa.gov/hazard/earthqk.shtml ,last accessed 23.02.2020.

50. https://earthquake.usgs.gov/earthquakes/search/ ,last accessed 23.02.2020.

51. Robinson W. H., Seismic Isolation of Civil Buildings in New Zealand, John Wiley & Sons Ltd., New Zealand, 2000.

52. Skinner R.I., Robinson W.H., McVerry G.H., An Introduction to Seismic Isolation, John Wiley & Sons Ltd., England, 1993.

53. Jules Touaillon, Improvement in buildings, Letters Patent No. 99,973, patented February 15, 1870.

54. Raufaste NJ (ed) (1992): Earthquake Resistant Construction Using Base Isolation. National Institute of Standards and Technology Special Publication, 832 (1), Washington, USA.

55. Jacob Bechtold, Earthquake-proof building, Letters Patent No. 845,046, patented February 26, 1907.

56. J. A. Calantarients, Building construction to resist the action of earthquakes, Letters Patent No. 932,443, patented August 31, 1909.

57. F. Naeim and J. M. Kelly, Design of Seismic Isolated Structures from Theory to Practice, John Wiley & Sons Inc., 1999.

58. Robinson, W., "Lead-rubber hysteretic bearings suitable for protecting structures during earthquakes.", Seismic Isolation and Protective Systems 2.1, 2011.

59. Victor Zayas, Stanley Low, S. M. (1987). "The FPS earthquake resisting system experimental report." Report No. UCB/EERC 87/01, University of California, Berkeley Earthquake Engineering Research Center.

60. Victor Zayas, S. L. (1990). "A simple pendulum technique for achieving seismic isolation." Earthquake Spectra.

61. Constantinou, M., Mokha, A., and Reinhorn, A. (1990). "Teflon bearings in base isolation II: Modeling." Journal of Structural Engineering, 116(2), 455-474.

62. Mokha, A., Constantinou, M., and Reinhorn, A. (1990). "Teflon bearings in base isolation I: Testing." Journal of Structural Engineering, 116(2), 438-454.

63. Mokha, A., Constantinou, M., Reinhorn, A., and Zayas, V. A. (1991). "Experimental study of friction-pendulum isolation system." Journal of Structural Engineering, 117(4), 1201-1217.

64. Calvi, G., Ceresa, P., Casarotti, C., Bolognini, D., and Auricchio, F. (2004). "Effects of axial force variation in the seismic response of bridges isolated with friction pendulum systems." Journal of Earthquake Engineering, 8(spec01), 187-224.

65. Casarotti, C. and Pavese, A. (2014). "Statistical results of a wide experimental campaign on full scale curved surface sliders." Proceedings of the 2nd ECEE&S, Istanbul.

66. Calvi, P. M., Moratti, M., and Calvi, G. M. (2016). "Seismic isolation devices based on sliding between surfaces with variable friction coeffcient." Earthquake Spectra, 32(4), 2291-2315.

67. Calvi, P. M. and Ruggiero, D. M. (2016). "Numerical modelling of variable friction sliding base isolators." Bulletin of Earthquake Engineering, 14(2), 549.

68. Gillich G.R., Amariei D., Iancu V., Jurcau C., Aspects behavior of bridges which use different vibration isolating systems, 10th WSEAS International Conference on Automation & Information (ICAI'09), Prague, March 23-25, 2009, pp. 140-145.

69. Wilde K., Garboni P., Fujino Y., Base isolation system with shape memory alloy device for elevated highway bridges, Engineering Structures, 22(3), 2000, pp. 222-229.

70. Taylor A., Lin A., Martin J., Performance of Elastomers in Isolation Bearings: A Literature Review, Earthquake Spectra, 8(2), 1992, pp. 279.

71. Kelly J.M., Konstantinidis D., Mechanics of rubber bearings for seismic and vibration isolation, Wiley, 2011.

72. Robinson W.H., Lead-rubber hysteretic bearings suitable for protecting structures during earthquakes, Earthquake Engineering & Structural Dynamics, 10(4), 1982, pp. 593-604.

73. Gillich G.R., Bratu P., Frunzaverde D., Amariei D., Iancu V., Identifying mechanical characteristics of materials with non-linear behavior using statistical methods, Proceedings of the 4th WSEAS International Conference on Computer Engineering and Applications, Harvard USA, 2010, pp. 96-103.

74. Constantinou M.C., Behavior of the double concave Friction Pendulum bearing, Earthquake engineering and Structural dynamics, 35(11), 2006, pp. 1403-1424.

75. Fenz D.M., Constantinou M.C., Spherical sliding isolation bearings with adaptive behavior: experimental verification, Earthquake Engineering and Structural Dynamics, 37(2), 2008, pp. 185-2015.

76. Minda A.A., Gillich G.R., Iavornic C.M., Minda P.F., Analytical and Finite Element Study for Friction Pendulum with Parameterized Sliding Surfaces, Proceedings of the World Congress on Engineering 2012, Vol. 3, WCE 2012, July 4 - 6, 2012, London, U.K.

77. Tanaka K., Hirasawa M., Ishiguro Y., Ohyama H., Nakamura Y. Base-Isolation System with Hybrid Lead Rubber Bearings. SMiRT- 12, paper K25/5, p. 381.

78. Lu L.-Y., Lee T.-Y., Juang S.-Y., Yeh S.-W. Polynomial friction pendulum isolators (PFPIs) for building floor isolation: An experimental and theoretical study, Engineering Structures, Vol. 56, 2013, p. 970–982.

79. Tsai C.S., Lin Y.C., Su H.C. Characterization and modeling of multiple friction pendulum isolation system with numerous sliding interfaces. Earthquake Engineering & Structural Dynamics, Vol. 39, Issue 13, 2010, p. 1463 – 1491.

80. Cheng, F.Y., Jiang, H. and Lou, K., Smart Structures Innovative Systems for Seismic Response Control, Taylor & Francis Group, LLC, 2008, ISBN: 9781420008173.

81. Derham, C. J., Kelly, J. M. (1985), ''Non-linear natural rubber bearings for seismic isolation'', Nuclear Eng. Design, Vol. 84, No. 3, 417-428.

82. EN, 15129:2009, Anti-seismic devices; European Committee For Standardization, 2009.

83. Cruciat, R.-I., Reducerea efectului acţiunii seismice asupra clădirilor prin metoda izolării - Teză de doctorat, UTCB, Facultatea Construcții Civile Industriale şi Agricole, 2013.

84. Den Hatog, J. P. (1956), Mechanical vibration, 4th edition, McGraw-Hill, USA.

85. Westermo, B., Udwadia, F. (1983), ''Periodic response of a building to harmonic excitations'', Earthquake engineering and structural dynamics, 11, 135-146.

86. Mostaghel, N., Hejazi, M., Tanbakuchi, J. (1983), ''Response of sliding structures to harmonic support motion'', Earthquake engineering and structural dynamics, 11, 355-366.

87. Mostaghel, N., Tanbakuchi, J. (1983), ''Response of sliding structures to earthquake support motion'', Earthquake engineering and structural dynamics, 11, 729-748.

88. Mostaghel, N., Davis, T. (1997), ''Representation of Coulomb friction for dynamic analysis'', Earthquake engineering and structural dynamics, 26, 541-548.

89. Mostaghel, N., Khodaverdian, M. (1987), ''Dynamic of resilient friction base isolator (RFBI)'', Earthquake engineering and structural dynamics, 15, 379-390.

90. Mostaghel, N., Khodaverdian, M. (1988), ''Seismic response of structures supported on RFBI system'', Earthquake engineering and structural dynamics, 16, 839-854.

91. Su, L., Ahmadi, G., Tadjbakhsh, I. G. (1989), ''A comparative study of performances of various base isolation systems'', Earthquake engineering and structural dynamics, 18, 11-32.

92. Guiraud, R., Noelleroux, J.P., Livolant, M. and Michalopoulos, A.P. (1985) " Seismic Isolation Using Sliding-Elastomer Bearings." Nuclear Engineering and Design, 84, 363-377.

93. Ibrahim, R.A., Recent advances in nonlinear passive vibration isolators, Journal of Sound and Vibration, vol.314, no.3-5, 2008, p.371-452.

94. Hsiang-Chuan Tsai and Guan-Cheng Lin(1993)," Optimum Tuned Mass Damper for Minimizing Steady State Response of Support-Excited and Damped System", Journal of Earthquake Engineering and Structural Dynamics, Vol. 22, pp 957-973, year 1993.

95. Gillich N., Mituletu I.C., Gillich G.R., Chioncel C.P., Hatiegan C., Frequency and magnitude estimation in voltage unbalanced power systems. 10th International Symposium on Advanced Topics in Electrical Engineering (ATEE), Bucharest, March 23-25, 2017, p. 1-4.

96. Malin T.C., Gillich G.R., Nedelcu D., Study on the behavior of the isolated structures with friction pendulums and a counterweight, AVMS 2021.

97. LabVIEW™ Joint Time-Frequency Analysis Toolkit Reference Manual.

98. Nedelcu, D., Gillich, G.R., Iancu, V., Mălin. C.T. Study on the effect of a simple friction pendulum radius on the response of isolated structures. ICMSAV 2018 & COMAT 2018 & Emech 2018, Brasov, Romania, 25-26 October 2018.

99. Gillich, Gilbert-Rainer, et al. "A versatile algorithm for estimating natural frequencies with high accuracy." Vibroengineering Procedia, vol. 57, 15 Sept. 2019

TIMIS GABRIELA-VASILICA
2022.01.13 14:18

APPENDIX A

Study 1 (in chapter 4.2):

Contact case	Components	Contact type	μ_D [-]	v_D [mm/s^2]	μ_S [-]	v_S [mm/s^2]	R [mm]	f [Hz]	A [mm]	Time [s]
1	Structure	Acrylic	0.05	10.16	0.08	0.1	110 ÷ 960	1	10	30
	Shaking plate	Steel (greasy)								

Study 2 (in chapter 4.3):

Contact case	Components	Contact type	μ_D [-]	v_D [mm/s^2]	μ_S [-]	v_S [mm/s^2]
1	Structure	Steel (dry)	0.25	10.16	0.3	0.1
	Shaking plate	Steel (dry)				

Study 3 (in chapter 4.4):

- ***Case 1***

Contact case	Components	Contact type	μ_D [-]	v_D [mm/s^2]	μ_S [-]	v_S [mm/s^2]	R [mm]	f [Hz]	A [mm]	Time [s]
1	Structure	Steel (dry)	0.25	10.16	0.3	0.1	260	0.75 ÷ 6	5	10
	Shaking plate	Steel (dry)								
2	Structure	Acrylic	0.05	10.16	0.08	0.1	260	0.75 ÷ 6	5	10
	Shaking plate	Steel (greasy)								
3	Structure	Custom	0.03	10.16	0.05	0.1	260	0.75 ÷ 6	5	10
	Shaking plate									

- ***Case 2***

Contact case	Components	Contact type	μ_D [-]	v_D [mm/s^2]	μ_S [-]	v_S [mm/s^2]	R [mm]	f [Hz]	A [mm]	Time [s]
1	Structure	Steel (dry)	0.25	10.16	0.3	0.1	110 ÷ 960	1	10	30
	Shaking plate	Steel (dry)								
2	Structure	Acrylic	0.05	10.16	0.08	0.1	110 ÷ 960	1	10	30
	Shaking plate	Steel (greasy)								
3	Structure	Custom	0.03	10.16	0.05	0.1	110 ÷ 960	1	10	30
	Shaking plate									

Study 4 (in chapter 4.5):

- ***Case 1 - circle***

Contact case	Components	Contact type	μ_D [-]	v_D [mm/s^2]	μ_S [-]	v_S [mm/s^2]	R [mm]	f [Hz]	A [mm]	Time [s]
1	Structure	Steel (dry)	0.25	10.16	0.3	0.1	110 ÷ 960	1	10	30
	Shaking plate	Steel (dry)								
2	Structure	Steel (greasy)	0.05	10.16	0.08	0.1	110 ÷ 960	1	10	30
	Shaking plate	Steel (greasy)								
3	Structure	Teflon	0.03	10.16	0.05	0.1	110 ÷ 960	1	10	30
	Shaking plate	Steel (greasy)								

- ***Case 2 - ellipse***

Contact case	Components	Contact type	μ_D [-]	v_D [mm/s^2]	μ_S [-]	v_S [mm/s^2]	R_V [mm]	R_H [mm]	f [Hz]	A [mm]	Time [s]
1	Structure	Steel (dry)	0.25	10.16	0.3	0.1	960	110 ÷ 960	1	10	30
	Shaking plate	Steel (dry)									
2	Structure	Steel (greasy)	0.05	10.16	0.08	0.1	960	110 ÷ 960	1	10	30
	Shaking plate	Steel (greasy)									
3	Structure	Teflon	0.03	10.16	0.05	0.1	960	110 ÷ 960	1	10	30
	Shaking plate	Steel (greasy)									

Study 5 (in chapter 4.6):

- ***Case 1*:**

➢ **contact with friction** between the structure and the shaking plate, and **without friction** between the structure and the counterweight.

➢ **constant k of the springs: - k=0.01 N/mm** (structure – shaking plate)

- k=0.004÷0.01 N/mm (structure - counterweight)

Contact case	Components	Contact type	μ_D [-]	v_D [mm/s^2]	μ_S [-]	v_S [mm/s^2]	R [mm]	f [Hz]	A [mm]	Time [s]
1	Structure	Steel (greasy)	0.05	10.16	0.08	0.1	-	1	20	30
	Shaking plate	Steel (greasy)								

- ***Case 2*:**

➢ **contact with friction** between the structure and the shaking plate and between the structure and the counterweight.

➢ **constant k of the springs:** - ***k=0.01 N/mm*** (structure – shaking plate)

- k=0.004÷0.01 N/mm (structure - counterweight)

Contact case	Components	Contact type	μ_D [-]	v_D [mm/s^2]	μ_S [-]	v_S [mm/s^2]	R [mm]	f [Hz]	A [mm]	Time [s]
1	Structure	Steel (greasy)	0.05	10.16	0.08	0.1	-	1	20	30
	Shaking plate	Steel (greasy)								

APPENDIX B

The Python code of the PySEMO application contains 1801 lines, from which only the lines of code corresponding to the signal generation and the antiderivative calculation were extracted for example.

```
def ChartGeneration(self): # Signal generation
    self.Local_TIMP=[]
    self.Local_SINUS=[]
    self.Local_NOISE=[]
    self.Local_DAMP=[]
    self.Local_SIGNAL=[]

    self.NOS=int(self.txt_NOS.GetValue().strip())
    self.FR=int(self.txt_FR.GetValue().strip())
    self.DT=1/self.FR
    self.a=float(self.txt_a.GetValue().strip())
    self.b=float(self.txt_b.GetValue().strip())
    self.c=float(self.txt_c.GetValue().strip())
    self.f1=float(self.txt_f1.GetValue().strip())
    self.f2=float(self.txt_f2.GetValue().strip())
    self.f3=float(self.txt_f3.GetValue().strip())
    self.Noise=float(self.txt_Noise.GetValue().strip())
    self.Dump=float(self.txt_Dump.GetValue().strip())

    self.faza1 = float(self.txt_Ph1.GetValue().strip())
    self.faza2 = float(self.txt_Ph2.GetValue().strip())
    self.faza3 = float(self.txt_Ph3.GetValue().strip())


    LimTest=int(4 * max(self.f1,self.f2,self.f3))
    if self.FR < LimTest:
        msj="Frequency rate="+str(self.FR)+"\n"+"Must be "+str(LimTest)+"\n"+"Please increase 'Frequency
rate' !"
        wx.MessageBox(msj, "ERROR", wx.OK | wx.ICON_ERROR)
        return

    xyz=[]
    xyz.append(self.f1)
    xyz.append(self.f2)
    xyz.append(self.f3 )
    xyz[:] = (value for value in xyz if value != 0) # Se elimina valorile nule din lista de frecvente "f1, f2, f3"
    fmin=min(xyz)
    Nr_Rec_Cycles=6
    Perioada=1/fmin
    Treal=self.NOS*self.DT
    Tnecesar=Nr_Rec_Cycles*Perioada
    msj="No. of samples NOS="+str(self.NOS)+"\n"
    msj=msj+"Frequency rate="+str(self.FR)+"\n"
    msj=msj+"Delta T="+str(self.DT)+"\n"
    msj=msj+"Frequency min="+str(fmin)+"\n"
    msj=msj+"Minimum number of requested cycles="+str(Nr_Rec_Cycles)+"\n"
    msj=msj+"Period="+str(Perioada)+"\n"
    msj=msj+"Required time="+str(Tnecesar)+"\n"
    msj=msj+"Real time="+str(Treal)+"\n"
    msj=msj+"'Required time' must be smaller then 'Real time'"+"\n"
```

```
msj=msj+"Increase 'NOS' at minim value "+str(int(self.FR*Tnecesar)+1)  +"\n\n"
if Tnecesar>Treal:
   wx.MessageBox(msj, "ERROR", wx.OK | wx.ICON_ERROR)

f1f2=abs(self.f1-self.f2)
f1f3=abs(self.f1-self.f3)
f2f3=abs(self.f2-self.f3)
Freper=min(f1f2, f1f3, f2f3)

if Freper==0:
   conditie2=5000
else:
   conditie2=2*self.FR/Freper

msj="Frequency minim difference="+str(Freper)+"\n"
msj=msj+"No. of samples NOS="+str(self.NOS)+"\n"
msj=msj+"Frequency rate="+str(self.FR)+"\n"
msj=msj+"Two Frequency are too close. Increase NOS !!!"+"\n"
msj=msj+"Minimum requested NOS must be "+str(int(conditie2)+1)+"\n"

if self.NOS<conditie2:
   wx.MessageBox(msj, "ERROR", wx.OK | wx.ICON_ERROR)

self.DateIn="No. of samples="+self.txt_NOS.GetValue().strip()+"\n"
self.DateIn=self.DateIn+"Frequency rate ="+self.txt_FR.GetValue().strip()+"\n"
self.DateIn=self.DateIn+"Delta T="+self.txt_DT.GetValue().strip()+"\n"
self.DateIn=self.DateIn+"a="+self.txt_a.GetValue().strip()+"\n"
self.DateIn=self.DateIn+"b="+self.txt_b.GetValue().strip()+"\n"
self.DateIn=self.DateIn+"c="+self.txt_c.GetValue().strip()+"\n"
self.DateIn=self.DateIn+"f1="+self.txt_f1.GetValue().strip()+"\n"
self.DateIn=self.DateIn+"f2="+self.txt_f2.GetValue().strip()+"\n"
self.DateIn=self.DateIn+"f3="+self.txt_f3.GetValue().strip()+"\n"
self.DateIn=self.DateIn+"Ph1="+self.txt_Ph1.GetValue().strip()+"\n"
self.DateIn=self.DateIn+"Ph1="+self.txt_Ph2.GetValue().strip()+"\n"
self.DateIn=self.DateIn+"Ph1="+self.txt_Ph3.GetValue().strip()+"\n"
self.DateIn=self.DateIn+"Noise amplitude="+self.txt_Noise.GetValue().strip()+"\n"
self.DateIn=self.DateIn+"Damping="+self.txt_Dump.GetValue().strip()+"\n\n"

if self.OpenedFile==0:
   # Keyboard input of the file name
   tit = "File name" ; msg = "Enter the file name for data saving... "
   dlg = wx.TextEntryDialog(self, msg, tit, "DataTest", style = wx.OK | wx.CANCEL)
   if dlg.ShowModal() == wx.ID_CANCEL:
      dlg.Destroy()
      self.Close(True)
      self.Destroy()
      return
   self.NumeFileMemo=str(dlg.GetValue())
   file_name1=os.getcwd()+"/"+self.NumeFileMemo+"_Parameter.CSV"
   file_CSV1 = open(file_name1,'w')
   file_CSV1.write(self.DateIn)
   file_CSV1.close

samples = np.random.normal(0, 0.25, size=self.NOS)
min1=min(samples)
max1=max(samples)
maxabs=max1
if abs(min1)>maxabs: maxabs=abs(min1)
samples = self.Noise*samples/maxabs
```

```
        Zgomot=samples.tolist()

        self.IDP="" ; self.IDP_Excel="" ; t=0 ; Time=[] ; Amplitudine=[] ; Sinus=[] ; Amortizare=[]
        if self.OpenedFile==1:
           file_name=os.getcwd()+"/"+self.FILENAME_DATA
        else:
           file_name=os.getcwd()+"/"+self.NumeFileMemo+".CSV"

        self.txt_DT.SetValue(str(self.DT))  # A nu se muta in fata
        self.FILE_img_NAME=file_name
        file_name_Plus=file_name[0:file_name.rfind(".")]+"_PLUS.CSV"
        file_CSV = open(file_name,'w')
        file_CSV.write(str(self.NOS)+'\n')

        file_PLUS_CSV = open(file_name_Plus,'w')
        file_PLUS_CSV.write(self.DateIn)

sir="n"+","+"Time"+","+"a*sin[(2*Pi*f1*t)+Pi*Ph1]"+","+"b*sin[(2*Pi*f2*t)+Pi*Ph2]"+","+"c*sin[(2*Pi*f3*t
)+Pi*Ph3]"+"," \
              +"a*sin[(2*Pi*f1*t)+Pi*Ph1]+b*sin[(2*Pi*f2*t)+Pi*Ph2]+c*sin[(2*Pi*f3*t)+Pi*Ph3]" \
              +","+"Noise"+","+"Damping"+","+"Signal Generated"+'\n'
        file_PLUS_CSV.write(sir)


        if self.Noise==0: Zgomot=[0] * len(samples)
        if self.Dump==0: Amortizare=[0] * len(samples)

        RMS_Noise=0 ; RMS_SG=0
        for i in range(1,self.NOS+1):
           s1=self.a * math.sin((2*Public_PI*self.f1*t) + Public_PI * self.faza1)
           s2=self.b * math.sin((2*Public_PI*self.f2*t) + Public_PI * self.faza2)
           s3=self.c * math.sin((2*Public_PI*self.f3*t) + Public_PI * self.faza3)
           Sinus.append(s1+s2+s3)
           if self.Dump<>0:
              Amort=math.exp( self.Dump*t)
              Amortizare.append(Amort)
              Ampl=Amort *((s1+s2+s3)+Zgomot[i-1])
           else:
              Amort=0
              Ampl=(s1+s2+s3) + Zgomot[i-1]
           Amplitudine.append(Ampl)
           Time.append(t)

           self.Local_TIMP.append(t)
           self.Local_SINUS.append(s1+s2+s3)
           self.Local_NOISE.append(Zgomot[i-1])
           self.Local_DAMP.append(Amortizare[i-1])
           self.Local_SIGNAL.append(Ampl)

           RMS_Noise=RMS_Noise+Zgomot[i-1]*Zgomot[i-1]
           RMS_SG=RMS_SG+(s1+s2+s3)*(s1+s2+s3)
           self.IDP=self.IDP+("%5d" % i)+"\t"+("%0.4f" % t) + "\t"+("%0.4f" % s1) + "\t"+("%0.4f" % s2)+
"\t"+("%0.4f" % s3)+ "\t"+ ("%0.4f" % (s1+s2+s3)) + "\t"+("%0.4f" % Zgomot[i-1]) + "\t"+("%0.4f" %
Amort)+ "\t"+("%0.4f" % Ampl)+"\n"
           self.IDP_Excel=self.IDP_Excel+("%5d" % i)+"\t"+("%0.4f" % t) + "\t"+("%0.4f" % Ampl)+"\n"
           file_CSV.write(str(t)+","+ str(Ampl)+"\n")

           file_PLUS_CSV.write(("%5d" % i) + "," + \
                 ("%0.4f" % t) + "," + \
```

```
                ("%0.4f" % s1) + "," + \
                ("%0.4f" % s2) + "," + \
                ("%0.4f" % s3) + "," + \
                ("%0.4f" % (s1+s2+s3)) + "," + \
                ("%0.4f" % Zgomot[i-1]) + "," + \
                ("%0.4f" % Amort) + "," + \
                ("%0.4f" % Ampl) +  \
                "\n")
            t=t+self.DT
        file_CSV.close
        RMS_Noise=RMS_Noise/self.NOS
        RMS_SG=RMS_SG/self.NOS
        SQRT_RMS_Noise=math.sqrt(RMS_Noise)
        SQRT_RMS_SG=math.sqrt(RMS_SG)
        SNR=0
        if RMS_Noise<>0 :
            SNR=RMS_SG / RMS_Noise

        self.DateRMS="RMS_SG^2= "+("%0.4f" % RMS_SG)+"\n"
        self.DateRMS=self.DateRMS+"RMS_Noise^2= "+("%0.4f" % RMS_Noise)+"\n"
        self.DateRMS=self.DateRMS+"SNR= "+("%0.4f" % (SNR))+"\n"
        self.DateRMS=self.DateRMS+"RMS_SG= "+("%0.4f" % SQRT_RMS_SG)+"\n"
        self.DateRMS=self.DateRMS+"RMS_Noise= "+("%0.4f" % SQRT_RMS_Noise)+"\n"

        file_PLUS_CSV.write(self.DateRMS)

        file_PLUS_CSV.close

        sirtxt="RMS_SG^2= "+("%0.3f" % RMS_SG)+ " "
        sirtxt=sirtxt+"RMS_Noise^2= "+("%0.3f" % RMS_Noise)+" "
        sirtxt=sirtxt+"SNR= "+("%0.3f" % (SNR))+" "
        sirtxt=sirtxt+"RMS_SG= "+("%0.3f" % SQRT_RMS_SG)+" "
        sirtxt=sirtxt+"RMS_Noise= "+("%0.3f" % SQRT_RMS_Noise)

        msg="Signal Generated for Tmax="+str((self.NOS-1)*self.DT)+ " sec. in file: " + file_name+"\n"
        msg=msg+sirtxt
        self.file_name=file_name

        self.axa1.set_title(msg , fontsize=14)

        self.axa1.lines.remove(self.Curve_Sinus)
        self.Curve_Sinus, = self.axa1.plot(Time, Sinus, '.-',   linewidth=2, color="Cyan", la-
bel="a*sin[(2*Pi*f1*t)+Pi*Ph1]+b*sin[(2*Pi*f2*t)+Pi*Ph2]+c*sin[(2*Pi*f3*t)+Pi*Ph3]")

        self.axa1.lines.remove(self.Curve)
        self.Curve, = self.axa1.plot(Time, Amplitudine, '.-', markersize=4, linewidth=2, color="Red", label="Gene-
rated signal")

        self.axa1.lines.remove(self.Curve_Noise)
        self.Curve_Noise, = self.axa1.plot(Time, Zgomot, '.-', markersize=4,  linewidth=0.5, color="Gray", la-
bel="Noise")

        self.axa1.lines.remove(self.Curve_Damp)
        self.Curve_Damp, = self.axa1.plot(Time, Amortizare, '.-',  linewidth=0.5, color="Green", label="Damping")

        self.axa1.legend(prop={'size': 9})
        self.axa1.relim()
        self.axa1.autoscale_view(True,True,True)
        self.axa1.figure.canvas.draw()
```

```
def CALCULATE(self): #Antiderivate calculus

    Verify_Excel()
    self.Recreate_Axis()

    self.OPTIUNE = self.lst_VARIANTA.GetStringSelection().strip()
    if self.OPTIUNE =="Displacement":
        fex1=os.getcwd()+"/RESULTS/Displacement.xlsx"
        macheta="Macheta - Displacement.xlsx"
        FisierExcel="Displacement"
    if self.OPTIUNE =="Velocity up":
        fex1=os.getcwd()+"/RESULTS/VelocityUp.xlsx"
        macheta="Macheta - VelocityUp.xlsx"
        FisierExcel="VelocityUp"
    if self.OPTIUNE =="Velocity down":
        fex1=os.getcwd()+"/RESULTS/VelocityDown.xlsx"
        macheta="Macheta - VelocityDown.xlsx"
        FisierExcel="VelocityDown"
    if self.OPTIUNE =="Acceleration":
        fex1=os.getcwd()+"/RESULTS/Acceleration.xlsx"
        macheta="Macheta - Acceleration.xlsx"
        FisierExcel="Acceleration"

    connection = sqlite.connect(os.getcwd()+'\Config.db') ; cursor = connection.cursor()
    blob=ExtragTextMemory(cursor, macheta)
    cursor.close() ; connection.close()

    open(fex1, 'wb').write(blob)
    xlApp = Dispatch("Excel.Application")   # Connect Excel
    xlApp.Visible=False
    xlWb = xlApp.Workbooks.Open(fex1)
    XLSheet=xlWb.Worksheets(FisierExcel)
    sheets = xlWb.Sheets

    self.L0=self.L1=self.L2=self.L3=self.L4=self.L5=""

    if self.OPTIUNE =="Displacement":

        #--------------  1 ----------------
        msg=self.OPTIUNE+ " signal for Tmax="+str((self.NOS-1)*self.DT)+ " sec.from file: " + self.fex1
        self.axa_Disp.set_title(msg , fontsize=14)
        label1="Initial displacement"
        self.DispCurve1, = self.axa_Disp.plot(self.Time, self.Amplitudine, '.-',
              linewidth=2, color="Red", label=label1)

        #--------------  2 ----------------
        TimeDer1, Derivare1 = self.DERIVARE(self.Time, self.Amplitudine)
        label2="Velocity 1 calculated - Derivated"
        self.VeloCurve1, = self.axa_Velo.plot(TimeDer1, Derivare1, '.-',
              linewidth=2, color="Green", label=label2)

        #--------------  3 ----------------
        TimeDer2, Derivare2 = self.DERIVARE(TimeDer1, Derivare1)
        label3="Acceleration 1 calculated - Derivated"
        self.AcceCurve1, = self.axa_Acce.plot(TimeDer2, Derivare2, '.-',
              linewidth=2, color="Blue", label=label3)

        #--------------  4 ----------------
```

```
    TimeInt1, Integrala1 = self.INTEGRARE1(TimeDer2, Derivare2)
    TimeInt1=TimeInt1[0:len(TimeInt1)-1]
    label4="Velocity reconstructed - Integrated"
    self.VeloCurve2, = self.axa_Velo.plot(TimeInt1, Integrala1, '.-',
          linewidth=2, color="Blue", label=label4)

    #--------------  5 ----------------
    TimeInt2, Integrala2 = self.INTEGRARE2(TimeInt1, Integrala1)
    label5="Displacement reconstructed  - Integrated*"
    self.DispCurve2, = self.axa_Disp.plot(TimeInt2, Integrala2, '.-',
          linewidth=2, color="Blue", label=label5)

    for x in self.Time:        self.L0=self.L0+("%0.4f" % x)+"\n"
    for x in self.Amplitudine:  self.L1=self.L1+("%0.4f" % x)+"\n"
    for x in Derivare1:        self.L2=self.L2+("%0.4f" % x)+"\n"
    for x in Derivare2:        self.L3=self.L3+("%0.4f" % x)+"\n"
    for x in Integrala1:       self.L4=self.L4+("%0.4f" % x)+"\n"
    for x in Integrala2:       self.L5=self.L5+("%0.4f" % x)+"\n"


if self.OPTIUNE =="Velocity up":

    #--------------  1 ----------------
    msg=self.OPTIUNE+ " signal for Tmax="+str((self.NOS-1)*self.DT)+ " sec.from file: " + self.fex1
    self.axa_Velo.set_title(msg , fontsize=14)
    label1="Initial velocity"
    self.VeloCurve1, = self.axa_Velo.plot(self.Time, self.Amplitudine, '.-',
          linewidth=2, color="Red", label=label1)

    #--------------  2 ----------------
    TimeDer1, Derivare1 = self.DERIVARE(self.Time, self.Amplitudine)
    label2="Acceleration 1 calculated - Derivated"
    self.AcceCurve1, = self.axa_Acce.plot(TimeDer1, Derivare1, '.-',
          linewidth=2, color="Red", label=label2)

    #--------------  3 ----------------
    TimeInt1, Integrala1 = self.INTEGRARE1(TimeDer1, Derivare1)
    label3="Velocity 1 calculated - Integrated"
    self.VeloCurve2, = self.axa_Velo.plot(TimeInt1, Integrala1, '.-',
          linewidth=2, color="Blue", label=label3)

    #--------------  4 ----------------
    TimeInt2, Integrala2 = self.INTEGRARE2(TimeInt1, Integrala1)
    label4="Displacement calculated - Integrated*"
    self.DispCurve1, = self.axa_Disp.plot(TimeInt2, Integrala2, '.-',
          linewidth=2, color="Blue", label=label4)

    #--------------  5 ----------------
    TimeDer1, Derivare2 = self.DERIVARE(TimeInt2, Integrala2)
    label5="Velocity reconstructed - Derivated"
    self.VeloCurve3, = self.axa_Velo.plot(TimeDer1, Derivare2, '.-',
          linewidth=2, color="Green", label=label5)

    for x in self.Time:        self.L0=self.L0+("%0.4f" % x)+"\n"
    for x in self.Amplitudine:  self.L1=self.L1+("%0.4f" % x)+"\n"
    for x in Derivare1:        self.L2=self.L2+("%0.4f" % x)+"\n"
    for x in Integrala1:       self.L3=self.L3+("%0.4f" % x)+"\n"
    for x in Integrala2:       self.L4=self.L4+("%0.4f" % x)+"\n"
    for x in Derivare2:        self.L5=self.L5+("%0.4f" % x)+"\n"
```

```
if self.OPTIUNE =="Velocity down":

    #-------------- 1 ----------------
    msg=self.OPTIUNE+ " signal for Tmax="+str((self.NOS-1)*self.DT)+ " sec.from file: " + self.fex1
    self.axa_Velo.set_title(msg , fontsize=14)
    label1="Initial velocity"
    self.VeloCurve1, = self.axa_Velo.plot(self.Time, self.Amplitudine, '.-',
          linewidth=2, color="Red", label=label1)

    #-------------- 2 ----------------
    TimeInt1, Integrala1 = self.INTEGRARE1(self.Time, self.Amplitudine)
    Integrala1=Integrala1[0:len(Integrala1)-1]
    label2="Displacement calculated - Integrated"
    self.DispCurve1, = self.axa_Disp.plot(TimeInt1, Integrala1, '.-',
          linewidth=2, color="Blue", label=label2)

    #-------------- 3 ----------------
    TimeDer1, Derivare1 = self.DERIVARE(TimeInt1, Integrala1)
    label3="Velocity 1 calculated - Derivated"
    self.VeloCurve2, = self.axa_Velo.plot(TimeDer1, Derivare1, '.-',
          linewidth=2, color="Blue", label=label3)

    #-------------- 4 ----------------
    TimeDer2, Derivare2 = self.DERIVARE(TimeDer1, Derivare1)
    label4="Acceleration 1 calculated - Derivated"
    self.AcceCurve1, = self.axa_Acce.plot(TimeDer2, Derivare2, '.-',
          linewidth=2, color="Red", label=label4)

    #-------------- 5 ----------------
    TimeInt2, Integrala2 = self.INTEGRARE1(TimeDer2, Derivare2)
    label5="Velocity reconstructed - Integrated"
    TimeInt2=TimeInt2[0:len(TimeInt2)-2]
    self.VeloCurve3, = self.axa_Velo.plot(TimeInt2, Integrala2, '.-',
          linewidth=2, color="Green", label=label5)

    for x in self.Time:        self.L0=self.L0+("%0.4f" % x)+"\n"
    for x in self.Amplitudine:  self.L1=self.L1+("%0.4f" % x)+"\n"
    for x in Integrala1:       self.L2=self.L2+("%0.4f" % x)+"\n"
    for x in Derivare1:         self.L3=self.L3+("%0.4f" % x)+"\n"
    for x in Derivare2:         self.L4=self.L4+("%0.4f" % x)+"\n"
    for x in Integrala2:       self.L5=self.L5+("%0.4f" % x)+"\n"

if self.OPTIUNE =="Acceleration":

    #-------------- 1 ----------------
    msg=self.OPTIUNE+ " signal for Tmax="+str((self.NOS-1)*self.DT)+ " sec.from file: " + self.fex1
    self.axa_Acce.set_title(msg , fontsize=14)
    label1="Initial acceleration"
    self.AcceCurve1, = self.axa_Acce.plot(self.Time, self.Amplitudine, '.-',
          linewidth=2, color="Red", label=label1)

    #-------------- 2 ----------------
    TimeInt1, Integrala1 = self.INTEGRARE1(self.Time, self.Amplitudine)
    Integrala1=Integrala1[0:len(Integrala1)-1]
    label2="Velocity 1 calculated - Integrated"
    self.VeloCurve1, = self.axa_Velo.plot(TimeInt1, Integrala1, '.-',
          linewidth=2, color="Blue", label=label2)
```

```
        #--------------  3 ----------------
        TimeInt2, Integrala2 = self.INTEGRARE2(TimeInt1, Integrala1)
        label3="Displacement calculated - Integrated*"
        self.DispCurve1, = self.axa_Disp.plot(TimeInt2, Integrala2, '.-',
              linewidth=2, color="Green", label=label3)

        #--------------  4 ----------------
        TimeDer1, Derivare1 = self.DERIVARE(TimeInt2, Integrala2)
        label4="Velocity reconstructed - Derivated"
        self.VeloCurve2, = self.axa_Velo.plot(TimeDer1, Derivare1, '.-',
              linewidth=2, color="Red", label=label4)

        #--------------  5 ----------------
        TimeDer2, Derivare2 = self.DERIVARE(TimeDer1, Derivare1)
        label5="Acceleration reconstructed - Derivated"
        self.AcceCurve2, = self.axa_Acce.plot(TimeDer2, Derivare2, '.-',
              linewidth=2, color="Green", label=label5)

        for x in self.Time:         self.L0=self.L0+("%0.4f" % x)+"\n"
        for x in self.Amplitudine:  self.L1=self.L1+("%0.4f" % x)+"\n"
        for x in Integrala1:        self.L2=self.L2+("%0.4f" % x)+"\n"
        for x in Integrala2:        self.L3=self.L3+("%0.4f" % x)+"\n"
        for x in Derivare1:         self.L4=self.L4+("%0.4f" % x)+"\n"
        for x in Derivare2:         self.L5=self.L5+("%0.4f" % x)+"\n"


    Put_Clipboard(self.L0); XLSheet.Cells(4,1).Select() ; XLSheet.Paste()
    Put_Clipboard(self.L1); XLSheet.Cells(4,2).Select() ; XLSheet.Paste()
    Put_Clipboard(self.L2); XLSheet.Cells(4,3).Select() ; XLSheet.Paste()
    Put_Clipboard(self.L3); XLSheet.Cells(4,4).Select() ; XLSheet.Paste()
    Put_Clipboard(self.L4); XLSheet.Cells(4,5).Select() ; XLSheet.Paste()
    Put_Clipboard(self.L5); XLSheet.Cells(4,6).Select() ; XLSheet.Paste()
    XLSheet.Cells(1,1).Select()

    xlWb.Close(SaveChanges=1)
    xlApp.Quit()

    self.axa_Disp.legend()
    self.axa_Disp.relim()
    self.axa_Disp.autoscale_view(True,True,True)
    self.axa_Disp.figure.canvas.draw()

    self.axa_Velo.legend()
    self.axa_Velo.relim()
    self.axa_Velo.autoscale_view(True,True,True)
    self.axa_Velo.figure.canvas.draw()

    self.axa_Acce.legend()
    self.axa_Acce.relim()
    self.axa_Acce.autoscale_view(True,True,True)
    self.axa_Acce.figure.canvas.draw()

    sir="\nThe numerical results were exported to Excel file:\n\n  "+fex1+"\n"
    wx.MessageBox(sir, "Info", wx.OK )
```